OPEN ACCESS

University of BRISTOL

This electronic thesis or dissertation has been downloaded from Explore Bristol Research, http://research-information.bristol.ac.uk

Author:
Ullah, Sami

Title:
Sustainable functionalization of diamond surface with tin, lithium, and oxygen for low work function applications

General rights
Access to the thesis is subject to the Creative Commons Attribution - NonCommercial-No Derivatives 4.0 International Public License. A copy of this may be found at https://creativecommons.org/licenses/by-nc-nd/4.0/legalcode This license sets out your rights and the restrictions that apply to your access to the thesis so it is important you read this before proceeding.

Take down policy
Some pages of this thesis may have been removed for copyright restrictions prior to having it been deposited in Explore Bristol Research. However, if you have discovered material within the thesis that you consider to be unlawful e.g. breaches of copyright (either yours or that of a third party) or any other law, including but not limited to those relating to patent, trademark, confidentiality, data protection, obscenity, defamation, libel, then please contact collections-metadata@bristol.ac.uk and include the following information in your message:

•Your contact details
•Bibliographic details for the item, including a URL
•An outline nature of the complaint

Your claim will be investigated and, where appropriate, the item in question will be removed from public view as soon as possible.

Sustainable Functionalization of Diamond Surface with Tin, Lithium, and Oxygen for Low Work Function Applications

By

Sami Ullah

School of Physics

UNIVERSITY OF BRISTOL

A dissertation submitted to the University of Bristol
in accordance with the requirements of the degree of
DOCTOR OF PHILOSOPHY in the Faculty of Science.

JANUARY 2023

Word Count = ~ 36000

Abstract

The overarching goal and ambition of this research is to realise a potential solution to the chemical instability found with known functionalised diamond surfaces. A sub-set of these form a dipole that gives rise to a negative electron affinity property that promotes enhanced electron emission at thermionic temperatures and has numerous technological applications including concentrated solar thermal power generation.

The prime focus of the research presented in this thesis is the use of tin (Sn), a very nontoxic, abundantly available, less expensive heavy metal, as an alternative termination of the diamond surface. The suitability of tin was established using the density functional theory (DFT) where Sn and tin monoxide (SnO) groups used as a termination on the diamond (100) surface have resulted in a large adsorption energy of -4.4 eV in half monolayer configuration (HML) with an electron affinity of −1.43 eV and up to -6.5 eV in HML configuration with an electron affinity up to −1.37 eV, respectively. The NEA occurs as a result of dipole formation on the surface due to the shift in the electron density toward or in the vicinity of surface carbon atoms, realised through the electrostatic potential and density of states calculations.

Lithium nitride solution was deposited on the diamond surface with subsequent annealing at higher temperatures to gain an insight into the mobility of the Li atoms on the diamond. Li atoms were seen to move from the surface into the near surface bulk and then back to the surface through the temperatures of 650 °C – 750 °C – 850 °C, at which point the LiO was completely desorbed from the surface. This was seen to affect the bulk properties of diamond.

An air stable sub monolayer of SnO nanoclusters was formed “reliably” on the surface of diamond (100) using physical vapor deposition. SnO was seen to impart an NEA of -0.02 eV to the diamond surface along with a reduction in the WF by 1.8 eV. Inclusion of Li atoms into this structure resulted in Li atoms taking up oxygen from SnO and forming SnO_x-LiO_2 heterostructure with an NEA of – 0.42 eV and WF reduction by 2.3 eV. This interaction has also resulted in the increased stability of the Li on diamond surface. Only about 15% of Li was lost in the case of Li_2O-SnO_x termination on diamond (100) compared to 47% lost in case of LiO terminated diamond at similar elevated temperatures.

Acknowledgement

All praises to the One who has adorned mankind with the light of His knowledge and who has sent His Messengers *peace be upon them all*, as torch bearers to the "Truth". I thank Almighty Allah and His Beloved *peace be upon Him* for inspiring me, guiding me, helping me towards finishing one the major goals of my life. I am also thankful to my spiritual mentor, the light of my eyes and the peace of my mind, soul and heart, the most perfect guide Maulana Muhammad Ameen Owaisi *peace be upon him* for always being with me with his spiritual courage (*himmah*) during my stay in the UK.

As our Beloved has said one who doesn't thank people, hasn't thanked Almighty at all. I would like to express that I have an incredibly long list of people to thank for. These people have not only been helpful and supportive but without them this journey wouldn't have been possible especially my supervisor Professor Neil Fox whose guidance, care, supervision, support is enough to nourish an inadept into a doctor. The people from BCFN such as Professor Annela Seddon, Dr. Ian Lindsay, Dr. Duncan Casey, Becky Freshwater were these ones who received me in the University on my first day and since then have been taking care of my academic needs perfectly. I must say the environment that BCFN provides is amazing in terms of culturing such relationships among various people that not only prove helpful during the long journey of PhD but also make one feel at home. I am incredibly thankful to Dr. Paul May, Dr. Mattia Cattelan, Dr. Jude Laverock, Dr. Gary Wan, Dr. Tahani Al-Mutairi, Dr. Ed Smith, Dr. Ramiz Zulkharnay, etc. for providing guidance and support at various points during this journey. Although we did spend a considerably huge amount of time in the physical and mental quarantine during and after the pandemic that has left us broken. But I am optimistic that we have come out of it stronger than before and calmer than ever *in sha Allah*. I am also thankful to the University of Bristol, UK for providing me with the Zutshi Smith Scholarship without which this journey would have been impossible. Finally, I am thankful and indebted to my beloved parents without the prayers and blessings of whom I wouldn't be where I am today and to my precious wife, Nayeema Ji, for enduring and surfing over the high and low tides of PhD life with me. Lastly, I must acknowledge and be thankful that I was blessed with a baby boy, Mir Hasnain Ali Andjani, whose presence and little smiles would relieve me from the stress and anxiety during my PhD.

Covid Statement

The COVID-19 pandemic had an immense impact on my studies. It left me without any practical work during the period from January 2020 till March 2021, as the labs were inaccessible, and everybody was worried about the survival. The pandemic had a severe impact on my health as well. I was not able to read, write or learn anything due to the overwhelming fear and hence emotional instability during the initial period of the pandemic. My supervisor Professor Neil Fox was extremely supportive with his fortnightly meetings and encouragement. Later in the pandemic, I was able to work due to being used to the new "normal" but at a snail's pace. Later in 2021, the labs were opened but with overwhelming load on the lab incharges and hence slow progress. My sponsors at the University of Bristol, UK were extremely supportive by providing me with a funded extension of 6 months, knowing which brought relief and peace. Thankfully, I was able to cope up with the situation and continue my studies.

Author's declaration

I declare that the work in this dissertation was carried out in accordance with the requirements of the University's Regulations and Code of Practice for Research Degree Programmes and that it has not been submitted for any other academic award. Except where indicated by specific reference in the text, the work is the candidate's own work. Work done in collaboration with, or with the assistance of, others, is indicated as such. Any views expressed in the dissertation are those of the author.

SIGNED: .....DATE: .....

List of Publications

1. S. Ullah, N.A. Fox, "Modification of the Surface Structure and Electronic Properties of Diamond (100) with Tin as a Surface Termination: A Density Functional Theory Study", J. Phys. Chem. C 125 (2021) 25165.

This manuscript was written through contributions of all authors as mentioned below. All authors have given approval to the final version of the manuscript. This publication has contributed to chapter 2, chapter 3 and chapter 4.

2. S. Ullah, L. Cullingford, T. Zhang, J.R. Wong, G. Wan, M. Cattelan, N.A. Fox, "An investigation into the surface termination and near-surface bulk doping of oxygen-terminated diamond with lithium at various annealing temperatures", MRS Adv. (2021). pdf [doi: 10.1557/s43580-021-00060-x].

This manuscript was written through contributions of all authors as mentioned below. All authors have given approval to the final version of the manuscript. This publication has contributed to chapter 2, chapter 3 and chapter 5.

3. S. Ullah, G. Wan, C. Kouzios, C. Woodgate, M. Cattelan, N.A. Fox, "Structure and electronic properties of Tin monoxide (SnO) and lithiated SnO terminated diamond (100) and its comparison with lithium oxide terminated diamond", Appl. Surf. Sci. 559 (2021) 149962.

This manuscript was written through contributions of all authors as mentioned below. All authors have given approval to the final version of the manuscript. This publication has contributed to chapter 2, chapter 3 and chapter 6.

***Sami Ullah**: Investigation, Methodology, Conceptualization, Software, Visualization, Writing - original draft. **L. Cullingford:** Investigation, Validation. **T. Zhang:** Investigation, Validation. **J.R. Wong:** Investigation, Validation. **Gary Wan**: Validation, Resources, Writing - review & editing. **Christos Kouzios**: Investigation, Writing - review & editing. **Cameron Woodgate**: Investigation, Validation. **Mattia Cattelan**: Conceptualization, Resources, Data curation, Writing - review & editing. **Neil Fox**: Writing - review & editing, Supervision, Funding acquisition.*

List of Acronyms

Symbol	Full form
ARPES	Angle Resolved Photo Emission Spectroscopy
ARXPS	Angle Resolved X- Ray Photoelectron Spectroscopy
BE	Binding Energy
BDD	Boron Doped Diamond
CASTEP	Cambridge Serial Total Energy Package
CBM	Conduction Band Minimum
CVD	Chemical Vapor Deposition
DFT	Density Functional Theory
DOS	Density of States
EF-PEEM	Energy Filtered Photo Emission Microscopy
E_F	Fermi level
E-beam	Electron Beam
EP	Electron Potential
ESCA	Electron Spectroscopy for Chemical Analysis
FCC	Face Centred Cubic
FML	Full Mono Layer
GGA	Generalised Gradient Approximation
HPHT	High Pressure High Temperature
HML	Half Mono Layer
HF CVD	Hot Filament CVD
KE	Kinetic Energy
LDA	Local Density Approximation
MWCVD	Micro Wave CVD
MFC	Mass Flow Controller
NEA	Negative Electron Affinity
NDD	Nitrogen Doped Diamond
OTD	Oxygen Terminated Diamond
PVD	Physical Vapor Deposition

PV	Photovoltaic
PEA	Positive Electron Affinity
PCD	Poly Crystalline Diamond
QML	Quarter Mono Layer
RT	Room Temperature
SCD	Single Crystal Diamond
SPA-LEED	Spot Profile Analysis- Low Energy Electron Diffraction
TEC	Thermionic Energy Converter
UHV	Ultra-High Vacuum
UPS	Ultraviolet (UV) Photoelectron Spectroscopy
VBM	Valence Band Maximum
WF	Work Function
XPS	X-ray Photoelectron Spectroscopy

Contents

List of Figures

Figures Page

List of Tables

Chapter 1

Introduction

Summary

This is the introductory chapter of the thesis which mentions the climate change and the other issues associated with it. How industrial revolution and/or "the activities of human" have led to the climate catastrophe and its effects on the energy sources has been discussed along with how material science could help mitigate the climate change by focusing towards net zero emission goals.

Moreover, diamond as a candidate for energy conversion devices has been described. The types and properties of diamond have been mentioned along with how the properties of diamond can be changed for it to have important and interesting properties so that it can be effectively used in energy applications.

1.1. Introduction: Climate change a global challenge

Our scriptures speak of an important role of human being as a viceroy among the creation on the planet earth. A viceroy is a guardian over all other things present on the face of earth whether it be animals, plants, earth itself. A guardian is meant to take care of the things he or she watches over (i.e. the environment). The crisis of the time, well known by climate change and environmental degradation that our mother earth is facing are mostly due to the acts of human [13] in the form of excesses in the industrial revolution. Figure 1.1 shows the levels of carbon dioxide emission (CO_2), a chief cause for environmental degradation, since the ancient time which indicates a spike in the levels of CO_2 emitted since the industrial revolution, breaking the records of thousands of years in 1950 without any halt.

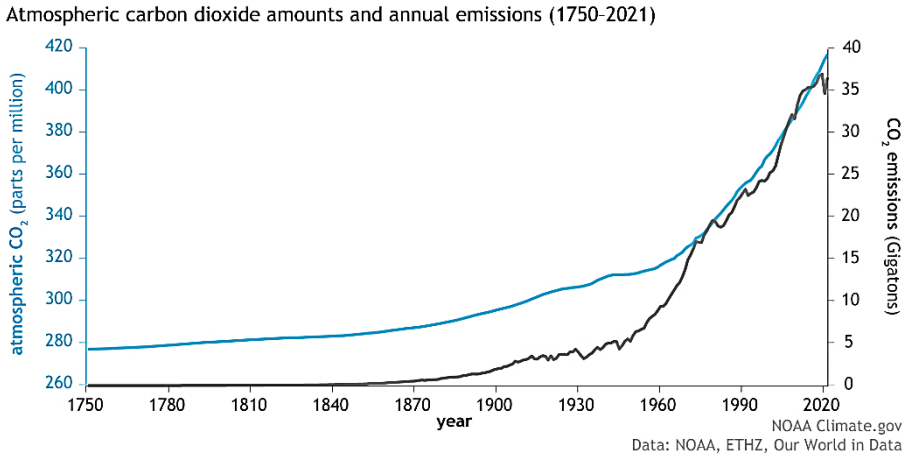

Figure 1.1 : CO2 in air since the ancient times till modern times. It shows record increase in the levels of CO2 mostly due to the industrial activities of human. Emissions increased slowly nearing 5 billion tons per year in the mid-20th century before rapidly spiking to more than 35 billion tons per year by the end of the century. Reproduced from [14]

From our homes to mega industries, from modern scooters to aeroplanes and space shuttles, etc. the fossil fuels are burnt for the purpose of getting energy, releasing massive amounts of CO_2. As the days go by, the population increases tremendously (tripled in past 70 years) [15] and this increases the use of energy-yielding fossil fuels and other such products which release harmful gases (Figure 1.2).

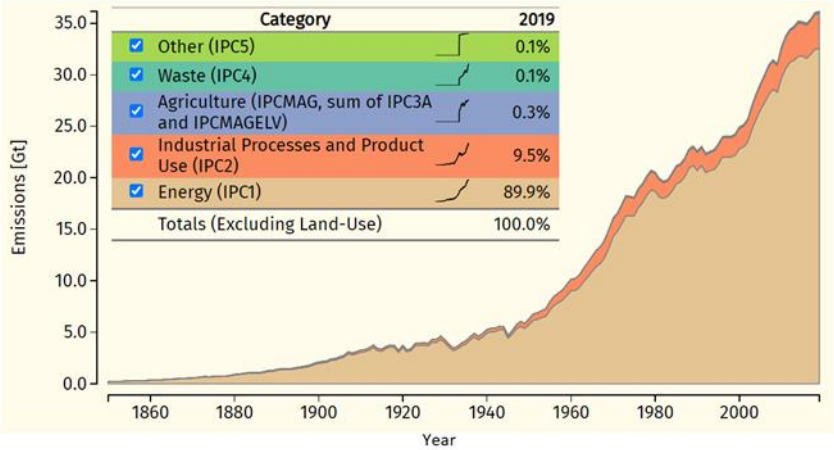

Figure 1.2: Energy harvesting from fossils as chief reason for CO_2 emission. The Potsdam Institute for Climate Impact Research study reveals nearly 90% (32.1 billion tonnes) of the atmospheric CO_2 contributed by the energy consumption, be it because of the lamps in our rooms or the HVAC systems running in huge buildings. Source [16, 17]

Due to the presence of increased levels of such gases as CO_2 and methane, visible spectrum absorption and re-radiation in the IR region occurs as a result of which heat gets trapped which increases the temperature on the earth, famously called greenhouse effect. The most concerning aspect of greenhouse effect is the rate at which the temperature is increasing. To put everything in simple terms, according to a report by the UN [18, 19], our world is hotter by 1 °C than the pre industrial time (i.e. around 1800 A.D.) which doesn't seem as an immediate threat to humankind or the planet earth. Even a rise of 1.5 to 2 °C global temperature by 2100 has been predicted to be "not a cause for concern". What really terrifies the scientists is the current rate at which the temperature is rising which is 1.5 °C in about 10 years which would be catastrophic for the nature, the symptoms of which the world is already facing in the form of many devastating natural phenomenon (rather natural reactions) for example the rise of sea water levels, famines, less food, floods.

This has resulted in a famous agreement between the world leaders on climate change, although many have acted in denial, called the Paris agreement in 2015 in which the world leaders met and pledged to build the worldwide framework for mitigating the dangerous climate change by avoiding the rise of temperature beyond 2°C and developing strategies to limit it well under 1.5 °C along with an intention to strengthen the different countries in dealing with the impacts of climate change and strengthen their efforts in this journey [20, 21].

Globally approximately 84% of our energy needs are still met with the fossil fuels which release nearly 50 billion tons of CO_2 each year [22]. Instead of erasing the 200 years history of scientific and technological achievements and going back to candles and horses, the reduction in the use of fossil fuels for energy needs is stressed. This entails strengthening the awareness and implementation of renewable energy sources and harnessing, the only alternative to fossil fuels that can heal the earth to a significant extent. This would mean developing the science and technology to harness the natural sources of energy by exploring the wide range of materials and their design and application in energy conversion and storage devices. This would also help in tapping the waste heat from various other sources like nuclear reactors, geothermal sources, etc. (which is nearly 2/3rd of the total thermal energy produced). Emphasis has to be laid on other aspects too like carbon capture, water splitting for hydrogen release and its storage so that it can be a clean alternative to the fuel, etc. All of these efforts were the outcomes of the various scientific explorations and topics of discussion between the world leaders in COP26 as well which happened in Glasgow UK where the world leaders met in 2021 [23] to discuss the outcome of their pledge in Paris agreement (which was nowhere near the goal) and to renew their pledge more empathetically for the greater good of humanity. This has resulted in developing the "Net Zero Emission" goal in which different countries under the leadership of the United Kingdom have promised to reach the goals of net zero carbon dioxide and methane emissions by restricting or eliminating the use of dangerous fossil fuels and promote the use of clean sources of energy by a certain target year (2030) and provide financial help to the developing nations to combat the symptoms of climate change. Thus, every single step towards the production and implementation of technology and materials for green energy counts as a milestone in this age of crisis which is actually the aim of this study.

1.2. Material science and its role in fulfilling our 'Net zero emission' goal

Let us illustrate this with an example set by the UK which became the first global economy to set a net zero emission target for 2050 [24]. In this regard, an initiative was taken by The Henry Royce Institute (Royce) in collaboration with the Institute of Physics (IOP) to involve academic and industrial material scientists to find the role of material science in delivering affordable, reliable and green energy. The outcome of this initiative was a set of roadmaps illustrating how material science can contribute to the UK's low carbon

energy transition. It was shown that novel materials and processes need to be developed and implemented in photovoltaic systems, low carbon production of hydrogen (water splitting), thermoelectric energy conversion, caloric energy conversion, and low loss electronics in order to achieve the mentioned goals [25].

As an example, PV energy conversion has been considered as one of the means to address the UK's net zero goals for energy generation as it has the potential to meet 50% of the UK's total generation capacity by 2030 which of course depends on how quickly the existent technologies (in which the UK has world leading position in PV field) are translated into working devices [26].

Another example is that of hydrogen generation at low carbon expenditure to develop green energy from clean fuels which involves a range of interdisciplinary skills and knowledge in which the modelling, surface science and process engineering among others play crucial role which beckons towards the role of material science in this aspect [27].

Research aimed towards the development and characterisation of novel materials for thermoelectric and caloric energy conversion devices would be another milestone in this journey of reaching net zero target as research shows the impact of caloric only to UK heating and cooling is a 50% reduction in energy consumption. These devices are manufactured using non-polluting, efficient, reliable, compact and sustainable methods and are meant for refrigeration, air conditioning, and heating, such day-to-day processes which add up to the energy demands significantly.

Hence these examples highlight the importance of material science and technology, in the words of Henry Royce Institute Chair, Baroness Brown of Cambridge (Julia King), as an "important means in this major energy transition to deliver the disruptive technologies that will develop the energy-efficient applications and processes, urgently needed to achieve 2050 net-zero goal"[28].

One thing that is being stressed again and again while looking for the solutions to the crisis of the time is to use the renewable sources of energy for most of our needs. As of 2021, renewable sources satisfy 15% of the global energy demand which is forecasted to increase up to 20-30% by 2040 and by 2050 , world should be able to completely derive energy from the renewables only, hence reaching the net zero target [29].

Furthermore, what should motivate us to innovate in harvesting the renewable sources of energy is the fact that the renewable sources are abundantly available in every country, is cheaper and healthier, creates more jobs. This stresses upon material science and its role in the process of evolving such materials and design which could render the energy harvesting devices more efficient and economical. It is due to the innovations facilitated by the material science that the solar photovoltaic module costs have been reduced by 80% while the wind turbine costs have been reduced by 30-40% [30].

1.3. Climate change and its effect on the renewable sources of energy

Various renewable sources of energy can be identified, the most prominent being hydroelectric power generation, wind generation, solar power generation, etc. A new line of research has studied the effect of climate change on these sources themselves which can be summarised here. One of the most important factors is climate change induced change in rainfall patterns which in turn affect the river flows and water levels and hence production. This can also cause changes in precipitation and temperatures which could have an adverse effect on the moisture level of soil and hence cause run off. Flooding and intense rains can cause a significant damage to the dams, turbines and crucial infrastructure. Changes in the air temperature can induce surface evaporation, reduce water storage and hence power output. This could also lead to the melting of glaciers which anyway is a serious threat [31].

In the case of wind energy, changes in wind speed can reduce the power generation as the turbines cannot work in very high or very low winds. The power generation can also be affected by the daily or seasonal distribution of wind leading to a mismatch between wind energy input to the grid and daily load demand. Changes in air temperature can lead to slight declines in air density and hence output. The turbines can be damaged by the drifting ice. The offshore infrastructure might be damaged by the rising sea levels. There is a threat of damage to the infrastructure due to the extreme whether events like hurricanes and storms which could cause the shutdown of the system altogether.

A lot of focus is being given on the solar energy harvesting using the solar PV technology. However, climate change can pose a serious threat to this avenue as well. Changes in mean temperature due to climate change could negatively affect the efficiency of the cells and hence power output e.g. it has been realised that every 0.5% drop in the efficiency of a solar module is attributed to 1°C increase in temperature [31]. The conductors used for transporting the electric energy would also face similar situation in terms of their

capacity to conduct the electricity. All of this might increase the operational cost of the solar modules, hence affecting this technology seriously. Climate change could also cause changes in solar irradiation by cloudiness, dirt, dust, snow in the atmosphere, thereby affecting the output power generation. High speed winds, fires, and other extreme weather conditions can cause damage to the infrastructure.

In spite of these adverse effects of climate change on the renewable sources of energy, the development and innovation in this sector is very crucial to replace the current sources of energy and reach the net zero emission goals. Having mentioned these, more focus can be laid on a well-known classical phenomenon namely thermionic energy conversion (towards green energy generation) which has a potential of generating electricity not only using the commonly known sources of renewable energy such as solar energy but also could generate power from the sources of waste energy found in many installations on the earth such as nuclear reactors, factories, human bodies, car exhausts, etc. Furthermore, the thermionic converter devices will have lesser chances of degradation due to climate changes (as found in case of solar energy converters) due to their application and scope in diverse areas. For example, a solar panel can be affected by the adverse climate change which could render it useless, but a thermionic converter can still be used to harness waste heat from nuclear reactors and other factories.

1.4. Sources of waste heat and their utilisation

Waste heat refers to the energy that is generated in industrial processes and discarded without being put to practical use. Heat is an outcome of almost every thermal and mechanical process in the form of hot gases released into the atmosphere, hot by products released as waste or the heat transfer from the equipment surfaces. Be it the factories or the home installations, or nuclear reactors, even the human bodies, a significant amount of heat is lost as waste during the normal activities of the set up. It has been estimated that 60% of the heat from the nuclear reactors is wasted into the sea or other water bodies [32]. 20 to 50% of the industrial energy consumption is released as waste heat [8]. However, most of this waste heat can be recovered and used by developing proper methodologies and equipment or devices which can capture and transform this heat into some form of mechanical or electrical work in order to reduce the burden on energy sources and to make our appliances and industries cost effective. Some of the sources of the waste heat and their proper utilisation has been mentioned in the table 1.1 below.

Table 1.1: Showing sources of waste heat and their proper utilisation. Reproduced with modification from [8]

Waste Heat Source	Uses for Waste Heat
• Combustion Exhausts: Glass melting furnace Cement kiln Fume incinerator Aluminium reverberatory furnace Boiler • Process off-gases: Steel electric arc furnace Aluminium reverberatory furnace • Cooling water from Furnaces Air compressors Internal combustion engines • Conductive, convective and radiative losses from equipment and products: Hot cokes	• Combustion air preheating • Boiler feedwater preheating • Load preheating • Power generation • Steam generation for use in: Power generation Mechanical power Process steam • Space heating • Water preheating • Transfer to liquid or gaseous process streams

Power generation through thermionic emission could be one of the most efficient and effective ways of recovering the waste heat from various sources especially from the nuclear reactors and industrial set ups. The waste heat could be tapped to heat a low work function emitter that releases electrons which are then collected by a collector with a lower work function. The bias created in this process drives the load connected between the electrodes (emitter and collector).

1.5. Diamond as a potential candidate for energy conversion devices

Carbon is the 4th most common element in our galaxy due to its ease of production in nuclear fusion reactions. However, it is usually found bonded to other elements in various organic and inorganic substances. When the atoms of carbon share sp^2 hybridised orbitals with each other in a three-fold coordinated structure, materials like graphite and graphene are formed, however, when these atoms share sp^3 hybridised orbitals in a σ

bond and in a fourfold coordinated structure, diamonds are formed. Diamond has a tetrahedral structure with face centred cubic (FCC) lattice with a basis of two atoms per lattice point located at (0,0,0) and (1/4,1/4,1/4) along the unit cell (figure 1.3). Naturally diamonds are formed deep into the earth's crust at very high pressures and temperatures. Due to the innovation and development in the synthetic diamond producing technologies, an interest has risen in diamonds for their use in various applications such as thermionic emission, nuclear batteries, radiation detectors, solar panels, heat sinks, etc. This is due to diamond being a novel wide band gap material and its interesting properties, which will be discussed in the next section, that enable it to be used in such cutting-edge applications.

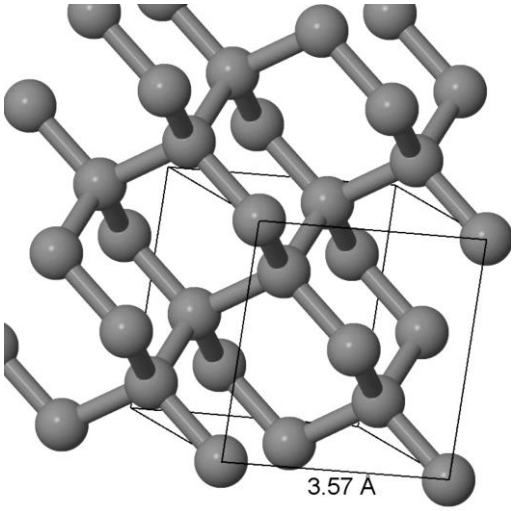

Figure 1.3: The conventional unit cell of diamond where the balls represent carbon atoms, and the rods represent the bonds between them as outlined in black.

1.5.1. Properties of diamond

Some of the interesting properties of diamond are mentioned in table 1.2. These properties of diamond are attributed to the diamonds' stronger sp^3 bonds and the short bond length of carbon atoms which results in low compressibility and hence increased hardness and strength. In fact, diamond is regarded as the hardest material known among all the 3D materials known at over 130 GPa which makes it useful in various industrial and surgical tools. Due to its sp^3 bonds, diamond is chemically inert and hence can be used in various chemical processes.

Table 1.2: Key physical and electronic properties of diamond. Reproduced from [9].

Property	Value	units
Hardness	10000	Kg/mm^2
Tensile Strength	>1.2	GPa
Compressive strength	>110	GPa
Density	3.52	g/cm^3
Young's modulus	1.22	GPa
Thermal expansion coefficient	0.0000011	/K
Thermal conductivity	20	W/ cm-K
Dielectric constant	5.7	Dimensionless
Dielectric strength	10,000,000	V/cm
Electron mobility	2200	$Cm2/V^{-s}$
Hole mobility	1600	$Cm2/V^{-s}$
Band gap	5.45	eV
Resistivity	10^{13} - 10^{16}	Ω
Electron saturated velocity	27,000,000	Cm/s
Hole saturated velocity	10,000,000	Cm/s

The thermal conductivity of diamond at RT is highest at 22 $Wcm^{-1}K^{-1}$ compared to 4 $Wcm^{-1}K^{-1}$ for copper. This property enables diamond to be used in replacing massive heat sinks and noisy air coolers in electronic devices and also as a heat spreader to improve functioning of devices (for example GaN based devices) in power electronics. Particularly, diamond is very well suited to the high temperature applications, a crucial feature in thermionics, due to its low thermal expansion coefficient of 1.1×10^{-6} K^{-1}.

Diamond is wide band gap semiconductor material with an indirect band gap of 5.45 eV which allows doping of a number of elements within the diamond lattice in order to derive many interesting electronic properties from diamond. Diamond is also very resistant to radiation damage and chemically and biologically inert which makes it useful in various applications and also as coating in nuclear fusion system and high energy particle accelerators.

1.5.2. Types of diamond

Natural diamond

The rarity, hardness, colour and brilliance of diamond has rendered it as one of the most sought after and attractive material for its use not only in jewellery as diamond is known to reflect light brilliantly when cut properly, but also in industrial application as tips on the drills and cutting devices. The natural source of diamond is found in the upper mantle some 120 to 200 km below the Earth's surface where it is formed from the silicate magma solution at pressures of 4 - 7 GPa and temperatures of 900 – 1350 °C. The fact that not much of this diamond reaches the surface makes it one of the most expensive items on the face of earth.

High pressure High Temperature (HPHT) Diamond

Also recognised as one of the forms of synthetic diamond, HPHT process imitates nature to form diamonds. As the name suggests it uses a very high pressure (5–6 GPa) and temperature (1300–1400 °C) for the transformation of carbon in graphite to the diamond. The enthalpy of formation between graphite and diamond actually differs only by 2.9 kJ mol^{-1}, however it is due to the large activation energy barrier of 728 kJ mol^{-1} (for graphitisation at 110 surface) that the transition from diamond back to graphite is not possible and hence diamond remains in its meta stable state besides graphite being a stable allotrope of carbon at a normal temperature and pressure.

These diamond stones are mainly used in industries for cutting and abrasion applications and also in the labs for the research on diamonds. However, these cannot be used in jewellery due to the these not being in a shape and also mainly due to the problem of incorporation of impurities such as nitrogen giving it a yellow colour. Also the diamond due to their shape cannot be used in other applications such as heat sinks and coatings. These diamonds have a limited usage in electronic industry as well due to the lack of precision in controlling the impurities.

Chemical Vapour Deposition (CVD) diamond

A CVD process in which the gas phase reactions at a temperature of 800 °C and pressure < 0.3 bar deposit carbon atom by atom on the surface of a substrate (molybdenum, diamond, silicon, etc.) from the radicals (such as CH_3) formed from the gas mixtures that include CH_4 as a carbon source and H_2 to etch away the sp^2 carbon preferentially over sp^3 carbon and hence allow for the growth of diamond. Various methods can be

employed to modify the quality, purity and orientation of diamond using CVD growth for example by changing the concentration of carbon source (CH_4) between 1 to 4% in H_2 that increases the diamond quality and reduces the growth rate. Various dopants or impurities can be introduced into the diamond lattice by adding gases such as B_2H_6 for boron doping, N_2 for nitrogen doping, PH_3 for phosphorous doping, etc. As the CVD growth is directional, orientation of the growing diamond can be selected by choosing a suitable single crystal diamond substrate. CVD diamond can be grown using either hot filament CVD method or by using more advanced and widely used microwave CVD method which will be described in a later chapter.

1.5.3. Altering the properties of diamond (doping)

Pure diamond intrinsically has a large band gap and behaves as a perfect insulator. However, its electronic properties can be modified by chemically doping the diamond crystal with different elements e.g. boron and nitrogen in order to make it p- type or n-type, respectively, for it to be useful in many device applications. This works by changing the position of the Fermi level within the diamond as due to doping electronic states are added within the band gap, hence altering the occupancy of states near the conduction and minimum (CBM) and valence band maximum (VBM). A p-type doping of diamond is achieved by using a substitutional boron within the diamond lattice which brings the fermi level close to the VBM (by creating an acceptor level of 0.37 eV above the VBM) as a result of which holes can exist within the valence band to carry the positive charge and hence conduct electricity. In order to make a metallic diamond (i.e. diamond with conductivity like metals, doping concentration needs to be increased so that the acceptor level comes very close to the VBM, which otherwise is very deep. Similarly, in case of n-type diamond which is made by adding substitutional nitrogen or phosphorous into the diamond crystal. These create very deep donor levels of approximately 1.7 and 0.4 eV, respectively, below the CBM and hence do not result in electrical conductivity of diamond at RT. Nitrogen doping is known to cause stress and vacancies in the diamond lattice, therefore no n-type diamond can be used for device applications like p-n junctions transistor applications.

1.5.4. Positive electron affinity (PEA) and negative electron affinity (NEA) on the surface of diamond

Surface properties of diamond have been widely investigated as many interesting phenomenon occur due to the functionalisation of surface carbon atoms, possessing

dangling bonds, with various atoms and molecules, called terminating species [33]. A surface dipole is generated between the surface carbon atoms and the terminating species due to the difference in the electronegativities. This can result in the shifting of the electron density towards or away from the surface carbon atoms, hence resulting in the widely known properties such as negative electron affinity (NEA) or positive electron affinity (PEA) on the surface of diamond [34]. PEA is defined as the condition in the electronic structure of diamond when the vacuum level lies above the conduction band and hence there is a barrier to the electron emission while NEA is the opposite phenomenon where the vacuum level lies below the conduction level and hence reducing or eliminating the barrier to the electron emission (i.e. lower WF), due to which the electrons can easily exit the diamond surface (figure 1.4).

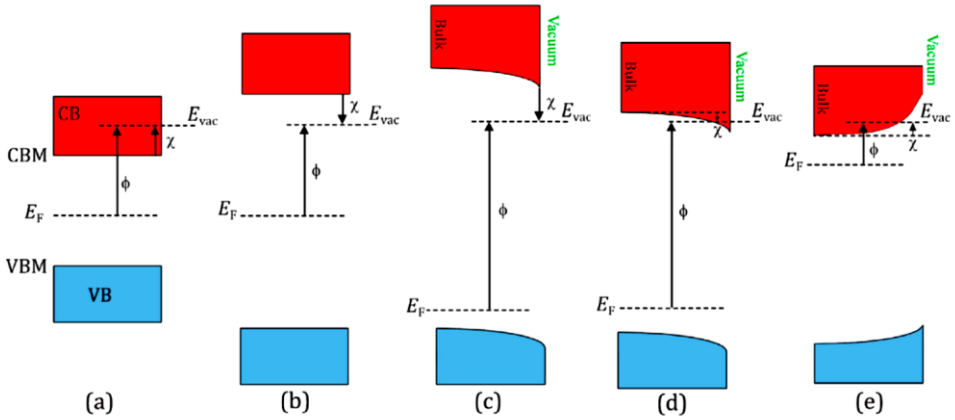

Figure 1.4: Schematic diagram illustrating the electron affinity and its relation to WF relative to a fixed vacuum energy level. VB, VBM, CB and CBM indicate the valence band, valence band maximum, conduction band and conduction band minimum, respectively. The fermi level position is dependent upon the doping condition (n doped or p doped). a) PEA, showing vacuum level in the conduction band; b) true NEA where the vacuum level is significantly below the CBM, c) true NEA in a p doped material with downward band bending. d) effective NEA where the downward band bending pushes the CBM below the vacuum level and e) PEA in an n doped material where upward band bending has pushed the CBM above the vacuum level. Reproduced from [35].

Common terminations that have been studied as PEA imparting and NEA imparting are oxygen termination and hydrogen termination respectively. Various metals also have resulted in PEA and NEA on the surface of diamond. PEA and NEA diamond surfaces have applications in various emerging fields such as quantum sensing, electrochemical applications (catalysis, etc.), thermionic emission, radiation conversion and detection, green energy generation, etc.

1.6. Application: Diamond in Thermionic Energy Converter (TEC) devices

Materials with enhanced thermal stability, low work function (WF) (i.e. low barrier to electron emission), less degradation at elevated temperatures, etc. are an ideal candidate for TEC devices. In thermionic emission, the thermal energy provides the electrons in the emitter with the energy to overcome the WF of the emitter. The electrons are emitted by the emitter and then collected by a cathode through a small gap while creating a self-bias which drives a load (figure 1.5a). A TEC device normally operates under the vacuum condition in order to increase the mean free path of the electrons between the electrodes which otherwise would affect the current negatively. Vacuum also ensures that the thermal conductance between the electrodes is negligible.

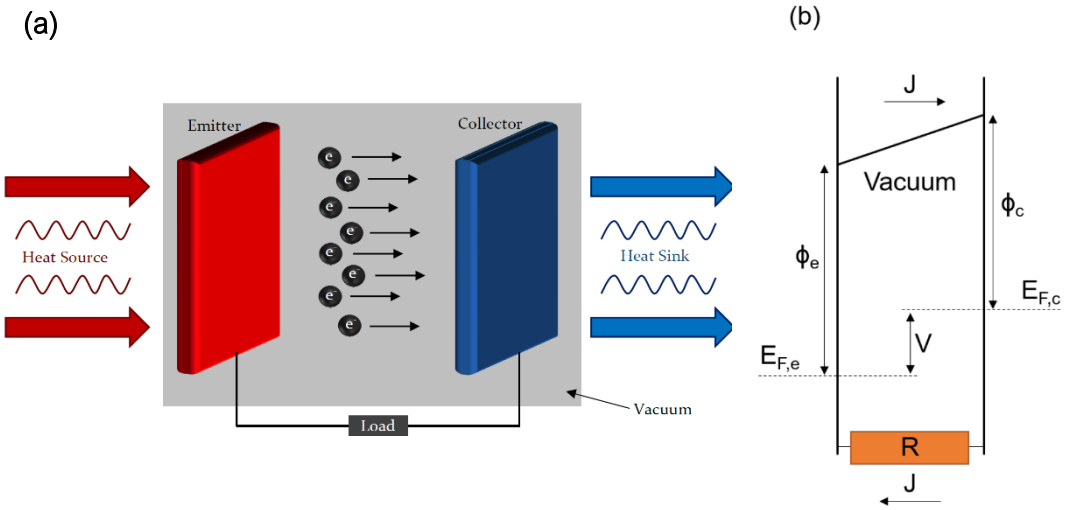

Figure 1.5: A TEC device which shows an emitter and collector electrode connected through a load. The heat source and heat sinks are also shown for convenience in understanding the process. Reproduced from [36]*; The basic workings principle of a TEC, where the heat energy can be supplied through various means to the emitter/cathode, emitting electrons to drive a load. (b) An energy diagram of a basic TEC in operation, where J is the current, V is the contact potential, - is the WF, and EF is the Fermi level. Reproduced with modification from* [3]*.*

As shown in the figure 1.5b, the emitted electrons raise the Fermi level of the collector which leads to the increase in the contact potential difference between the electrodes, hence driving the current through the load or external circuit [37]. The operating potential (V) in this device depends on the external load or resistance in order that the current flowing between the electrodes is equal to the current flowing through the load. The emitter WF needs to be low enough to emit the electrons at lower energies (red heat) while the collector WF needs to be further lower in order to accept the electrons that

might have lost some amount of energy while travelling between the electrodes and also so that the reverse current or back flow of electrons is reduced [38]. The most important factor to determine the proper and efficient functioning of the TEC device is keeping a small gap between the electrodes to reduce V between the electrodes which otherwise would increase the barrier height for the electrons at the collector side (preventing the electrons from being collected if V increases) [39]. Another advantage of small gap between the emitter and the collector electrode is the mitigation of space charge region which occurs due to the increased concentration of low energy electrons in the vacuum gap between the emitter and the collector electrode. But if the gap is made too small, it may be difficult to maintain the temperature difference between the hot and cold side. The point being that the optimum separation may be material dependent, a larger gap of hundreds of microns is easier to engineer.

The physics behind the thermionic emission is described by the famous Richardson Dushman equation (also known as the Richardson or Richardson-Laue-Dushman equation) [40] which is;

$$J = AT^2 \exp(-\varphi / k_B T) \quad \text{.....(1.1)}$$

Here A is the Richardson constant (also called as the emission constant) of the material, φ is the emitter material WF and k_B is the Boltzman constant. From this equation it is evident that in order to achieve thermionic emission at a lower temperature material with lower WF are needed, due to the exponential nature of the term ($-\varphi/kBT$). In the past TECs had been used for certain space programs with operating temperatures in excess of 1500 °C [41]. The research in TECs had been eclipsed by the advances in other alternative technologies such as photovoltaics and thermoelectric. However, recent advances in wide band gap material such as diamond have shown that a significant amount of thermionic emission can be achieved from the diamond as an emitter material in a TEC device, at a low temperature of 600 °C which has renewed the interest in TECs [42–47]. This feat has been attributed to the lowering of WF of diamond due to doping and surface termination using various elements such as H, Li, Cs, etc.

These devices have many advantages over other power generating devices some of which are their simple design, compact size, lack of moving parts, and high theoretical efficiency. The thermal energy could be provided by a wide spectrum of sources for example solar energy, nuclear energy, burning fuel, or waste heat from many other sources like human

body and car and industrial exhausts. Hence a wide scope for this type of utilisation or devices is possible.

1.7. Thesis outline

The theoretical and experimental investigation in this thesis are intended to study tin and tin monoxide (SnO) along with its heterostructure with lithium oxide as a stable and efficient surface dopant or termination of diamond for producing enhanced materials for electron emission in thermionic energy convertor devices.

Chapter 2 discusses the overall literature survey around the topic. It builds the case for tin based surface terminations of diamond.

Chapter 3 discusses various theoretical techniques for studying such terminations and also discusses experimental techniques for the deposition and characterisation of tin based terminations on diamond.

Chapter 4 discusses the theoretical results on tin and tin oxide based termination of diamond using density functional theory (DFT) performed on Cambridge Serial Total Energy Package (CASTEP) program, establishing the potential of tin as a NEA imparting, WF lowering and stable termination of diamond.

Chapter 5 discusses the initial results shedding light on the behaviour of lithium on the surface of oxygen terminated diamond at elevated temperatures. These form important part in studying the tin and lithium oxide based heterostructure of diamond.

Chapter 6 discusses the experimental results on tin oxide and tin/lithium oxide based heterostructure termination of diamond (100) evidencing the early theoretical results and also establishing the possibility of forming an more efficient heterostructure based termination on diamond.

Chapter 7 concludes the main and important outcomes of the thesis along with identifying the problems associated with this research area, hence, laying a foundation for the future investigation into this research area.

Chapter 2

Background

Summary

This chapter describes the background, current state of the art and the importance of this piece of research. The novelty of the work has also been described. It has been discussed how tin could be a sustainable solution to the problems associated with the efficient and effective terminations of diamond surface for low work function applications. The 'novel' heterostructure termination based on alkali and heavy metal alloys on the surface of diamond and their potential properties have been discussed to lay a stress on this type of study. Most of the material has been taken from the papers:

1. S. Ullah, *L. Cullingford, T. Zhang, J.R. Wong, G. Wan, M. Cattelan, N.A. Fox, "An investigation into the surface termination and near-surface bulk doping of oxygen-terminated diamond with lithium at various annealing temperatures", MRS Adv. (2021). pdf [doi: 10.1557/s43580-021-00060-x].*

This manuscript was written through contributions of all authors as mentioned below. All authors have given approval to the final version of the manuscript.

2. S. Ullah, *N.A. Fox, "Modification of the Surface Structure and Electronic Properties of Diamond (100) with Tin as a Surface Termination: A Density Functional Theory Study", J. Phys. Chem. C 125 (2021) 25165.*

This manuscript was written through contributions of all authors as mentioned below. All authors have given approval to the final version of the manuscript.

3. S. Ullah, *G. Wan, C. Kouzios, C. Woodgate, M. Cattelan, N.A. Fox, "Structure and electronic properties of Tin monoxide (SnO) and lithiated SnO terminated diamond (100) and its comparison with lithium oxide terminated diamond", Appl. Surf. Sci. 559 (2021) 149962.*

This manuscript was written through contributions of all authors as mentioned below. All authors have given approval to the final version of the manuscript.

Sami Ullah*: Investigation, Methodology, Conceptualization, Software, Visualization, Writing - original draft.* ***L. Cullingford:*** *Investigation, Validation.* ***T. Zhang:*** *Investigation, Validation.* ***J.R. Wong:*** *Investigation, Validation.* ***Gary Wan****: Validation, Resources, Writing - review & editing.* ***Christos Kouzios****: Investigation, Writing - review & editing.* ***Cameron Woodgate****: Investigation, Validation.* ***Mattia Cattelan****: Conceptualization, Resources, Data curation, Writing - review & editing.* ***Neil Fox****: Writing - review & editing, Supervision, Funding acquisition.*

2.1 Literature Survey

The 21st century has seen a huge demand placed on energy sources to provide for daily consumption which cannot currently be fulfilled by renewable sources forcing a reliance upon fossil fuel alternatives. One way of mitigating the burden on limited renewable sources of energy is to produce materials with low WF. Using these materials in energy harvesting technologies that produce electrical power from heat would allow such systems to be efficient enough to be integrated into concentrated solar thermal power generation plants to help deliver more generating capacity at lower cost electricity. One such technology is the Thermionic Energy Converter (TEC) that uses the temperature and WF differences between a heated and cooled electrode pair configured in a vacuum enclosure, to generate a DC high current, low voltage output [35, 48]. Synthetic diamond is an ideal electrode material due to its chemical stability and ability to engineer its surface electronic properties through functionalisation with elemental species [49, 50].

Tuning of the electrical properties of diamond by controlled surface doping of elements like oxygen, nitrogen, lithium, sodium or boron [51, 52] has multiplied the interest in diamond technology research for novel applications including, thermionic emission, catalysis, quantum sensing, etc. [35, 53]. A key goal for diamond-based TEC devices would be the demonstration of low temperature, high current thermionic emission. This should be possible by engineering certain diamond surfaces to exhibit NEA which promotes enhanced surface electron emission [46, 54–57]. NEA exists when the vacuum level lies below the conduction level in a semiconductor material, hence a negligible energy barrier to electron emission. The existence of NEA on the surface of diamond has been attributed to the formation of a surface dipole between surface carbon atoms and the terminating species [57]. The terminating species need to be a more electropositive atom or a group relative to the surface C atoms because of which the electron density shifts towards more electronegative C atoms and hence NEA. Achieving NEA in narrow band gap semiconductors is difficult but in wide band gap semiconductors, such as diamond, due to the natural proximity of the vacuum energy level to the CBM, any suitable surface termination changes the surface dipole in such a way that the CB lies above the vacuum level. The existence of true NEA, where CBM at the surface is higher than the local vacuum level, $E_{vac,}$ is crucial for achieving significantly higher electron yield, which is desirable in applications like current amplifiers, vacuum electronics, thermionic converters, and even new forms of photo- chemistry [58]. True NEA can be differentiated from the effective NEA as in the latter case the CBM at the surface is very close to the

vacuum level which qualifies it for the positive electron affinity (PEA), however, due to sufficient downward band bending towards the surface deep in the bulk of the material, the CBM is above the vacuum level. This encourages the tunnelling of electrons from the CBM into the vacuum region without encountering a barrier if the space charge region is narrow enough [59].

Also, the induction of NEA leads to the reduction in the ionisation energy, a feature which is very critical for surface transfer doping application used in many diamond based electronic devices. Moreover, diamond has also been explored as an important material in a quantum sensing application due to the discovery of various elemental vacancy centres in it. Nitrogen and silicon vacancy centres with negative charge (as NV^- and SiV^-) have been explored in detail in different types of diamond material e.g., nano diamonds etc. as candidates of interest for such applications. NEA would neutralise the negative charged NV^- and SiV^- species, hence giving rise to the need of having a positive electron affinity diamond surface (PEA) which can preserve the charge state of vacancies in the diamond [53].

Various atoms or groups have been investigated as a potential PEA and NEA terminating species to the diamond surfaces with various orientations. The most common PEA and NEA imparting atoms that have been researched widely are oxygen (O) and hydrogen (H), respectively [60-61]. O terminated diamond (OTD) surfaces have been researched widely as a PEA imparting surface termination [57]. Many processes with diamond as simple as acid washing results in the O surface termination of diamond [62]. Experimentally O has been seen to occupy a mix of both the ether and the ketone (carbonyl) position. Theoretically ether terminated diamond has been found to be the most stable form of OTD as has been found in this work as well. OTD has been seen to possess a PEA of up to 2.7 eV and 3.8 eV with large adsorption energies per atom in case of ether and ketone terminations, respectively [61, 63-64]. Experimentally, the PEA value of 0.89 eV per atom for oxygen terminated diamond has been reported [5]. This has resulted in O being studied as potential candidate in quantum sensing and electrochemical applications along with other elements like boron [10, 65]. H termination of diamond has been found to possess an NEA of -1.96 eV theoretically and -1.3 eV experimentally [10, 66-67]. However, hydrogen has been seen to desorb at elevated temperatures greater than 700 °C which makes it challenging to use in a diamond TEC device that needs to be designed to withstand repeated cycling to temperatures that approach or exceed this temperature.

Many alternatives, involving a monolayer or sub-monolayer coverage of some electropositive group I or II metals have been proposed [68-69], as well as first row transition metals (TMs) [70-71] on bare and oxygenated diamond surfaces. Transition metals like Cu, Ti, Ni and Co metals have been found theoretically to impart NEA to the diamond surface however their ability to do so depends upon the ease with which they form a carbide on the diamond surface and for which only Ti and V have been able to show higher NEA value than others [50-72]. Most of these metals, however, do not form a stable monovalent bond with carbon which was solved by using an oxygen terminated diamond (OTD) surface instead of a bare diamond surface. The key here being to induce stronger bonding between the metal layer and the underlying diamond surface and hence a large surface dipole. Alkali metals like Na, K and Li have been explored as potential terminations on diamond surfaces. Petrich and Bennedorf found a much higher sticking coefficient and hence a prospect of stronger bonding of K on oxygen terminated diamond than on hydrogen terminated diamond [73]. In other words metal oxygen and carbon oxygen bonds have been found to be stronger and more stable than metal carbon bonds [74-75]. James [76] has theoretically demonstrated Al termination of 1 ML on the surface of diamond with an adsorption energy (E_a) value of - 4.11 eV and NEA of - 1.47 eV. A larger value of adsorption energy (E_a), - 5.24 eV with an NEA of - 1.36 eV, was obtained with Al termination of 0.25 ML on the OTD. Cs-O terminated diamond surface has been found to possess a very low WF of ~1.5 eV but despite this it is highly unstable due to the loss of Cs above 400 °C [68]. As mentioned before, stable low WF surfaces in thermionic emission devices are required to work at higher temperatures. Kane M O'Donnell [77] was able to demonstrate air stable lithium (Li) -O terminated NEA diamond surface successfully with controlled atomic layer coverage and stability at 800 °C. However, in this work it is found that Li desorbs at 800 °C along with most of the oxygen from the diamond surface [5], which demands investigating methods to increase the stability of Li on the surface of diamond. One such method is to explore a suitable metallic termination on the diamond surfaces which can render Li adsorption on the surface of diamond more stable at higher temperatures and help in decreasing the WF further for thermionic emission. Moreover, Li is unstable in ambient environment and hence not suitable for device formation. Li atoms have been found to enter the near surface bulk of diamond at elevated temperatures and hence alter the bulk properties of diamond which affects the surface properties as well [4]. These issues demand an investigation into a

sustainable and stable metallic termination of diamond which could impart NEA to the diamond surface and lower WF along with being eco-friendly and inexpensive.

Recently, the formation of Si and Ge terminated diamond surfaces have also been investigated. Alex Schenk [78, 79] has demonstrated the Si terminated diamond (100) surface with a two domain 3×1 reconstruction. This has resulted in an NEA of - 0.86 ± 0.1 eV. However, Si terminated diamond is unsuitable for the ambient environment due to its high reactivity and any application in the atmospheric environment would need a protective SiO_2 coating on the top. A similar structure has been obtained with Ge terminated diamond with a maximum coverage of 0.63 ML which has resulted in an NEA of - 0.71 eV as shown by Michael J Sear [80]. A novel termination that we explore in this study is tin (Sn), an element in the same group as C, Si and Ge, that has largely been ignored as a potential candidate for the studies on metal and metal-oxide termination on the diamond surface. It is widely known that SnO is a capable and promising p-type semiconductor with an experimentally-measured, indirect bandgap of only 0.7 eV [81] and a direct energy gap that ranges from 2.5 to 3 eV [82], Sn is naturally abundant, non-toxic in nature and hence doesn't pose any immediate threat to the environment unlike other metals. A Sn vacancy has been found to be the main source of p-type property of SnO which can be altered by proper doping. On top of that Sn, alloyed with alkali metals (Li, Na, etc.) in a specific stoichiometric ratio has been found to possess ultra-low WF in bulk form, for example, bulk Sn_2Li_5 has been found to possess a WF of 1.25 eV [83]. Investigation like this at thin film level on the surface of diamond with an intention to develop ultra-low WF surface for energy application would open a new chapter into the diamond-based surface science and technology and would potentially bring a remarkable achievement in this area, which is one of the motivations behind this thesis.

Also, Oxide-based 2D materials have been found to be dynamically stable and less susceptible to degradation in air [84-85]. Li intercalation into tin oxide (SnO_x) as an active electrode material for metal ion batteries has been widely studied in theory and experiment [86-87]. It has been found that lithiation of pristine SnO layers results in the formation of stable layered Li_xO structure. The expelled Sn atoms form atomic planes to separate the Li_xO layers [88]. The formation of such stable structures on the surface of diamond and the interaction of SnO_x with the diamond surface carbon atoms is an interesting area to investigate with the goal being to demonstrate a highly stable and temperature resistant, NEA imparting termination on the surface of diamond.

Chapter 3

Materials, Equipment and Methods

Summary

This chapter introduces the basic techniques and equipment (facilities) used to conduct the research presented in this thesis. The computational techniques using CASTEP program on the University of Bristol's supercomputer Blue Crystal 4, have been described in detail. The experimental techniques including deposition methods, characterisation tools are also detailed. The advanced spectroscopic techniques on a high end platform such as NanoESCA at the University of Bristol, UK, along with the experimental thermionic test equipment used to evaluate functionalised diamond are described. Some of the material has been taken from the papers:

1. S. Ullah, *L. Cullingford, T. Zhang, J.R. Wong, G. Wan, M. Cattelan, N.A. Fox, "An investigation into the surface termination and near-surface bulk doping of oxygen-terminated diamond with lithium at various annealing temperatures", MRS Adv. (2021). pdf [doi: 10.1557/s43580-021-00060-x].*

This manuscript was written through contributions of all authors as mentioned below. All authors have given approval to the final version of the manuscript.

2. S. Ullah, *N.A. Fox, "Modification of the Surface Structure and Electronic Properties of Diamond (100) with Tin as a Surface Termination: A Density Functional Theory Study", J. Phys. Chem. C 125 (2021) 25165.*

This manuscript was written through contributions of all authors as mentioned below. All authors have given approval to the final version of the manuscript.

3. S. Ullah, *G. Wan, C. Kouzios, C. Woodgate, M. Cattelan, N.A. Fox, "Structure and electronic properties of Tin monoxide (SnO) and lithiated SnO terminated diamond (100) and its comparison with lithium oxide terminated diamond", Appl. Surf. Sci. 559 (2021) 149962.*

This manuscript was written through contributions of all authors as mentioned below. All authors have given approval to the final version of the manuscript.

Sami Ullah*: Investigation, Methodology, Conceptualization, Software, Visualization, Writing - original draft.* ***L. Cullingford:*** *Investigation, Validation.* ***T. Zhang:*** *Investigation, Validation.* ***J.R. Wong:*** *Investigation, Validation.* ***Gary Wan****: Validation, Resources, Writing - review & editing.* ***Christos Kouzios****: Investigation, Writing - review & editing.* ***Cameron Woodgate****: Investigation, Validation.* ***Mattia Cattelan****: Conceptualization, Resources, Data curation, Writing - review & editing.* ***Neil Fox****: Writing - review & editing, Supervision, Funding acquisition.*

3.1 Introduction

Various theoretical and experimental methods were employed in this study which will be described here. The computational method employed to investigate the diamond surface termination was density functional theory (DFT) performed using Cambridge Serial Total Energy Package (CASTEP) program [89]. The practical experiments first required sample diamond substrates to be cleaned, oxygen terminated, and subsequently exposed under Ultra High Vacuum (UVH) to metal depositions with sub-monolayer thicknesses to generate a functionalised diamond surface. The prepared surfaces were characterised using Spectro microscopic techniques using a Scienta Omicron Nano-ESCA II platform. Further material characterisation was carried out using multi-wavelength Raman Spectroscopy (Renishaw 2000). Measurements of the electron emission properties of the functionalised diamond at elevated temperatures was performed using a home-built laser-heated vacuum test rig. This chapter will describe each piece of equipment in detail and shed light on the process of material deposition and characterisation using such equipment.

3.1.1 Computational modelling using DFT

The modelling of diamond surface was done using CASTEP program [89-90] on Blue Crystal 4 super computer of the University of Bristol, UK. Theoretical modelling is performed with an intention to easily characterise a material which is difficult to produce experimentally and to supplement experimental data for advanced understanding. So, the idea is to perform first principle (ab initio) electronic structure calculations using the physical constraints such as the position of nuclei and the number of electrons. The outcome of any theoretical investigation is usually in the form of physical structure (such as atomic structure, bond lengths, strengths, etc.) or electronic structure (such as band structure, WF, etc.) which is crucial to understand the material properties and behaviours [9]. DFT is designed to perform the energy minimisation to calculate the ground state

energy within a material, where the ground state can be found by converging the calculations through iterative steps to establish the lowest energy of the material system. A well converged calculation is defined as one in which the solution derived numerically can be considered as an accurate approximation of the true solution of the mathematical problem posed by DFT with a specific exchange – correlation functional to correct the kinetic and potential energy by summing up all the quantum mechanical interaction effects on the system.

3.1.2 Density functional theory (DFT)

A physical system is usually a combination of electrons and nuclei, and any investigation demands studying the interaction among these electrons and nuclei belonging to various elements/molecules. Generally, Schrodinger's equation is used to quantify the energy of the physical system which requires various types of approximations and simplifications to be made to reduce the time needed to perform the calculations. The Schrodinger equation consists of various terms and can be written as;

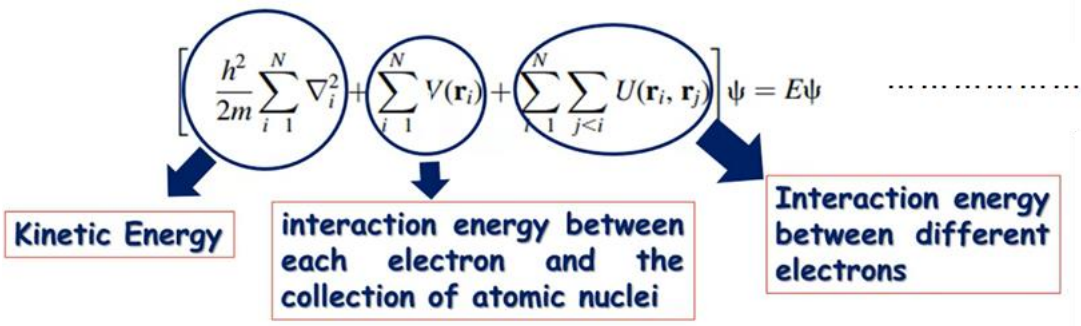

(3.1)

So, the total energy is an outcome of the sum of the totality of the kinetic energy of the particle and the different interactions such as nuclear - nuclear, electron - nuclear, and electron - electron coulombic interactions which form part of all the quantum mechanically non interacting effects. It also includes a factor of exchange and correlation functional (XC) which includes all the quantum mechanical interaction effects or the corrections to

the kinetic and potential energy. Since energy is a functional of electron density and XC functional is a part of energy, hence XC functional is dependent on electron density distribution. In order to exclude the nuclei-electron interactions and to simplify the electronic wavefunction calculation, the Born-Oppenheimer approximation [91] is used which assumes that the electronic motion and nuclear motion in molecules can be separated hence leading to a further assumption that the electronic wave function depends upon the nuclear positions but not upon their velocities as the nuclei are too heavy that they can be considered to be fixed. The core electrons are treated as fixed potentials, also referred to as pseudopotentials [92], due to the strong interaction of the core electrons and the nuclei which makes them behave independently in the chemical environment. This makes valence electrons the only potential candidates while solving the Schrodinger equations as the valence electrons would be the ones participating in any chemical interaction. The simplest form of exchange correlation interaction is Local Density Approximation (LDA) [93] in which the exchange correlation energy at each point in the system equals that of an uniform electron gas of the same density. LDA based calculations yield bond lengths and thus the geometries of molecules and solids typically with an astonishing accuracy of 1% [93]. The LDA was previously expected to be useful only for densities that are varying slowly however, practically LDA has been found to give extremely useful results for most applications. That being mentioned LDA is not suitable to calculate the energies and it drastically fails in situations where the density undergoes rapid changes such as in molecules. In order to be more accurate instead of homogeneous electron density, gradually changing density with space (the density gradient), called as Generalised Gradient Approximation (GGA) [94], was considered. In this case the XC functional depends upon both the electron density and the density gradient. GGA was used in the experiments reported in this thesis, as the exchange correlation potential for the system where a revised version of the Perdew-Burke-

Ernzerhof functional [94] was used. Some of the common disadvantages of DFT in general are:

a) DFT makes accurate predictions about the ground state properties however, the predictions made about the excited state properties are not similarly accurate.

b) Another very well-known inaccuracy with the GGA functional is the underestimation of calculated band gaps in semiconducting and insulating materials. In some situations, even larger than 1 eV error has become obtained.

c) DFT calculations cannot compensate for the inaccuracy caused by the weak Van der Waals (VdW) attractions that exist between atoms and molecules [95].

The CASTEP program uses a plane wave basis set with a defined maximum cut off energy to build the electron density. In order to approximate the electron density by sampling the K points over the Brillouin zone, a Monkhorst Pack (MP) grid [96] is used. For the calculation, Bloch's theorem demands forming an infinite crystal which is made possible by repeating a unit cell. The factors that determine the accuracy of the calculation are plane-wave energy cut-off, MP grid density and size of the unit cell, increasing these would cost the computational power and time.

In order to perform the actual calculations, a diamond slab is created (using software such as Vesta) from the sp^3 bonded C atoms, with a similar surface on each side of the slab. A wide and sufficient vacuum gap is made to exist between repeating slabs perpendicular to the slab surface. The slab thickness and the vacuum needs to be optimised before running the calculations.

CASTEP geometry optimisation output reveals information about the enthalpy, forces and bond positions for each iteration performed on a slab whose dimensions, lattice parameters and atomic positions along with symmetry operations are clearly indicated in

the input files. Mulliken bond populations [97] and charges are also outputted which help in determining the bonding structure between the species. One dimensional Electrostatic Potential (EP) can be generated with an in-built function "pot1d" which in our case outputted the electrostatic potentials, a combination of Hartree potential (Coulombic) and the local part of the pseudopotential, perpendicular to the surface of the diamond slab. Density Of States (DOS) calculations were performed using the OptaDOS code [98] with adaptive broadening method and a DOS spacing of 0.07 eV to sample the Brillion zone. All calculations were performed on the University of Bristol's Blue Crystal 4 supercomputer.

Adsorption Energy (E_a) Calculation

Adsorption energy [99] was calculated using equation;

$$\Upsilon = \frac{E_T - E_0 - \left(N_A \times E_{iso,A} + N_B \times E_{iso,B}\right)}{N_T} \quad \text{----------} \quad \textbf{(3.2)}$$

Where E_T is the energy of the diamond slab with adsorbates, E_0 is the energy of the bare diamond surface, N_A and N_B are the number of adsorbates A and B, $E_{iso,A}$ and $E_{iso,B}$ are the energy of A and B adsorbates and N_T is the total number of adsorbates. Negative sign of E_a indicates the exothermic reaction by convention.

Electron Affinity (EA) Calculations

Electron affinity (χ) is determined from the Ionisation energy (I) which is calculated using the method of Fall et. al. [99], as shown in equations;

$$\chi = I - E_g \quad \text{----------} \quad \textbf{(3.3)}$$

$$I = \left(V_{vac} - V_{av,slab}\right) - \left(V_{VBM,bulk} - V_{av,bulk}\right) \quad \text{----------} \quad \textbf{(3.4)}$$

where E_g is the experimental band gap (5.47 eV) used in this equation due to a well-known problem of underestimation of the band gap of diamond by gradient approximation (GGA) method. The energy difference between the vacuum potential and the average potential in the middle of the slab where the diamond is 'bulk-like' ($V_{vac} - V_{av,slab}$), is determined by performing the electrostatic potential calculation on the slab as shown in figure 3.1.

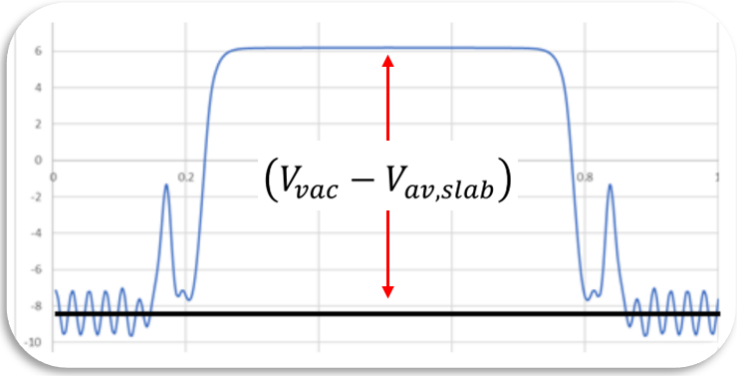

Figure 3.1: An example of the electrostatic potential graph of diamond taken perpendicular (in the z-direction) to the diamond slab.

The energy separation between the average electrostatic potential energy in the bulk and the bulk valence-band maximum is represented by $(V_{VBM,bulk} - V_{av,bulk})$. This is obtained by performing a band structure calculation on bulk diamond. By convention, the sign for the ionisation energy is positive. However, this difference has been calculated previously as 10.52 eV [100].

M. C. James et. al. [1] states "……DFT calculations are generally overestimating the magnitude of EAs compared with experimental measurements. Contributing factors for this discrepancy could be approximations in the DFT method, or the imperfect nature of experimental surfaces, such as an incomplete coverage of terminating species or a spatial variation in WF from a non-flat surface". Our main aim in this study would be to demonstrate the trend in the NEAs with different coverages and configurations of Sn on bare and OTD.

3.2 Methods

3.2.1 Diamond preparation

Diamond can be grown on certain suitable substrates such as molybdenum, silicon or even various types of diamond substrates itself, for example Single Crystal Diamond (SCD) and Poly Crystalline Diamond (PCD). The substrates need to be thermally stable at the growth temperatures and possess a thermal expansion coefficient similar to diamond so that the (diamond) thin films do not delaminate after the growth.

In order to proceed with the diamond growth, the non-diamond substrates (molybdenum and silicon) are initially seeded with nanodiamonds by submerging the clean substrates in a 25 % carboxyethylsilanetriol di-sodium salt solution in water (Fluorochem, 17191-40-7) for 5 minutes ensuring a full coverage, for growth uniformity [101]. Later the substrate is removed, and the excess solution is removed by rinsing in Milli-Q water thoroughly, leaving only a single layer of coverage which is then dried using compressed air. The dried substrate is then submerged into a suspension containing nanodiamonds (~6 nm) which are electrostatically attracted to the salt on the substrate. These nanodiamonds cover the surface of the substrate which is then removed, rinsed in water and dried. Diamond can also be grown on diamond substrates homoepitaxially in which a choice can be made from SCD or PCDs of various dimensions, for example in this work, undoped SCDs of dimension 3 mm × 3 mm × 0.25 mm were used. Before starting the actual growth, these diamond substrates are cleaned to remove any residual metallic particles resulting from the mechanical polishing, using a solution of aqua regia, prepared by addition of 2.5 mL HNO_3 (69%) to 7.5 mL HCl (37%) or a fuming mixture of H_2SO_4 and HNO_3 for a few hours (< 4 hours) [62, 57]. The substrates are then removed and rinsed with de-ionised water and isopropanol. A point worth mentioning here is that the acid cleaning results into oxygen termination of diamond surface and hence is considered

as an efficient and easy way to functionalise diamond with oxygen [1]. The substrates (both non- diamond and diamond) are then installed into various types of deposition chambers in CVD systems for diamond growth, cleaning and surface termination as well. The two most common CVD methods used generally in this research area and specifically for this work were hot filament CVD (HF CVD) and micro-wave CVD (MWCVD) as described in the next section.

3.2.2 CVD systems

The growth of synthetic diamond thin films for use in this research work was carried out using two different types of growth reactor, a hot filament CVD system for boron-doped diamond growth and a microwave plasma-assisted CVD reactor for intrinsic and nitrogen-doped diamond growth.

Hot filament CVD

A typical hot filament CVD system is shown in figure 3.2 and consists of a reaction chamber connected to a set of vacuum pumps to control the gas environment along with gas inlets, connected through gas mass flow controllers, and outlets, ensuring gas supply and exhaust. A demountable heating stage consists of a molybdenum substrate holder located 4 mm beneath three 0.25 mm diameter tantalum wires (filaments) that are spring loaded to stay taut. For boron doped diamond (BDD) layer growth, HPHT boron doped single crystal diamond (purchased from Element Six (145-500-0248 and MM 111/4010) substrate is placed in a central position on the sample stage and Ta wires are tightly connected. The heating stage is carefully lowered into the chamber which is then pumped down to 90 mTorr pressure. The sample stage is heated to a temperature of 120 °C for 30 minutes for de-gassing the adsorbates by passing a 4A current from an external power supply through the wires.

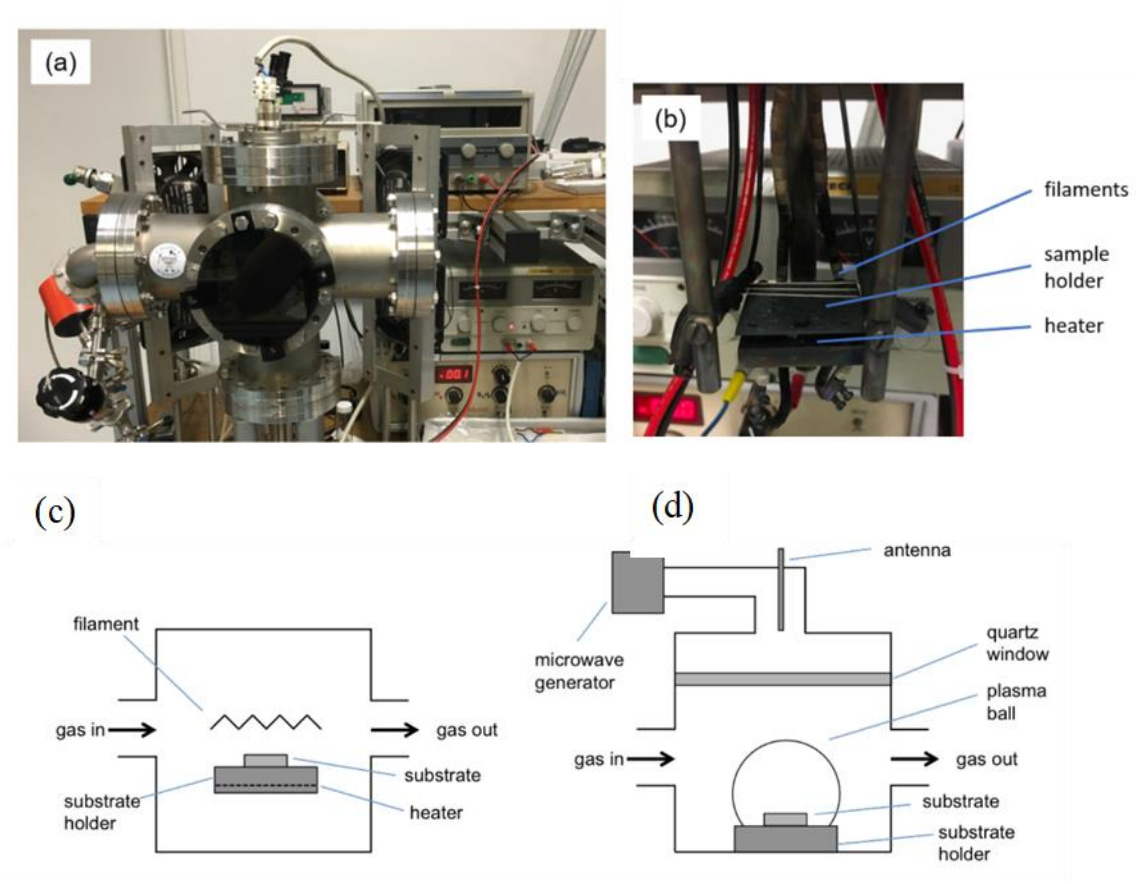

Figure 3.2: (a) One of the hot filaments (HF) CVD reactors. (b) The interior setup of the reactor. Adopted from [1] *(c) Schematic showing the process gases being dissociated with a heated filament in Hot filament CVD (d) Schematic showing a linear antenna-style microwave plasma CVD with an antenna that tunes the microwave radiations to form a plasma above the substrate. Adapted from May* [2]

Boron doped layer is grown using a gas mixture comprising H_2, CH_4 (both Air Liquide, Ltd) at a flow rate of 200 and 2 standard cubic centimetres per minute (sccm), respectively, i.e., 1% CH_4 in H_2, and 5% B_2H_6 in H_2 (BOC Group, plc) with a flow rate of 0.1 sccm for epitaxial B-doped layers on single crystal diamond. The Ta filament wires are supplied with a 25 A current at a voltage of ~ 9 V at which these wires get carburised by reacting with CH_4 and hence become brittle and unsuitable beyond one use. With carburisation, the voltage slightly increases to ~11 V as the resistance increases. The treatment is carried out for 60 minutes at a pressure of 20 Torr and a temperature of ~2300 K which enables a deposition of a good quality diamond thin film at a growth

rate of ~0.5 μm h^{-1}. BDD overlayers grown in the same reactor under the same conditions have previously been shown to contain a boron concentration of up to ~10^{20} cm^{-3}, measured from a depth profile using secondary ion mass spectroscopy [102].

Micro-wave CVD

Diamond can also be grown in microwave plasma enhanced CVD reactor (Applied Science and Technology (ASTeX)-type) with a vacuum chamber in which the gas is fed through mass flow controllers (MFC) and while the exhaust ports at the bottom are connected to a vacuum pump through an electrically controlled valve as shown in figure 3.3.

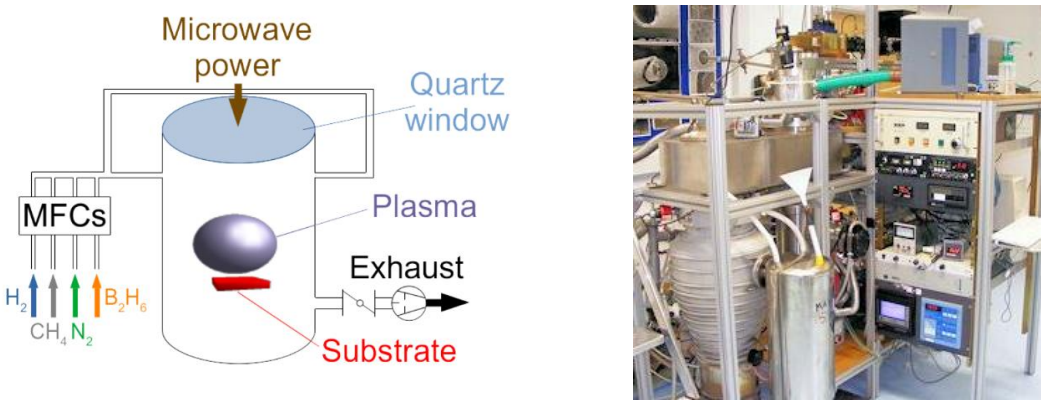

Figure 3.3: A sketch and a photograph of the microwave plasma enhanced CVD reactor. It shows the process of plasma generation from the reactant gases above the substrate for CVD of diamond. Adopted from [3]

A magnetron generates microwaves of 1500 W power which are transmitted by an antenna above the chamber. These microwaves travel through a quartz window into the chamber. The thermal energy/heat and the radicals needed for the diamond growth are provided by the plasma directly above the substrate. the combined effect of microwave power and the chamber pressure control the substrate temperature which can be monitored using single colour (λ = 2.2 μm) optical pyrometer (Thermalert SX, Raytex). The substrate is placed inside the chamber on a tungsten disc which is separated from the floor of the chamber using a molybdenum ring. This ring enables the thermal contact

of the substrate with the water-cooled base plate to be adjusted to achieve the desired growth temperature at the substrate surface facing the microwave plasma.

Typical diamond growth conditions include a substrate temperature of 850-900 °C, a chamber pressure of 130 Torr for a period of 15 min along with a gas mixture 4 % CH_4 diluted in H_2 for undoped diamond growth, with an additional 4 ppm of B_2H_6 for boron doping. However, we have used microwave CVD to clean the diamond surface along with hydrogen termination using a pure hydrogen plasma. The whole process involves a cleaning step of 2 min at 900 °C (~ 1200 W, ~ 85 Torr) followed by another 2 minutes of exposure at 500 °C (~ 700 W, ~ 35 Torr). After this the substrate is let cool down for another 2 minutes at RT under hydrogen gas exposure without plasma. This method has resulted into stable H termination and better coverage than other methods such as by using DC sputter coater etc.

3.2.3 Surface terminations

The functionalisation of diamond is a central topic of this thesis involving the generation and study of PEA and NEA on the diamond surface. The output of this work is applicable to the improved operation and performance of radiation conversion devices (diamond voltaic), diamond electrodes for photothermal electrocatalysis, quantum sensing (as PEA surfaces help in retaining the negative charge state of the nitrogen vacancies (NV^-) and silicon vacancies (SiV^-) while NEA nanodiamond surfaces covert these to neutral state[103]). Surface terminations of diamond were carried out as follows: Hydrogen is used to clean, and H terminate the diamond surface as described in the previous section. Diamond (100) surface was oxygen terminated using an ozone cracker. The sample sits on the tray with the workable surface facing upwards inside the cracker and the device runs for 30 minutes to render the surface oxygen terminated by UV-ozone treatment.

Another method is to oxygen terminate the diamond surface or supplement the oxygen termination at UHV conditions on NanoESCA facility by using the gas cracker.

Metal termination of diamond was carried out using physical vapor deposition (PVD) techniques such as E beam deposition and thermal evaporation for tin and lithium deposition, respectively which was done in a deposition chamber at a vacuum of ~10^{-9} mbar, mounted on the NanoESCA facility at the University of Bristol, UK.

3.3 NanoESCA Facility

Bristol Ultra-quiet NanoESCA Laboratory (BrUNEL) at the University of Bristol's Centre for Nanoscience and Quantum Information (NSQI) has a NanoESCA [104] facility sitting on a 28 tonne keel slab supported on pneumatic jacks as shown in figure 3.4 (a). The system consists of two ultra-high vacuum (UHV) chambers. One of these is configured with multi source X-ray photoelectron spectroscopy (XPS), Spot profile analysis- Low energy electron diffraction (SPA-LEED) and preparation tools including plasma etching and thermal annealing. A fast entry load lock is used to load samples into this UHV chamber for analysis. A second load lock allows a vacuum suitcase to be connected for sample transport under UHV. Additionally, this chamber is linked to the second chamber that is configured with a NanoESCA II analyser and VUV light sources. Samples that are transferred into the NanoESCA chamber are mounted on a five axis, sample manipulator that can be operated between 30K and 650K. A deposition chamber (pressure of ~10^{-9} mbar), where deposition of various metals and gas on the substrate surface is carried out, is connected to the vacuum suitcase port. These chambers each with different instruments attached are all interconnected under UHV enabling sample preparation and surface analysis with different tools to be performed under the same conditions, typically ~ 10^{-11} mbar (figure 3.4 (d)).

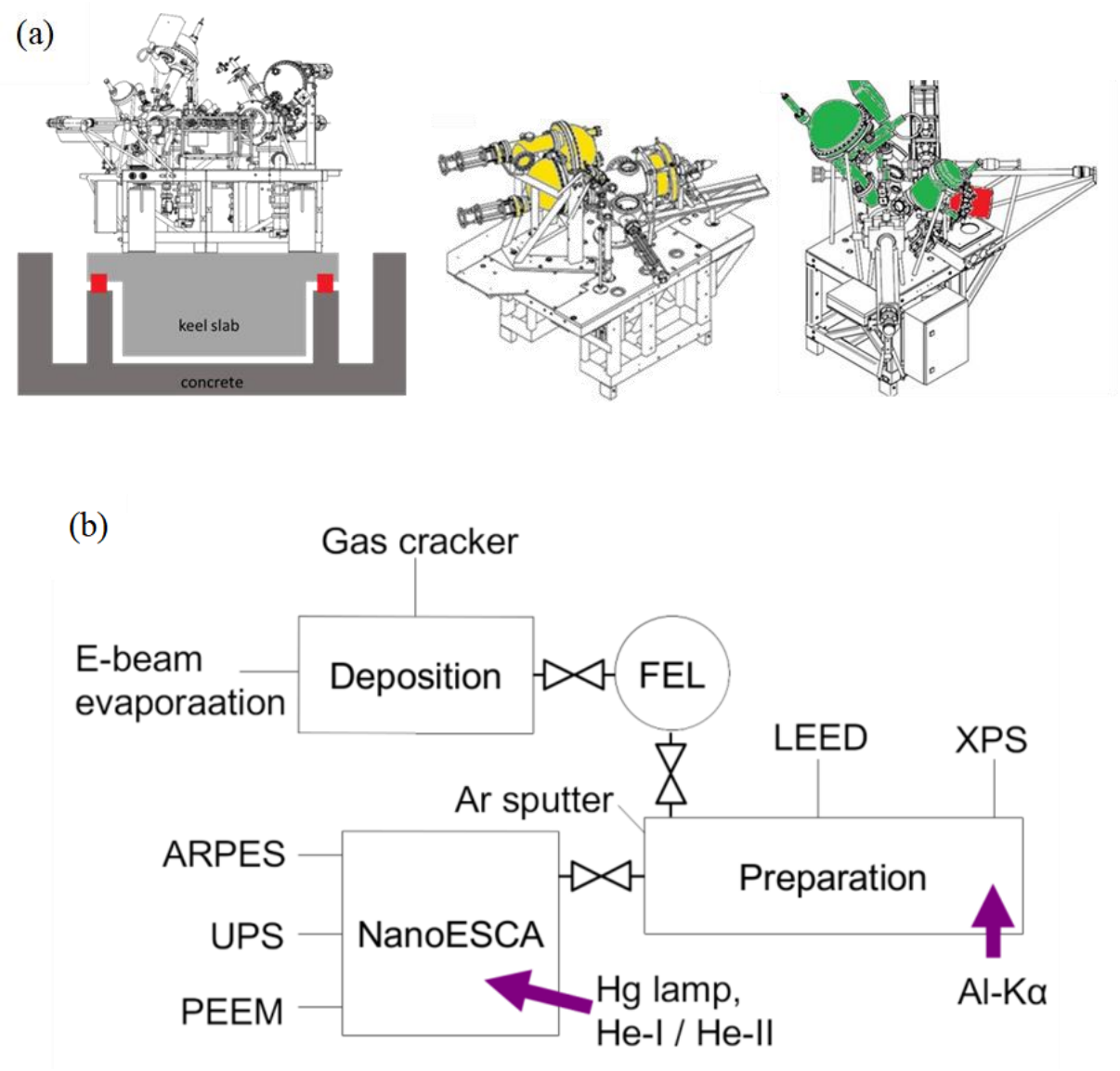

Figure 3.4: a) Shows the whole NanoESCA facility sitting on a 28-tonne keel slab supported on pneumatic jacks on concrete. b) Shows the preparation chamber or part of the facility while c) shows the NanoESCA or EF- PEEM side of the facility. d) Schematic shows the main parts of the NanoESCA facility in which a deposition chamber (pressure of ~ 10^{-9} mbar), a preparation chamber (pressure of ~ 10^{-11} mbar) and NanoESCA chamber (pressure of ~10^{-11} mbar) are shown to be connected through a fast entry load lock (FEL) (with a pressure of ~ 10^{-8} mbar) and various valves. Adopted from [3]

3.4 Deposition Techniques

The deposition of metals along with other sample preparation and modification processes are carried out in a deposition chamber at ultra-high vacuum (UHV) (figure 3.5). It consists of a wobble stick to bring the sample into the chamber from a FEL through mechanically controlled valves. A manipulator which is retractable and rotating acts like a joystick and

has a heating stage attached to the sample holder which can be made to face desired metal sources inside the chamber. A quartz microbalance is there to measure and optimise the thin film deposition of various metals while gas crackers, connected to external gas sources, are there to provide atomic gas exposure for surface modification. Physical vapour deposition (PVD) with e beam and thermal evaporation was carried out in this project to sub-monolayers of selected metals on the surface of diamond along with oxygen cracking to supplement the oxygen concentration on the surface of diamond (100).

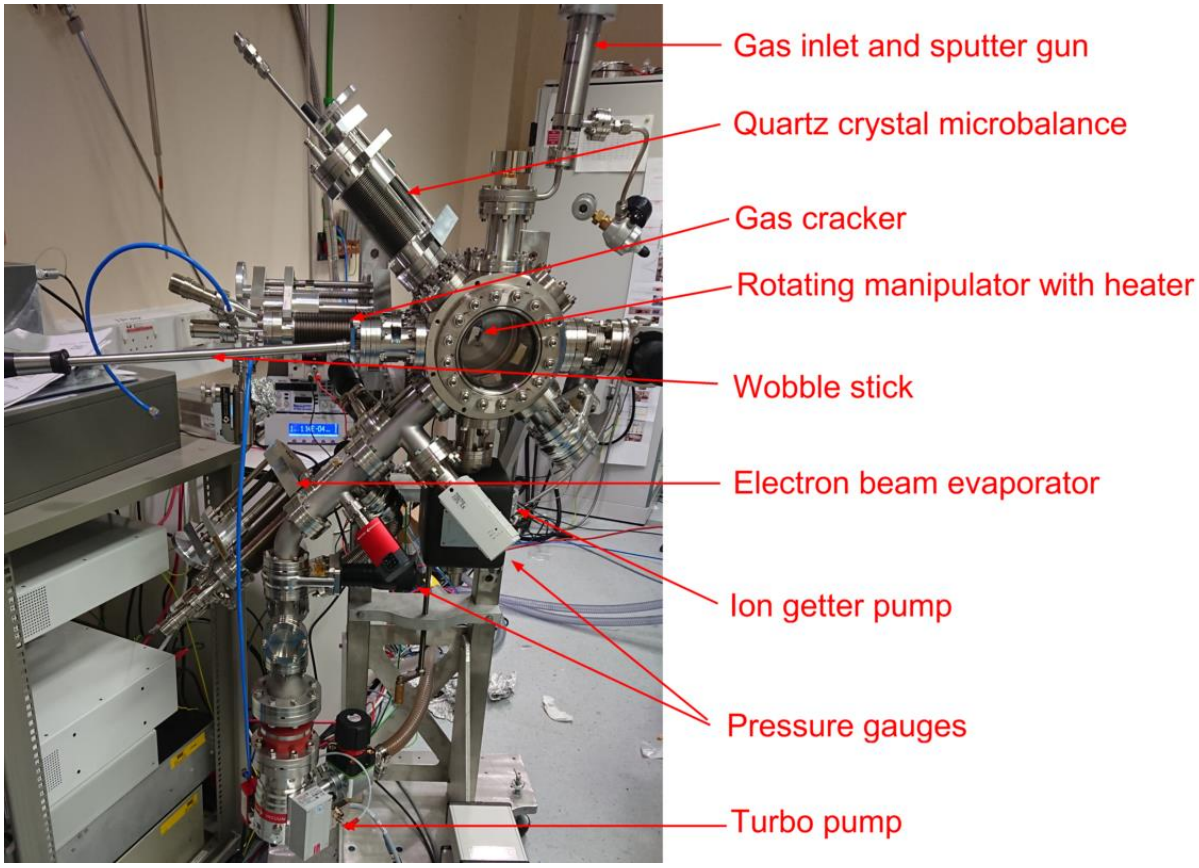

Figure 3.5: A labelled photo of the deposition chamber installed on the NanoESCA facility at the University of Bristol, UK. [3]

3.4.1 Physical vapour deposition (PVD)

This is a process in which a metal is vaporised from a condensed bulk phase using different techniques like electron beam or heat and later made to deposit on a substrate placed at a small distance from it into a condensed thin film phase. PVD techniques which have been used in our experiments are thermal evaporation using e-beam heating for tin deposition and direct current (ohmic) heating for lithium deposition. All PVD processes are carried out at high vacuum conditions (~10^{-9} mbar). The rate of deposition is measured and optimised using a Quartz microbalance with a precision of 1 Å thickness, placed in front of the crucibles/sources containing these metals. Later the microbalance is removed from the way and the substrate is brought in using a joy-stick type manipulator.

Lithium evaporation using thermal evaporation technique

In thermal evaporation by direct current or ohmic heating technique, the metal placed in a crucible is simply heated to the point when it starts vaporising after properly calibrating the current needed to bring about the point of vaporisation. The evolved metal vapour is directed to a substrate placed at 45° to the vertical axis of the crucible. Figure 3.6 demonstrates the configuration of the source and substrate used in our lab for the deposition of Li on the surface of diamond (100). The evaporator set-up is mounted on the NanoESCA facility and properly degassed before starting the actual deposition. The pressures are carefully maintained at high vacuum condition to eradicate the problems of contamination. The apparatus consisted of a boron nitride crucible, loaded into the evaporator compartment of the deposition chamber, wrapped in a tungsten coil with an integrated thermocouple and the whole configuration then sealed using a copper gasket as can be seen in figure 3.6.

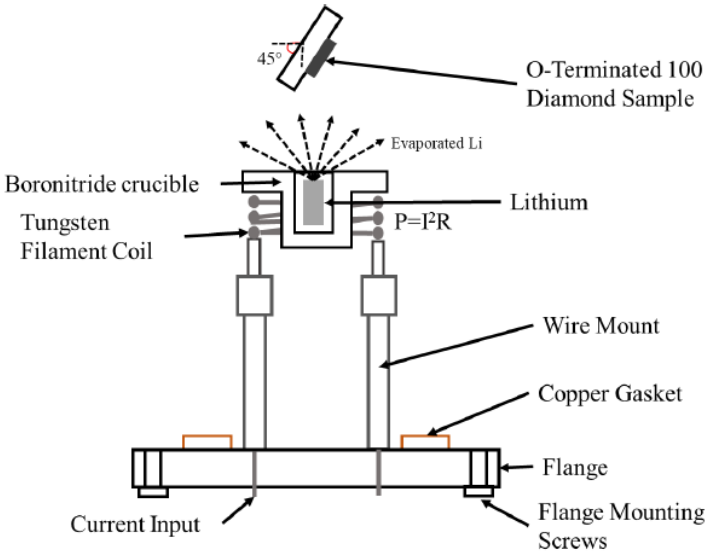

Figure 3.6: Schematic diagram showing the thermal evaporation set up for Li deposition with parts labelled. Base pressure is ~10^{-9} mbar.

The sample was held at 45° to the top of the evaporator before evaporating Li onto the diamond surface. After that 2.4 amps is passed through the tungsten filament (obtained from the calibration) taking the Li to 410°C where the evaporation takes place at a pressure below x10^{-6} mbar.

Tin deposition using e- beam technique

This technique uses high energy electron beam which is incident on a target material placed in a crucible as shown in figure 3.7. The e- beam vaporises the material which then starts depositing on a substrate placed facing it in the form of a thin film (figure 3.8 shows a schematic diagram showing the set up for E-beam deposition process.). An e-beam evaporator which is mounted at -45° to the horizontal contains different metal targets in four pockets. E beams are produced by heating a tungsten filament thermionically. The target is biased up to 2000 V relative to the filament and walls to accelerate the electrons towards it for heating.

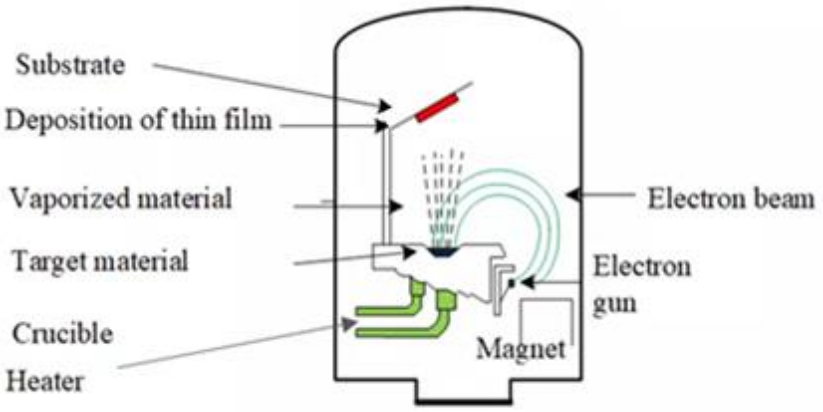

Figure 3.7: Schematic diagram demonstrating the E-beam technique for metal (Sn) deposition. The base pressure is around ~10^{-9} mbar. Adopted with modification from [105]

A molybdenum crucible is used to hold the evaporation target metal although these can be mounted as conductive rods mounted directly to the centre of the pocket. A quartz microbalance faces the pockets directly and was used to measure the evaporation rate of tin at a set value of current and voltage before depositing it on the surface of diamond.

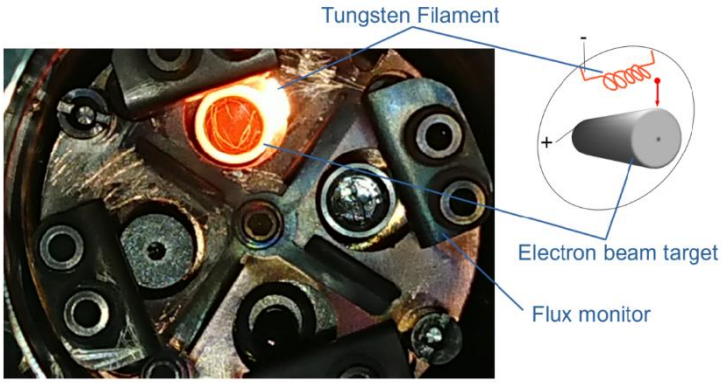

Figure 3.8: A picture of the e-beam evaporator showing four pockets containing different metals with a single pocket in use (orange) along with a labelled diagram for the components within a pocket. [3]

Tin granules were placed in a molybdenum crucible which was mounted on the evaporator and then installed into the deposition chamber. The crucible and the chamber were sufficiently degassed before starting the actual deposition. 0.8 ML of tin was deposited at a temperature of 327 °C on the surface of diamond, optimised using a

quartz crystal micro balance. Tin (Sn) metal deposition was performed using this method in the NanoESCA sample preparation chamber under UHV conditions (1.5×10^{-8} mbar)

Molecular oxygen dosing was performed at an oxygen pressure of ~1.5×10^{-6} mbar. Atomic oxygen dosing was performed by dosing O_2 through a gas cracker at 1.5×10^{-6} mbar.

3.5 XPS/SPA-LEED Chamber

This chamber consists of a manipulator with a heated stage attached to the sample holder module. The manipulator can be rotated and moved in and out of the chamber in a precisely controlled steps manually and by a motor, respectively. It also has an XPS system and a low energy electron diffraction (LEED) setup for characterisation. Moreover, an argon-based magnetron sputterer is also included for sample preparation.

3.6 Surface Characterization Techniques

Before explaining XPS and LEED in detail, the general concept of photoemission spectroscopy needs to be explained briefly.

3.6.1 Photo Emission spectroscopy:

Photoemission spectroscopy works on the principle of photoelectric effect where a sample is irradiated with energetic photons to expel electrons from the surface. These electrons when expelled can be collected by an analyser and yield a great deal of information about the nature of material being analysed. Figure 3.9 demonstrates the process of photoemission spectroscopy in which an electron (binding energy = E_b) expelled by impeding photon (Energy = $h\nu$) is collected by the analyser at a kinetic energy of E_k for further analysis.

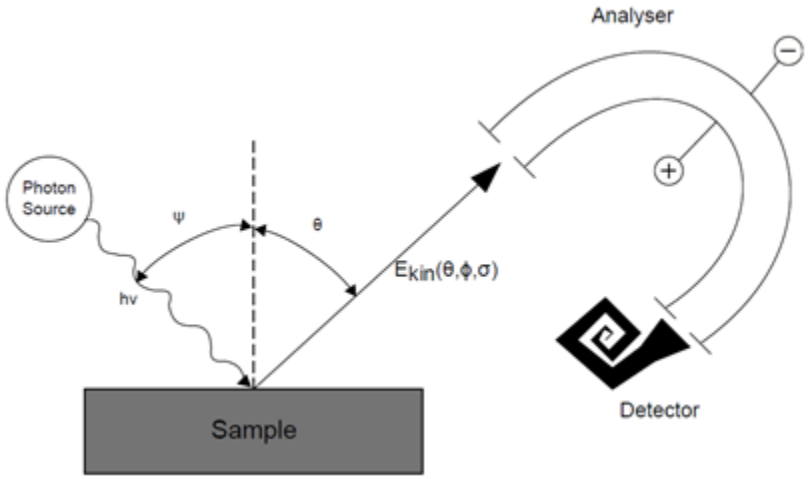

Figure 3.9: Schematic describing the general principle pertaining to the operation of a photoemission spectrometer. A photon source with energy hv (either X-ray or UV) emits light on a sample surface in an ultrahigh vacuum. The kinetic energy of the photoelectrons thus ejected is analysed by the electrostatic analyser. Adopted from [106]

The kinetic energy of the emitted electrons is recorded to produce the photoelectron spectrum by counting the ejected electron over a range of kinetic energies. Since each atom emits electrons of a characteristic energy, peaks appear in the spectrum. The peak shape, position and size can reveal a great deal of information about the species present on the surface of a material.

This kinetic energy (K.E.) is dependent upon the incident photon energy ($h\nu$) and the binding energy (B.E.) of the electron which can be defined as the energy required to expel the electron from the surface.

$$E_k = h\nu - E_b - \emptyset \qquad \text{..... (3.5)}$$

where Ø is the WF of the material, defined as the amount of energy required to bring the electron from within the material to the surface.

Photoemission processes are carried out in ultra-high vacuum (UHV) conditions to reduce the chances of ejected electrons interacting with gas molecules and losing energy. Photoemission spectroscopy can be used to study the core level electrons by using a monochromatic source of X rays with an energy of 1486.6 eV which gives information

about the chemical composition and bonding behaviour of the surface atoms. It can also be used to study the valence band electronic structure by irradiating the sample with vacuum ultraviolet beam of photons with an energy of 21.2 eV for He I or 40.8 eV for He II which excite and expel the valence band electrons from the surface of a material.

3.6.2 X-ray Photoelectron Spectroscopy (XPS)

The analysis of the surface chemistry of a material and determination of the surface composition, empirical formula, chemical and electronic state of the elements present is enabled by XPS within the 1-10 nm surface of the material. In this technique a monochromatic beam of X rays with an energy of 1486.6 eV is made to impede on the surface of the material which leads to the emission of photoelectrons which are then captured and sorted according to the energy by the analyser kept a meter away from the sample. Characteristic peaks for every element (except hydrogen and helium) are produced according to their binding energies in the material, with higher intensities corresponding to larger elemental concentration. The chemical structure of the material can be studied as shifts in the binding energy due to even a small change in the chemical environment of the sample. This technique is also known as Electron Spectroscopy for Chemical Analysis (ESCA).

With an incident monochromatic Al-Kα at +45° to the sample, a multi-channel ARGUS hemispherical analyser mounted at -45° from the vertical axis was used to collect the emitted electrons. The XPS data was analysed using CASA XPS software [107]. The stoichiometry between two elements was determined by finding the elemental ratios based on the background subtracted emission peak area of each element.

Angle Resolved XPS (ARXPS) was performed by tilting/rotating the manipulator, thereby varying the sample polar angle, between repeated measurements.

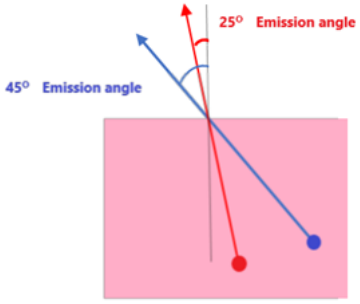

Figure 3.10: ARXPS showing XPS taken at less surface sensitive mode (LSS) i.e 25° and slightly more surface sensitive modes (MSS) i.e. at 45° to the normal of the sample. Adopted from [4]

ARXPS can be done in less surface sensitive mode (LSS) and slightly more surface sensitive modes (MSS) where the X rays have an emission angle of 25° and 45° (figure 3.10) to the normal of the sample surface and hence a great deal of information about the sample's near surface bulk and surface composition, respectively.

3.6.3 Spot Profile Area Low Energy Electron Diffraction (SPA-LEED)

Low-Energy electron diffraction (LEED) is a technique of surface structure determination of single-crystalline materials by bombardment, at an angle normal to the surface of the sample, with a collimated beam of low energy electrons (10-200 eV and 120 eV in our case) and observation of diffracted electrons as spots on a fluorescent screen as has been demonstrated in figure 3.11. This energy regime corresponds to the De Broglie wavelength of 1-4 Å which makes it possible for the very top atomic layers to participate in the diffraction. The vector difference between the incoming beam and the reflected beam represents the crystal surface's reciprocal lattice vector (if electron beam is kinematically reflected), which can lead us to the determination of the lattice type of the sample from the full 2D diffraction pattern.

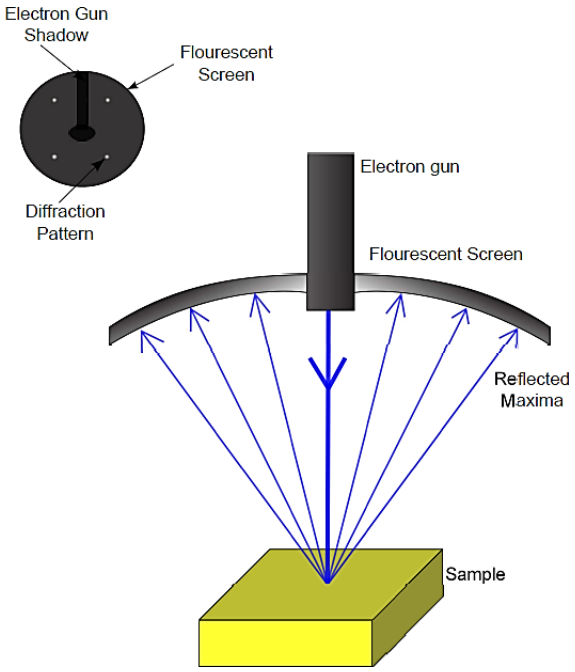

Figure 3.11: Schematic showing the basic working of a LEED set up where the low energy electrons from an electron gun are fired on a sample surface. The reflected beams are collected on a fluorescent screen which gives information about the crystal lattice structure of the sample" Adopted from [9]

LEED can also give us information about any surface reconstructions due to surface modification, where the reconstruction can be observed as a narrowing diffraction pattern in the corresponding axis. The surface roughness and impurities can be determined by the blur in the images while a sharper image represents a well-ordered crystal surface. A channeltron detector was used to detect the raster pattern of diffraction points through deflectors which allows for the Spot profile analysis- Low energy electron diffraction of the patterns to reveal the intensity ratios of the points or the reconstruction peaks along a path. SPA-LEED was used to investigate the surface roughness and reconstruction of the bare and Sn-O-C diamond 100 sample.

3.7 Energy Filtered Photoelectron Emission Microscopy (EF-PEEM)

NanoESCA or EF – PEEM works by acquiring a picture of the sample as a projection of the electron distribution onto a 2D image. In real space this is realised by mapping a

spatially resolved image of the sample while integrating over all emission angles in each point, while in momentum space it is obtained by mapping the momentum distribution of all electrons emitted from the sample while integrating over all sample area., These operations are usually performed at the low energy region of the photoemission due to high signal intensity and contrast of features for imaging. The projection is basically the emitted electrons, as described in the previous section, that have been accelerated into the microscope and passed through several electron lenses inside the microscope and the energy filter as described in a schematic figure 3.12. The data acquisition for photoemission microscopy in real space which is basically a map of the spatial resolved image and momentum space can be summarised in the following image and described later.

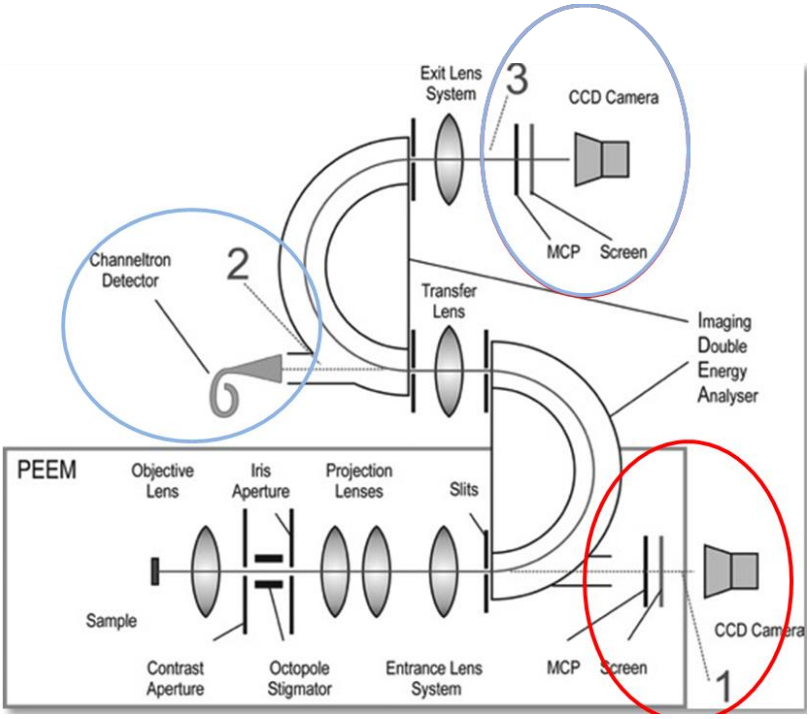

Figure 3.12: Showing various parts of PEEM / NanoESCA II with Spatial resolution in PEEM mode 13 nm. Spatial resolution in energy filtered mode 23 nm. Selected area spectroscopy Energy resolution at 29 K with Channeltron 30 meV. Energy resolution at 29 K in energy filtered mode 20 meV. Reproduced with modification from [108]

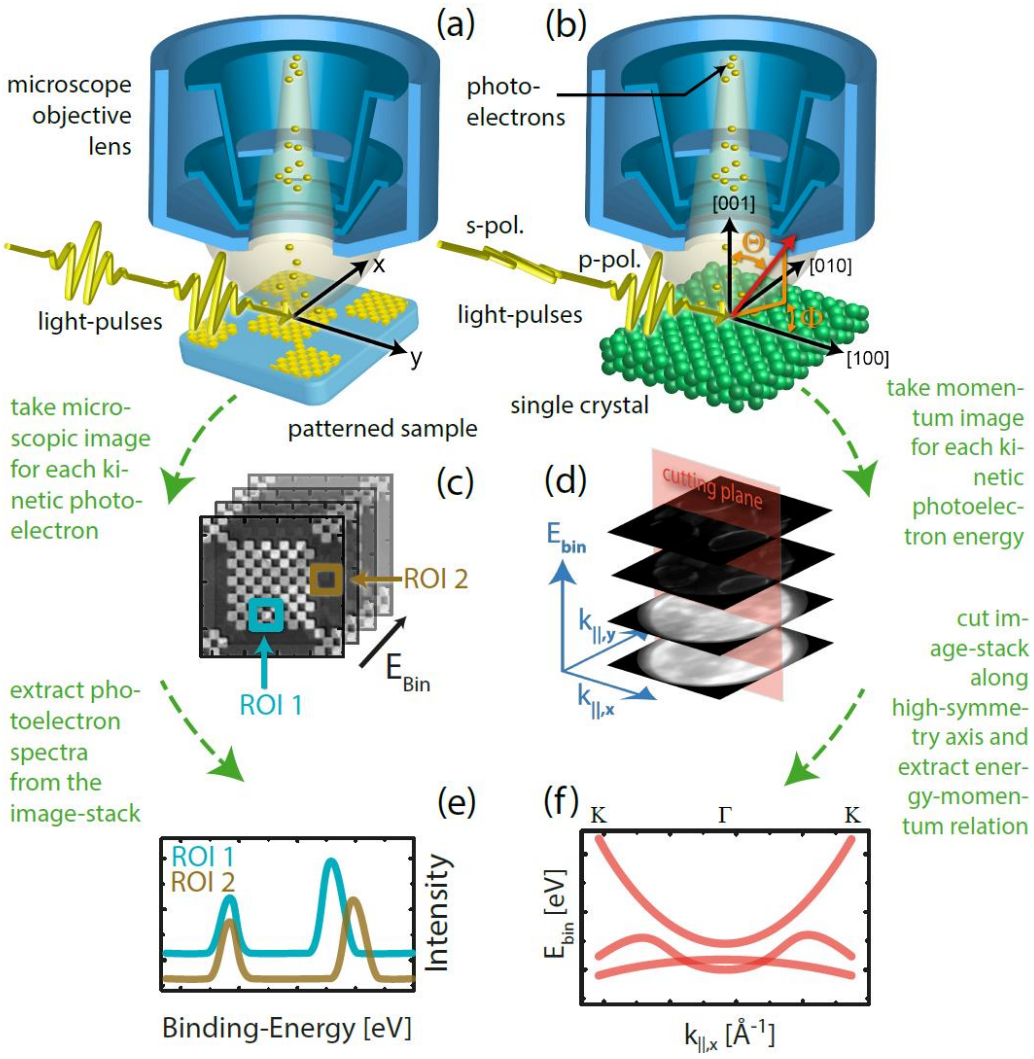

Figure 3.13.: "The scheme compares the two operation modes of energy-filtered photoemission microscopy and the process of data acquisition. In the real space mode (a) spatial resolved image spectra are acquired from a specimen (c). The chemical information can be evaluated for different sample positions (e). In momentum microscopy (b) the energy dispersion curve (f) is often of interest, which can be extracted from a stack of constant energy distributions (d)". Adopted from [104]

Momentum space microscopy is only possible for highly ordered periodic systems for example single crystal substrates, graphene, etc. as the integrated electron distribution of amorphous solids makes no sense due to the fact that the momentum maps from the amorphous solids differ so much inside the measured area.

As can be seen in figure 3.13, real space mode yields laterally resolved photoemission spectra (UPS) where each pixel is individual UPS spectrum, extracted from the lateral coordinates along the sample or regions of interest. These can be compared to reveal the chemical differences. Doing the scan over the low-energy cut-off region can therefore allow for WF determination at each point, this was done using Igor Pro script where pixel-by-pixel fitting was used to generate a WF map which involves finding the steepest gradient and extrapolating it to the background. While in momentum mode, cuts through the image spectrum perpendicular to the image plane reveal energy – momentum relations or band structures as described in later section.

These measurements are made using a double hemispherical energy analyser which offers energy resolved PEEM and in which the spherical aberrations introduced at the first hemispherical analyser are corrected at the second hemisphere. A bias applied to the sample selects the constant energy at which the analysers work.

The sample is inserted into the chamber at UHV ($\sim 10^{-11}$ mbar) using a wobble stick into the manipulator which can move in all the dimensions and rotate at all angles. The manipulator stage incorporates a heating stage and a liquid helium cryostat that can support sample temperatures from 30 K to 600 K. An extractor at a distance of 1.8 mm in front of the sample is biased at 12000 V. The entrance into the PEEM lens column consists of two integrated adjustable apertures. One of the apertures is at the Fourier plane which consists of a movable metal plate with different sized holes, thus set aperture sizes and its position along the plane can be selected, forming a contrast aperture which selects the momentum acceptance of incoming electrons. While the other aperture is at the image plane of the lenses and has a fixed position with an adjustable size, this forms an iris that selects a region of interest in real-space and leads to a better real-space lateral resolution.

The ideal light source for PEEM imaging would be a bright, low energy, non-focused and non-monochromatic light source which is fulfilled by a Hg vapor lamp ($h\nu \leq 5.8$ eV). The He lamp which is focused to a spot of about 300 µm and is monochromatic can operate under He-I ($h\nu = 21.2$ eV) or He-II ($h\nu = 40.8$ eV) conditions, at 100 mA, 3.3×10^{-9} mbar (chamber) and 150 mA, 1.5×10^{-9} mbar (chamber) respectively. The He lamp is focused to a spot of about 300 µm diameter and is monochromatic.

3.7.1 Ultra Violet (UV) Photoelectron Spectroscopy

This type of photoelectron spectroscopy uses photons with energy in the region of 5-40 eV (UV region) which excite the electron present in the valence band of a material. The emitted electrons are collected by the UV spectrometer which gives information about the density of states of the valence band of a material convoluted with a background of electrons inelastically scattered as they leave the sample. The ultra-violet photons are produced in a synchrotron facility or in a laboratory setting using Helium gas discharge lamp, although neon and argon gases can also be used. The photons emitted by He have energies of 21.2 eV (He I) and 40.8 eV (He II).

Two types of experiments can be performed using UPS: Valence band acquisition and WF measurement. UPS has greater surface sensitivity than XPS and the information depth in UPS is around 2-3 nm.

In order to take a standard UPS spectrum, a region of interest is select using the iris in PEEM and the emitted electrons are directed to the channeltron detector by a single (first) hemispherical analyser. The contrast aperture should be fully open for UPS measurements. This yields information about the sample constituents and components over a wide energy range.

3.7.2 Angle Resolved Photo Emission Spectroscopy (ARPES)

ARPES is an advanced form of photoemission process in which the emitted electrons are collected along with the angle of emission, usually called band mapping, which makes ARPES a direct experimental technique used to collect information about the electron distribution in the reciprocal space of a solid material. In other words, it can be defined as the direct method of studying the electronic structure of a surface. The information about the energy and momentum can be gained in this technique by probing the speed, direction and scattering process of valence electrons of a solid. Thus, the band dispersion and fermi surface of a solid can also be determined by this technique. In real photoemission, the excitation occurs in the vicinity of the crystal surface. The momentum component is believed to be conserved parallel to the surface (k parallel) due to periodicity of the surface crystal structure along that direction while k perpendicular is not conserved due to the fact that (as we cross into vacuum) the symmetry is broken in that direction. Thus, the conservation of energy and parallel momentum component in the photoemission process can yield important piece of information (parameters) about the initial electronic state in the crystal by taking into account the energy and momentum of the final electronic state, detected by the photoelectron analyser.

$$\varepsilon_i = \varepsilon_f - h\nu, \qquad \text{.....(3.6)}$$

$$k_i^{\parallel} = k_f^{\parallel} + G \qquad \text{.....(3.7)}$$

where ε and k represent energy and momentum, respectively while G represents the reciprocal lattice vectors.

Thus, according to the equation above, in ARPES, we can access the whole electronic band dispersion of a solid surface as the incoming electron randomly interacts with electrons, hence exciting electronic states from all bands and with all possible momenta.

The analyser thus catches all electrons going out in different directions and with different velocities which leads to the bright colours seen in the energy-momentum (ε- k) photo intensity distribution.

Thus, in ARPES a cube of E-k data is produced which reveals the valence band structure by cutting a sequence of parallel energy slices through the Brillouin zone as described in figure 3.14.

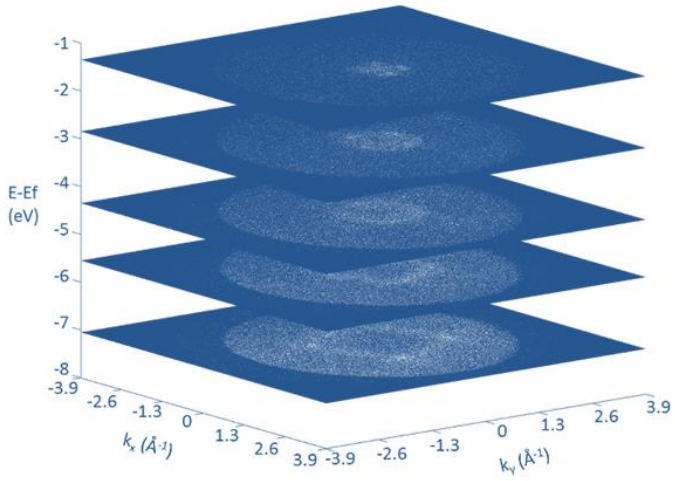

Figure 3.14: Selected ARPES stack of energy slices from Single Crystal C(100) diamond.

ARPES is taken by using the EF-PEEM imaging column to image in the Fourier plane which provides a full wave vector ARPES image compared to a single cut in $k_{//}$ with a resolution of 25 meV under liquid helium and 120 meV for RT measurements. To ensure a full unobstructed view of the e-k relation or the band structure, the contrast aperture is fully open. The iris size is tuned to balance the signal to noise ratio and analysis area. ARPES can reveal a great deal of information about the electronic interactions, doping and crystal orientations.

3.8 Thermionic emission Kit

In order to do the thermionic testing of the diamond samples, a set up at in the diamond lab at the University of Bristol's School of Chemistry was used which consists of a vacuum chamber along with a sample heater, electron collector and a feedthrough to measure the current between the sample and the collector. The details of the set can be seen in figure 3.15 and are available in a publication as well [109]. It consists of a collector attached to a motorised drive to control the distance or in other words vacuum gap between the emitter and the collector. The sample and the collector are both connected to electrical feedthrough while being electrically isolated from the rest of the chamber. An ammeter is connected to sample and the collector to give the sample to collector thermionic emission current while a power supply provides a negative bias of – 25 V on to the sample in order to minimise and ideally overcome the space charge and collector WF. In our experiments, the distance between the collector and emitter is set to 200 µm during the measurements with a chamber pressure of 5×10^{-6} Torr.

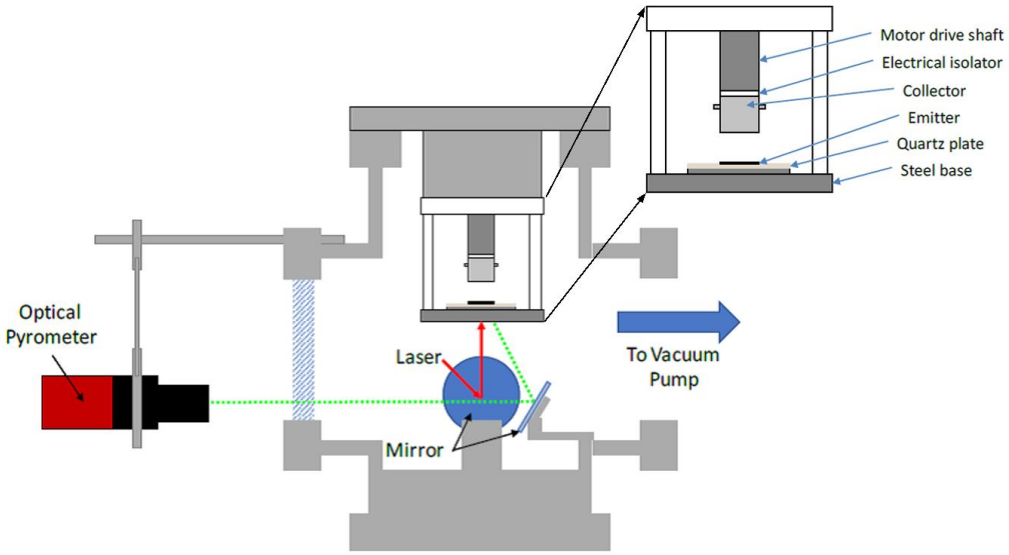

Figure 3.15: Schematic of the experimental thermionic emission testing kit, where a vacuum chamber along with other important parts of the laser heated system is shown. Extracted from a previous publication [3, 110]

An infra-red CO_2 laser (Firestar V40 series, Synrad) was employed to heat the sample directly in order to minimize the electrical background noise and maximise the control over sample temperature. There are mirrors to guide the laser on the base of the sample through an aperture on the sample stage base. In order to enhance the laser absorption through plasmonic coupling, a linear grating is inscribed on the molybdenum substrates [111]. A two-colour optical pyrometer (1.0 and 1.5 μm) aimed at the sample base measures the sample temperature. A PID feedback controls the laser power output which in turn controls the temperature of the sample.

Chapter 4

Modification of the Surface Structure and Electronic Properties of Diamond (100) with Tin as a Surface Termination: A Density Functional Theory Study

Summary

Most of the material for this Chapter has been taken from the paper;

***S. Ullah**, N.A. Fox, "Modification of the Surface Structure and Electronic Properties of Diamond (100) with Tin as a Surface Termination: A Density Functional Theory Study", J. Phys. Chem. C 125 (2021) 25165.*

This manuscript was written through contributions of all authors as mentioned below. All authors have given approval to the final version of the manuscript.

***Sami Ullah**: Investigation, Methodology, Conceptualization, Software, Visualization, Writing - original draft. **Neil Fox**: Writing - review & editing, Supervision, Funding acquisition.*

This chapter introduces various diamond surfaces and various types of terminations on the surface of diamond that yield different properties. Specifically, those metal and metal oxide-based terminations have been mentioned that yield negative electron affinity (NEA) on the surface of diamond. The importance of tin as a termination of diamond has been mentioned. The theoretical method in the form of the density functional theory-based modelling has been described. Various outcomes based on geometric optimisation, electrostatic potential calculation and projected density of states calculation have been described in detail to establish tin as one of the effective and efficient candidates for diamond surface termination. All of this was performed on the University of Bristol's High-Performance Computing (HPC) facility, a Blue Crystal 4 Supercomputer.

4.1 Introduction

Any investigation into metal and metal oxide termination of diamond would demand determining the surface and bonding structure on the surface of diamond. Although spectroscopic techniques such as SPA-LEED would reveal the surface structure experimentally, however, any surface irregularity would result in altering the surface structure and would result in a different output than expected. The shift in charge density between the surface carbon atoms and the terminating species is a crucial piece of information that enables us to determine the electronic structure or bonding structure between the surface species on a diamond surface. Shifts in core levels of carbon atoms are used to evaluate the relative shifts in charge density between the surface species however any charging of the sample would result in false shifts; false in the sense that the shifts in that case would be due to the accumulation of electrons on the surface rather than the differing electronegativities between the terminating species. Hence inputs from XPS core level shifts would not be sufficient for such purpose. Hence all of this demands, as an initial step into this study, a theoretical investigation on the possibility of terminating the diamond (100) surface (both bare and oxygen terminated) with Sn atoms at various coverages. This was done using the DFT code run through the CATSEP program as has been described in section 3.1.

4.2 The Diamond Surface

The surfaces of diamond are differentiated based on crystallographic orientations (shown by the Miller indices) that these possess for example C(100), C(111), C(110), C(113) etc. Out of these, as has been reported [9] that the slowly growing C(111) and C(100) ones are the most predominantly occurring as all other orientations grow out of the crystal faster. The clean C(100) diamond surface possesses two dangling bonds while (111) only one, per surface carbon atom. Due to this there is a reconstruction of the surface in the form of dimerization of the surface carbon atoms which results into a π-bonded surface

structure (and hence a (2 × 1) symmetry in the LEED pattern). Some of the reasons why 100 is preferred for the surface science experiments are very smooth surface growth (near atomic flatness) on 100 surface, lower defect concentration, etc. The monohydride surface (C(100)-(2×1):H bonds) is energetically more favourable than the clean surface due to the H atoms saturating the diamond surface. (111) surface occurs in an unreconstructed (1 × 1) pattern or a reconstructed (2 × 1) pattern, also known as Pandey chain reconstructed surface which is energetically more favourable. In this reconstruction π-bonds are formed in the first upper two layers of the surface only in the form of zigzag chains on its first layer (as shown in the figure 4.1). The dimerization or the reconstruction can be prevented and hence (1 × 1) favoured energetically by saturating the surface with the hydrogen atoms to form C-H bonds above the top layer carbon atoms.

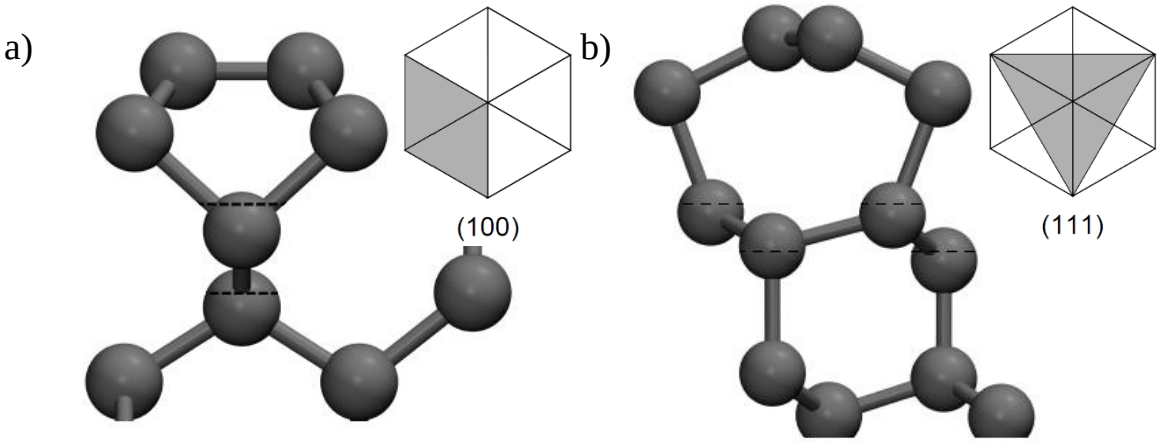

Figure 4.1: The optimized structure for the a) clean reconstructed C(100) surface and b) C(111) surface along with insets showing the 100 and 111 planes of an arbitrary unit cell.

Various atoms or groups have been investigated as a potential PEA and NEA terminating species to the diamond surfaces with various orientations. The most common PEA and NEA imparting atoms that have been researched widely are oxygen (O) and hydrogen (H), respectively [60-61, 112-113].

4.2.1 Hydrogen terminated diamond surface

H termination of diamond has been found to possess an NEA of -1.96 eV theoretically and -1.3 eV experimentally [10, 66-67], [114-115]. However, hydrogen has been seen to desorb at elevated temperatures (≥700 °C) which renders it non usable in the devices operating at high temperatures.

4.2.2 Oxygen terminated diamond surface

O terminated diamond (OTD) surfaces have been researched widely as a PEA imparting surface termination [57]. Many processes with diamond as simple as acid washing results in the O surface termination of diamond [62]. Experimentally O has been seen to occupy a mix of both the ether and the ketone (carbonyl) position. Theoretically ether terminated diamond has been found to be the most stable form of OTD as has been found in our study as well. OTD has been seen to possess a PEA of up to 2.7 eV and 3.8 eV with large adsorption energies per atom in case of ether and ketone terminations, respectively [61, 63, 64, 116]. Experimentally, we have found the PEA value of 0.89 eV per atom for oxygen terminated diamond [5]. This has resulted in O being studied as potential candidate in quantum sensing and electrochemical applications along with other elements like boron [10, 65] etc.

4.2.3 Metal and Metal oxide terminated diamond surface

As has been mentioned in chapter 2, various metal and metal oxide terminations of diamond surfaces have been explored [69, 117] backed by the fact that oxygen inclusion results in the stronger dipoles due to increased sticking coefficient between the metal atom and surface carbon atom [58, 76]. Research has mostly focussed on certain group of elements as potential termination of diamond surface. Alkaline metals, alkaline earth metals, transition metals have been a focus of most studies both theoretically and experimentally [4, 46, 59, 70, 118-120]. There are only a few studies that have focussed

on other elements like Al, Si, Ge, F, Sn etc. [5, 76, 78-80, 121] which have been shown to impart NEA to the diamond surface. The same group elements with Sn like Si and Ge have experimentally been studied as the surface terminations on diamond (100). Ge has been found to impart an NEA of – 0.71 eV on the surface of diamond (100) [80] while Si deposition on the surface of diamond (100) has resulted in an electron affinity of −0.86 ± 0.1 eV, however, both Si and Ge are determined to be unsuited for device application at ambient condition due to the high reactivity of unsatisfied silicon and germanium bonds which would demand a protective layer to be grown on top of the structure (e.g. in the form of SiO_2 layer) which could have a negative impact on NEA and lower WF in these structures. We have observed, experimentally, Sn to impart NEA on the surface of diamond (100) while being stable at ambient condition which is a crucial point as far as device application of these structures is concerned, as explained later in chapter 4. Table 4.1 shows the results of most stable terminations along with their corresponding EA's. Tin (Sn) has previously not been widely investigated as a termination of diamond surface. Sn is available in abundance, nontoxic and has the same valency as carbon (C), hence Sn atoms are expected to bond tetrahedrally like C atoms in diamond. Although the lattice constants for C (in diamond) and Sn are 3.6 Å and 6.5 Å, the difference in size will not play a significant role as the Sn coverage is only up to a monolayer.

Sn with a large electron cloud is expected to contribute to the redistribution of electron density towards more electronegative C and O due to which a surface dipole is generated with negative side of the dipole inclined towards the surface carbon atoms, a strong reason for the generation of NEA on the surface of diamond. Sn adsorption on an oxygen terminated diamond would also result in the formation of SnO on the surface of diamond. SnO has already been researched as a superior 2D material possessing various remarkable features and its conductivity can be altered using different doping approaches

[81, 82]. Moreover, lithiated tin has been shown to possess remarkably lower WF in bulk form (as alloys). Hence SnO terminated diamond would not only lead to modification of diamond surface properties impressively but also encourage other studies of combining alkali metals like Li with SnO thin films for revolutionary properties on the surface of diamond for various applications.

Table 4.1: Most stable coverages of different metals on the various orientations of diamond and their corresponding adsorption energies along with electron affinities taken from [10, 11, 12]. *Here bare means unterminated diamond while OTD represents oxygen terminated diamond (see figure 4.5).*

coverage (ML)	adsorbate	substrate	E_{ads} (eV)	χ (eV)
0.5	Al	bare	- 3.97	- 0.93
1	Al	bare	- 4.11	- 1.47
1	B	bare	- 6.85	- 1.39
1	Ti	bare	- 5.08	0.35
1	Cu	bare	- 2.93	- 0.55
0.5	Al	OTD	- 6.36	- 0.37
1	Al	OTD	- 4.58	- 0.54
0.5	B	OTD	- 9.0	0.49
1	Li	OTD	- 3.64	- 3.50
1	Na	OTD	- 1.62	- 1.42
0.5	Mg	OTD	- 3.92	- 2.77
0.5	Na	OTD	- 2.41	- 1.30
0.5	K	OTD	- 1.92	- 1.31
0.25	Cs	OTD	- 2.19	- 2.41

4.3 Method

A symmetrical 12 carbon atom thick periodic (in x and y) slab of carbon atoms with surface on both sides, representing diamond (100), with a 2×2 supercell on each (100) surface yielding 4 C atoms on the surface was used [122]. It has been established that the surface energy, bond angles and atomic charge reach desired stability and convergence under 12 layer slab thickness while the ideal bulk geometry inside the slab is also reached with 12 layers to ensure the convergence inner distances [123]. This enabled us to vary the coverage of Sn atoms from quarter monolayer (QML = 0.25 ML) to half mono layer (HML = 0.5 ML), to full monolayer (FML = 1 ML) by adsorbing one, two or four Sn atoms, respectively. For oxygen terminated diamond 8 oxygen atoms were used to terminate the 8 carbon atoms on both surfaces in ether and ketone configuration. The slab dimensions were fixed at 5.016 5 Å × 5.016 Å with a sufficient vacuum gap of 20-25 Å (~ 24.27 Å) in between the repeating cells such that the electrostatic potential had fully decayed in the vacuum. These slabs were used as samples for experiments on the CASTEP code [89] for performing the plane wave DFT calculations using Perdew–Burke–Ernzerhof (PBE) generalised gradient approximation (GGA) for the exchange-correlation functional [94] and Vanderbilt pseudopotentials [92]. The plane wave basis set of cut off energy 700 eV along with a Monkhorst-Pack [96] mesh with 6×6×1 k-points (18 k-points in total) was used for geometric optimisation while a 12×12×1 k point grid was employed for density of state calculation using OptaDOS code[98] (using adaptive broadening of DOS peaks and a spacing of 0.07 eV as optimised in [76], [121]). The BFGS algorithm resulted in the geometry optimised structure with tolerances of 0.05 eV/ Å and 2 × 10^{-5} eV per atom in ionic forces and total energy, respectively.

4.4 Results and discussion

Before performing the calculations on the actual metal i.e., Sn on diamond (100). The slabs were tested for convergence at different cut off energies and for k-points. The

structural calculations were converged using a cut off energy value of 700 eV and a Monkhorst-Pack grid of (6 × 6 × 1) k-points with a geometry convergence criterion (tolerances) of 0.05 eV/ Å and 2 × 10^{-5} eV per atom in ionic forces and total energy, respectively, a fixed unit cell and no restrictions on atomic positions. The energy was seen to converge fairly with the parameters used. The energy minimisation through geometry optimisation and electrostatic potential calculations were performed on bare, H terminated, and O terminated diamond (both ether and ketone) surfaces (table 4.2) which agree with the already available reports on these surfaces in the literature, hence demonstrating the viability of these parameters used for the future calculations.

Table 4.2: Electron affinity (χ) and adsorption energy (E_{ads}) for various diamond surfaces. Compared to the earlier studies as presented in the studies [1, 9]*, the values were found to be comparable.*

Sample	Source	E_{ads}(eV)	χ (eV)
Clean C	This work	------	0.73
	Previous DFT	------	0.51–0.69 [63], 0.62 [64], 0.86 , 0.28 [124]
H T D	This work	-4.16	-1.9
	Previous DFT	-4.14 [76], - 4.54 [125]	−1.95 [64], −2 [63], −2.2 [126]
OTD Ether	This work	-7.16	2.74
	Previous DFT	- 8.2 [64], - 6.21 [113]	2.61–2.7 [127], 2.63 [64]
OTD Ketone	This work	-6.78	3.73
	Previous DFT	- 7.88 [64], - 5.77 [10]	3.75 [64], 3.64 [127]

4.5 Tin termination of diamond (100) surface

After optimising and confirming the parameters, it was deemed necessary to select the sites of adsorption for Sn atoms on the diamond (100) surface. Most of the studies have adopted the traditional Levine structure to determine the high symmetry adsorption sites on the surface of Si and diamond [128], known as the Cave (T4), Pedestal (HH), Bridge (HB) and Valley Bridge (T3) sites as depicted in figure 4.2 a). A few studies have chosen other sites as well [10, 122].

This gave rise to a curiosity to test many other possible sites along with the above-mentioned sites at various coverages of Sn on diamond (100). Figure 1 shows the general structure of a (2 × 1) reconstructed diamond surface along with the different sites for Sn adsorption.

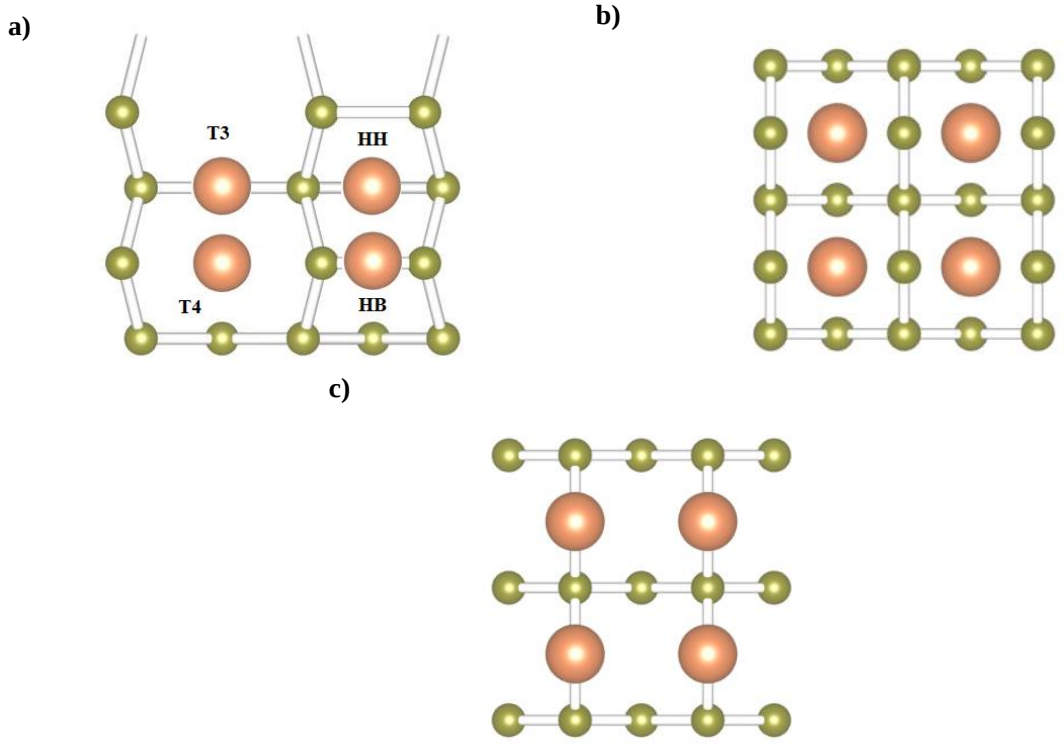

Figure 4.2: a) Plan view of the bare (2 × 1) reconstructed diamond surface showing the potential high symmetry adsorption sites for Sn on bare diamond surface. HH, HB, T3 and T4 refer to the hexagon hole, hexagon bridge, third-tier carbon, and fourth-tier carbon sites, respectively. Green balls represent carbon atoms while orange balls represent tin atoms. b) Unreconstructed diamond (100) surface with Sn atoms in ether configuration (bridge position). c) Unreconstructed diamond (100) surface with Sn atoms in ketone configuration (on top position).

4.5.1 Tin on bare diamond

As has been mentioned earlier, 4 Sn atoms on top of the surface with 4 C atoms gives 1 full monolayer (FML) adsorption. Hence 0.25 ML would need 1 Sn atoms anywhere on the 4 sites shown and described in figure 4.2. However, for half monolayer adsorption of Sn on diamond, 2 Sn atoms take up different combination of sites which are mentioned in the table 3. For 1 ML, there are only 2 most favourable ways (ether and ketone) in which Sn atoms could be placed on top of diamond surface. Ether and ketone configuration in case of FML coverage refers to the position of Sn atom in between the surface C atoms and on top of surface C atom, respectively. The unreconstructed surface of diamond (100) was found to be favourable for FML termination as it favours the bonding between the Sn and C atoms due to similar valency of the surface species. Any attempt to adsorb a FML of Sn in a different configuration or on a reconstructed diamond structure would output a HML terminated diamond with 2 Sn atoms unbonded which, in our opinion, satisfies the valency of both C and Sn atoms on the surface of diamond.

Hence, it can be concluded through the information presented in the table 4.3 that the most favourable adsorption site in case of 0.25 ML of Sn on diamond (100) is T4 site (figure 4.3 a) where the highest adsorption energy of – 4.27 eV with an NEA of – 0.39 eV is obtained. For HML case, the most stable and favourable site for Sn atoms is T4T4 (figure 4.3 b) with an adsorption energy value of – 4.4 eV and a NEA value of – 1.43 eV. As can be seen from the table 4.3, many other adsorption sites relaxed to T4T4 which indicates, again, this configuration to be the most stable and favourable one. Due to the large size of Sn atoms and heavy electron cloud, there is a possibility of interatomic repulsion between the Sn atoms which makes it relatively unfavourable for Sn atoms to achieve a full monolayer coverage on the diamond surface, hence giving a very small value of adsorption energy for both ketone and ether positions.

*Table 4.3: Values of electron affinity, χ, and adsorption energy, E_{ads}, calculated for various positions and at different surface coverages of Sn on the bare diamond (100) surface. * Represent the unreconstructed diamond structure.*

Coverage (ML)	Input sites	Output	Adsorption Energy, E_a(eV) /adsorbate	Electron Affinity, χ (eV)
0.25	HH	HH	- 3.45	- 0.58
0.25	HB	HB	- 3.8	- 0.8
0.25	T3	T3	- 3.8	- 0.89
0.25	T4	T4	- 4.27	- 0.39
0.5	HHHH	---	- 4.2	- 0.75
0.5	HBHB	---	- 3.75	- 1.6
0.5	T3T3	---	- 3.2	- 1.0
0.5	T4T4	---	- 4.4	- 1.43
0.5	HHHB	---	- 4.29	- 1.12
0.5	T3HB	T4HB	- 4.3	- 0.73
0.5	T3HH	---	- 4.1	- 1.01
0.5	T4HB	---	- 4.3	- 0.66
0.5	T4HH	T4HB	- 4.3	- 0.73
0.5	T4T3	T4T4	- 4.4	- 1.43
1	ETHER*	---	- 1.9	- 1.07
1	KETONE*	---	- 2.14	- 1.14

All other attempts to terminate diamond surface with a full monolayer coverage in different configurations resulted into the output structure relaxing into the HML terminated one with 2 Sn atoms left unbonded.

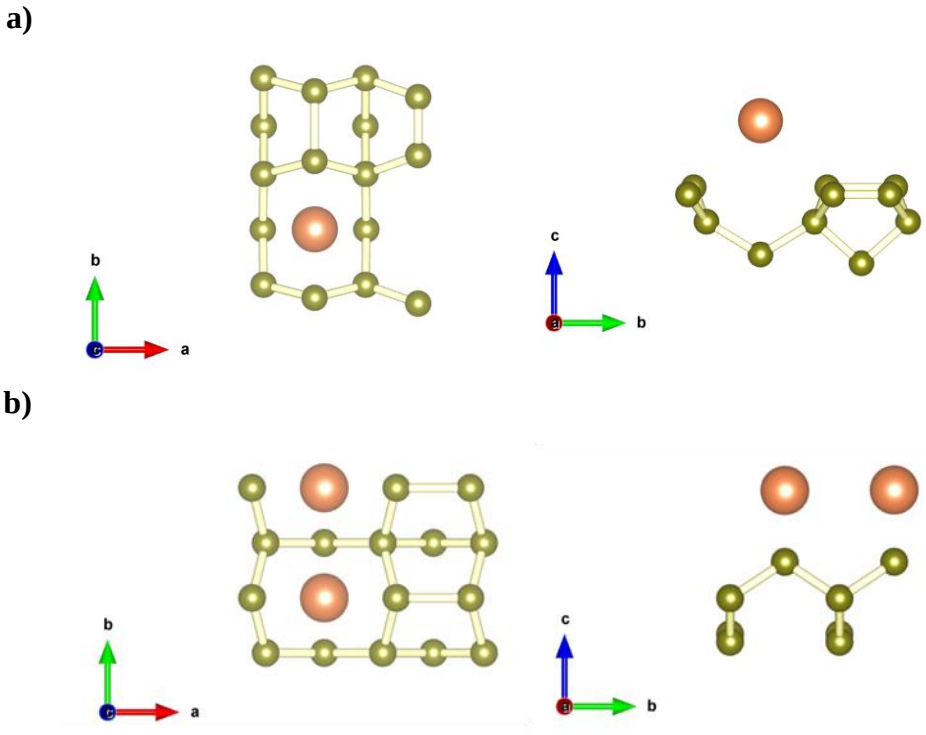

Figure 4.3: Most stable a) QML and b) HML of Sn on diamond (100). Note the reconstruction of the diamond surface has occurred due to Sn adsorption. Green balls represent carbon atoms while orange balls represent tin atoms.

Figure 4.4 shows the electrostatic potential for the HML (0.5 ML) of Sn on bare diamond (100) which shows the variation of electrostatic potential along the normal axis to the surface. The negative and positive sides of the dipole can be visualised in the form of crests and trough (or upswings and downswings by convention), respectively. The negative side of dipole is present towards (or on) the surface carbon atoms while the positive side of the dipole exists (localized) on Sn atoms. This dipole formation has been described as the source of NEA on the surface of diamond [57]. Mulliken bond population analysis is widely used to assess nature of the bond between any two species. A value of 0 indicates a perfectly ionic bond while an increasing value of bond population indicates increasing levels of covalency. In our case, the most stable HML adsorption exhibits the covalent nature of the bond between the surface C atoms and the adsorbed Sn atoms with a bond population value of 0.45.

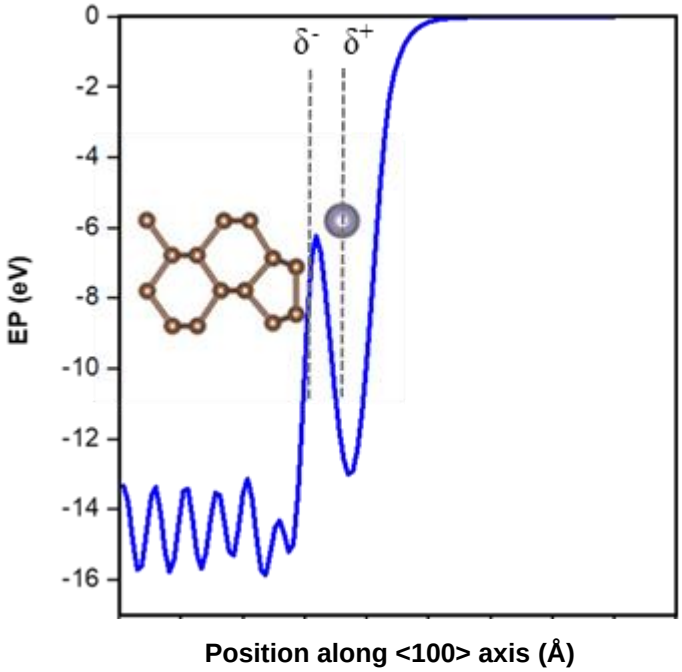

Figure 4.4: Electrostatic potential (EP) for the most stable configuration i.e., HML of Sn on bare diamond (100). The electrostatic potential is atom centric (localization of charges on or very near to the surface atoms) like H termination instead of bond centric (where delocalization of charges due to the lowering of electronic states causes the positive and negative sides of surface dipole sit between the surface species called bond centric) as seen in case of metal oxide (LiO) terminations of diamond. Here, brown balls represent carbon atoms grey balls represent tin atoms.

The adsorption of Sn atoms leads to increase in the C-C dimer bond length from nearly 1.38 Å to 1.7 Å which is expected due to the charge transfer between the C and Sn atoms and shows the dipole formation between more electropositive Sn atoms and the surface C atoms (C^- - Sn^+), also revealed by the Mulliken charge analysis which shows Sn gains a positive charge of 0.37e and 0.57e while the C atoms gain a charge of -0.20e again confirming the charge transfer between the surface species. In case of the HML and FML adsorption, a similar trend can be seen which indicates preferential covalent nature of Sn to surface C bond.

4.5.2 Tin on oxygen terminated diamond

To achieve a full coverage of oxygen on the surface of diamond, 8 oxygen atoms terminated both surfaces of diamond slab in ether and ketone configuration. Although it has been established widely using experimental and theoretical models that ether configuration is the most stable one [1], however, there are a few reports which mention ketone configuration as the most favourable termination of diamond [9]. In our study, ether configuration of oxygen termination came out to be the most stable one. However, when it comes to metal oxide termination of diamond, it has been found that metals can easily break the ketone bonds between surface carbon and oxygen atoms to form metal oxide on the surface of diamond with surface C atoms dimerising to reconstruct the diamond surface [76]. So, in order to establish which configuration of oxygen termination favours Sn deposition on the surface of diamond, both ether and ketone terminated surfaces were constructed and tested. Sn coverage varies in the similar manner as in case of bare diamond surface i.e., 0.25 ML or QML is represented by 1 Sn atom on each surface, while 0.5 ML or HML by 2 Sn atoms and 1 ML or FML by 4 Sn atoms on each surface of diamond (100). Figure 4.5 shows the ether and ketone clean unterminated diamond surfaces. The Sn atoms were placed on top of both the surfaces in different configurations and coverages which can be shown in Table 4.4 and 4.5. Here ether and ketone with regards to Sn means bridge site (between 2 O atoms) and on top (of O atoms) site, respectively.

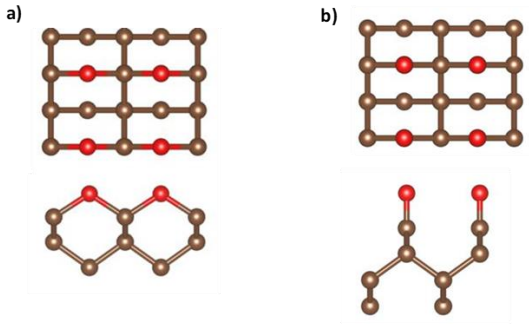

Figure 4.5: Showing clean diamond surfaces terminated with oxygen in a) ether (bridge between two C atoms and b) ketone (on top of each C atom) configurations. Brown balls represent carbon atoms while red balls represent oxygen atoms.

Table 4.4: Values of electron affinity, χ, and adsorption energy, E_{ads}, calculated for various positions and at different surface coverages of Sn on the oxygen terminated diamond (100) surface in ether configuration.

ETHER OXYGEN TERMINATED	Coverage (ML)	Sn configuration	Adsorption Energy, Ea (eV) per adsorbate	Electron Affinity, χ (eV)
	0.25	In between 4 O atoms	-5.9	- 0.86
	0.5	Ether	-5.6	2.31
	0.5	Ketone	-5.27	- 1.37
	1	Ether	-4.6	1.88

The ether bond being stronger and hence resilient to break with Sn adsorption yields lesser values of adsorption energy. A QML of Sn on the ether terminated diamond (figure 4.6a) is favoured which implies lesser chance for 2 Sn atoms to break the ether bonds probably due to interatomic repulsion between the Sn atoms which lessens the chance for them to interact with the surface oxygens which is not the case for a lone Sn atom. A FML of Sn on ether resulted in Sn atoms unbonded and going away from the surface, hence no adsorption due to the same reasons. It seems from the tables 4.4 and 4.5 that the most preferential configuration for Sn atoms on diamond (100) is QML (0.25 ML) of Sn atoms on top of the ketone terminated oxygen atoms (can be seen in figure 4.6b) which makes sense as it is expected that breaking a ketone bond would be easier for an Sn atom to bond with surface O than a more stable ether bond. However, this leads to a PEA value of 0.40 eV. It is the trend in the NEA rather than the actual numerical value that is important here as GGA is known to produce wrong estimates of electron affinity. Since the value of 0.40 is very small (very close to negative scale) and it has been experimentally seen that the sub–ML Sn adsorption leads to NEA on the surface of

diamond (100) [5] along with the fact that all other adsorption configurations (in tables 4.4 and 4.5) result into the NEA, hence it could be said that Sn leads to NEA on the surface of diamond (100) in most of the stable configurations.

Table 4.5: Values of electron affinity, χ, and adsorption energy, E_{ads}, calculated for various positions and at different surface coverages of Sn on the oxygen terminated diamond (100) surface in ketone configuration.

KETONE OXYGEN TERMINATED	Coverage	Sn configuration	Adsorption Energy, E_a (eV) per adsorbate	Electron Affinity, χ (eV)
	0.25	In between 4 O atoms	- 6.45	0.40
	0.5	Ether	- 5.8	- 2
	0.5	Ketone	- 6.03	- 1.37
	1	Ether	- 4.5	0.28

It can also be concluded that Sn prefers ketone terminated oxygen on the surface of diamond than the ether terminated one as can be seen from the larger adsorption energy values in the tables. HML coverage of Sn is the coverage of interest as nearly all the experiments investigating the surface properties of Sn terminated diamond would yield genuine insights into this field of study when the metal/ metal oxide layer is under 1 ML, especially when the advanced spectroscopic techniques are used. HML coverage of Sn on the ketone terminated diamond (can be seen in figure 4.6 c) also results in a large adsorption energy value of 6.03 eV with a large NEA value of – 1.37 eV which is an

important and a hopeful outcome that sets a base for the future theoretical and experimental investigation into this topic.

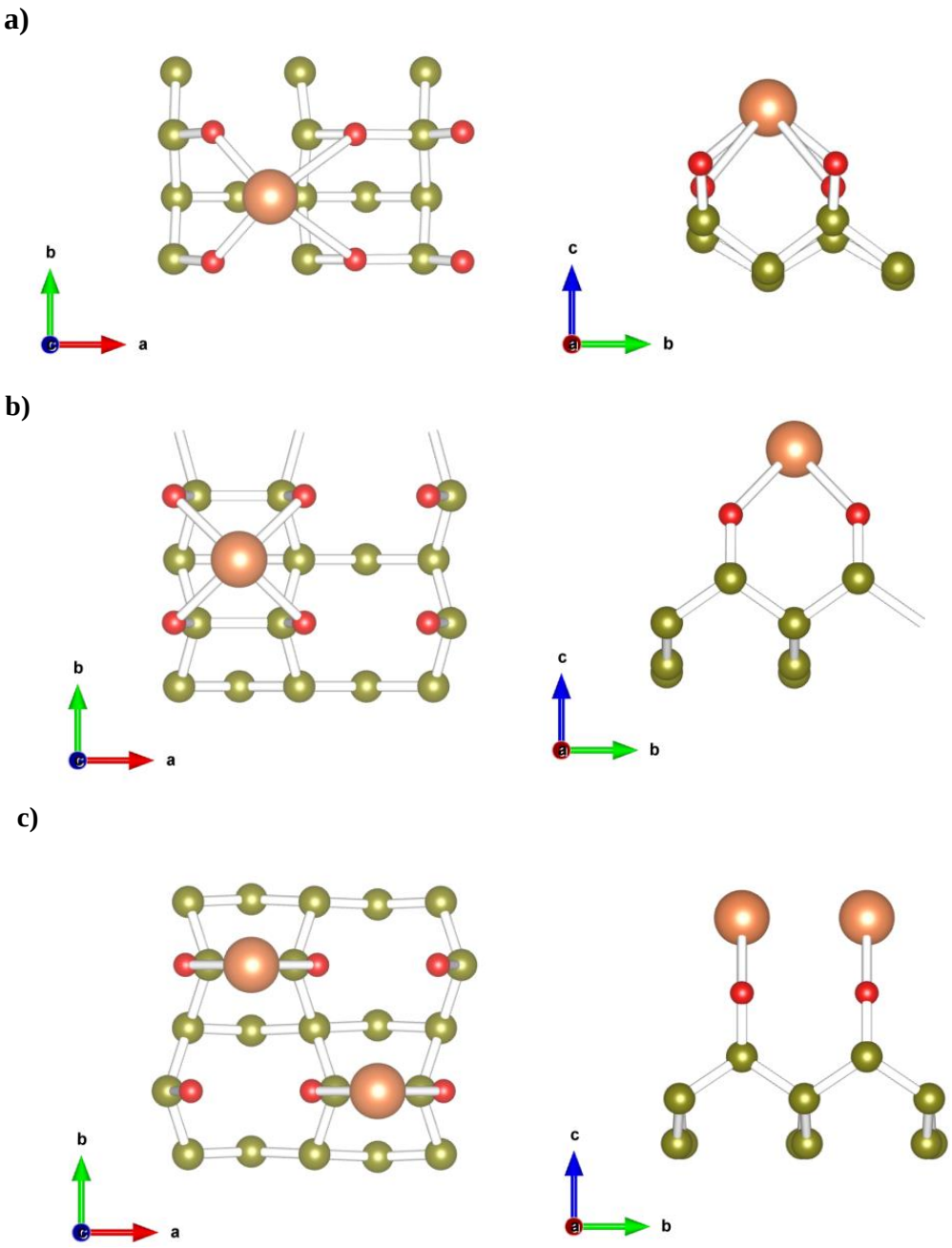

Figure 4.6: Geometry optimised most stable output structures showing a) QML (1 atom) Sn on the oxygen (ether) terminated diamond; no surface reconstruction has occurred due to Sn adsorption. b) QML adsorption where 1 Sn is shared by 4 O (ketone) atoms (4 coordination) hence resulted in reconstruction (or C-C bond) on the surface. c) HML adsorption where each Sn atom is shared by 2 O (ketone) atoms (2 coordination) hence resulted in reconstruction (or C-C bond) on the surface. Green balls represent carbon atoms while red balls and orange balls represent oxygen and tin atoms, respectively. Adopted with modification from [5].

The NEA values (more exactly trends) for Sn on bare and oxygen terminated diamond (100) surface are comparable to the ones obtained for the hydrogen terminated diamond and Li/ LiO terminated diamond (100) with larger adsorption energies implying stronger bonding between the surface species. A FML of Sn on ketone OTD resulted in Sn atoms unbonded and going away from the surface, hence no adsorption, similar to the ether OTD case.

In order to gain a further insight into the nature of the dipole at the surface, EP was generated for the most stable ketone terminated diamond surface as shown in figure 4.7.

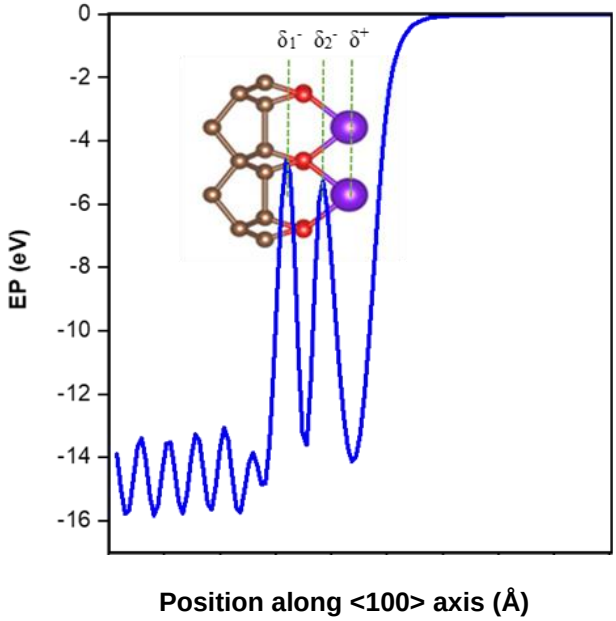

Figure 4.7: Electrostatic potential (EP) for the most stable configuration i.e., HML of Sn (ketone or on top) on oxygen (ketone) terminated diamond (100). The large surface dipole apparent in the potential is projected onto the structure. It shows the dipole is bond centric as has been found in case of LiO terminated diamond[5] rather than atom centric unlike H terminated diamond. Here in this figure, brown balls represent carbon atoms while red balls and purple balls represent oxygen and tin atoms, respectively.

Figure 4.7 shows the electrostatic potential (EP) along the normal to the surface of diamond (100). There is a complex interaction at the surface as compared to the bare surface. The downswing (trough) depicts the positive side of the surface dipole which is centred on the Sn atom as expected and seen in the Mulliken charge analysis too (discussed below). Since O atoms are more electronegative than both C and Sn, hence

attract the charge density towards itself resulting in the centring of the negative side of surface dipole between the C-O and O-Sn bonds in the form of δ_1^- and δ_2^+ (where it seems that $\delta_1^- > \delta_2^+$), respectively. This results in the net negative charge accumulation near the surface carbon atoms, giving rise to NEA on the surface of diamond.

Mulliken bond population value of 0.04 indicates the ionic nature of the bond between surface bonded O atoms and Sn atoms in case of ether terminated diamond with QML coverage along with an increase in the covalency (from 0.45 up to 0.74) of the bond between surface C and O atoms due to Sn adsorption. Mulliken charge analysis on the most stable configurations of Sn on oxygen terminated diamond reveals the formation of CO^- - Sn^+ dipole with Sn attaining a positive charge of 1.22e, O attaining a negative charge of -0.47e and C attaining a positive charge of 0.45e. The bond length is further reduced between C and O atoms due to Sn adsorption which again indicates increase in the covalency of the bond between the surface C and O and hence stronger bonding, in case of ether terminated diamond. However, in case of ketone terminated diamond the covalency between C and O atoms reduces considerably due to Sn adsorption. The bond length between C and O atoms increases which shows more tendency towards single bonded character which is expected as Sn atoms would break the double bond (π bond) between C and O atoms. A similar trend can be seen in case of the most stable HML coverage on ketone terminated diamond surface.

4.6 Projected Density of States calculation

Projected density of states (PDOS) calculations are performed using the OptaDOS code [98] in CASTEP to show the density of electronic states for individual atoms in the optimised structure. The adsorption of Sn on the bare and oxygenated diamond (100) results in a significant decrease in the WF, as has been seen experimentally also (see chapter 6), and NEA which occurs due to a shift in the electron density between the

surface atoms [5]. In case of Sn adsorption on the bare diamond surface, a simple explanation of surface dipole, as mentioned in the earlier sections of this chapter, can explain the mechanism of this shift, however, as has been seen in case of the oxygen terminated diamond, any explanation to this phenomenon demands a further support. Here projected density of states calculations before and after the Sn adsorption on the OTD will help us to understand further the distribution of electron density at the surface which accounts for the shift in the WF of the diamond surface.

Figure 4.8 a) shows the PDOS structure for the bulk and surface carbon atoms in the bare diamond (100), taken from the centre of the diamond slab and from the dimer row, respectively. Due to the sp^3 bonds being distributed across the diamond lattice, there are the indistinct, broader, and less intense peaks features present across the spectra especially towards the higher energy region. There are states within the band gap region of the diamond which originate from π and π* bonds of the surface carbon dimer rows. Figure 4.8 b) shows the PDOS spectra for the most stable QML of Sn adsorbed on the bare diamond (100) surface. The existence of a large peak which can be deconvoluted into a multiple peak structure, can be seen within 20 eV to 25 eV region, indicating the tin-oxide structure on the surface of diamond. This feature can be a distinguishing factor between SnO and tin dioxide as has been mentioned earlier. This feature is analogous to that of Sn4d peak's structure seen in XPS or the valence band structure of SnO on diamond [5]. There are states still present within the band gap of diamond and a match between the surface C states and Sn states indicates a covalent bonding between the two surface species is clearly visible. Figure 4.8c) shows the typical PDOS structure for ketone terminated diamond which shows the density of states for bulk carbon, surface carbon and oxygen atoms in ketone configuration. Again, due to the sp^3 bonds being distributed across the diamond lattice, there are the indistinct, broader, and less intense

peaks features between 5 and 15 eV corresponding to the sp^3 bonds than more localised features between -8 and 0 eV corresponding to sp^2 bonds. At higher energies, the PDOS presents similar distinct and sharp peaks for both surface C and O atoms at -6 eV and 24 eV, indicating the strong covalent bonding (sp^2 bonding character) between these species. In addition to these states the surface oxygens have three sharp nonbonding peaks within the band gap at around -0.5 eV, -2 eV and -3.5 eV corresponding to the lone pair electrons on the oxygens.

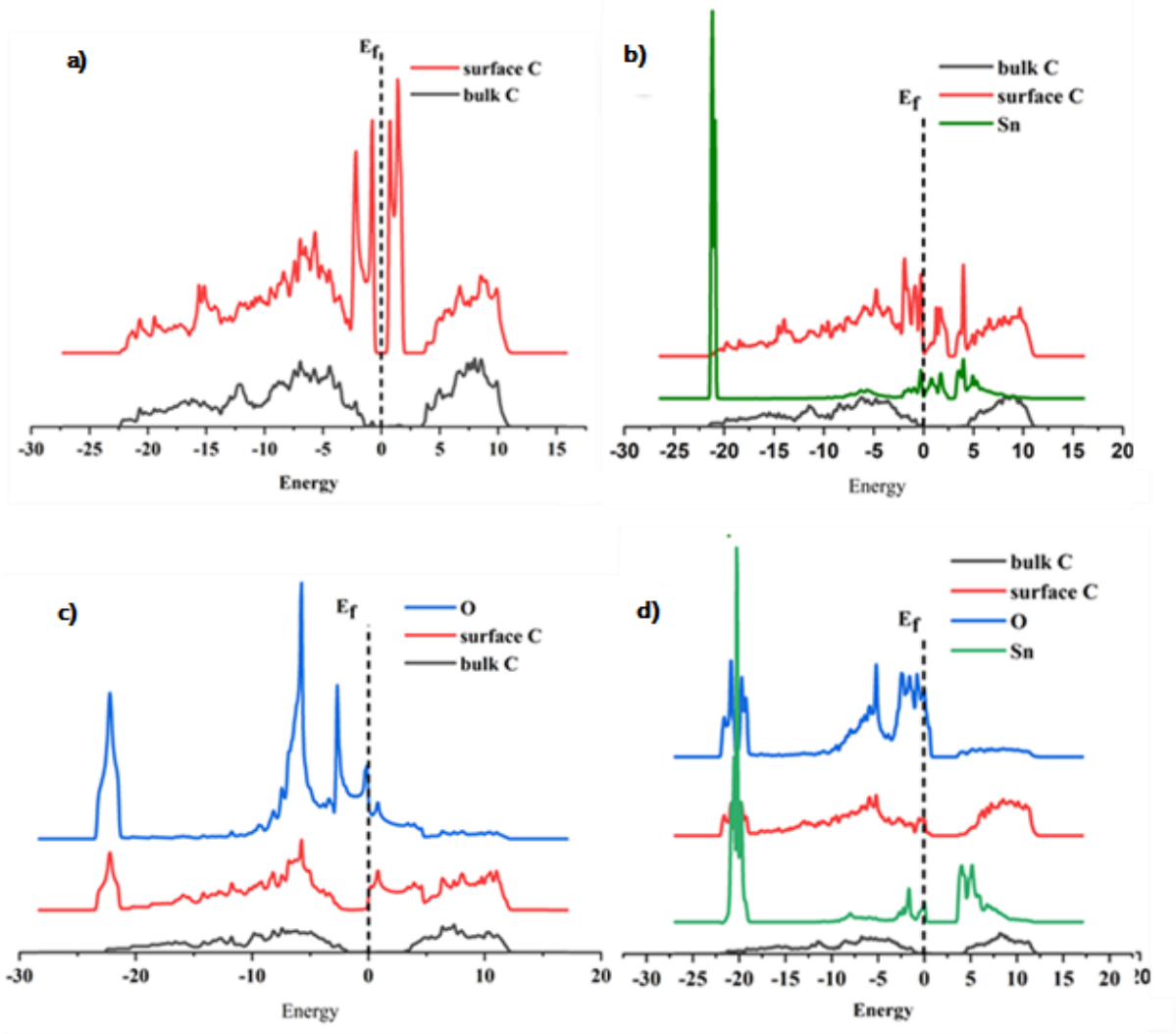

Figure 4.8: (a) Projected density of states (PDOS) for bulk C and surface C prior to Sn adsorption. (b) The PDOS for the same layers after QML of Sn adsorption (shifted vertically for clarity). (c) Projected density of states (PDOS) for bulk C, surface C and surface O (ketone) prior to Sn adsorption. (d) The PDOS for the same layers after QML of Sn adsorption (shifted vertically for clarity). All energies are relative to the Fermi level at 0 eV.

The adsorption of a HML of Sn on the ketone terminated diamond surface results in the significant change in the density of states of the surface species, as can be seen in figure 4.8d). The three sharp lone pair oxygen levels have been substantially downshifted in energy and seem to overlap with the bulk levels, indicating charge transfer from Sn to the other surface species (-O-C) as discussed in EP analysis too. There is an obvious evidence of match in PDOS spectra between surface C and O at many energy points which indicates strong covalent bonding between the species before Sn adsorption which seems to go away with Sn adsorption considerable indicating the breakage of the strong double bond between the surf C and O and formation of O-Sn single bond as can be seen in an excellent match between all three surface species between – 20 eV to – 26 eV. This also shows the charge redistribution between the surface species that leads to the lowering of WF and NEA.

4.7 Conclusion

This work describes the surface and electronic structure of the diamond (100) when Sn is adsorbed on the bare and oxygen terminated diamond in various coverages and configurations, which could serve as a foundation for any future theoretical and experimental investigation into the Sn surface doped diamond or Sn surface terminated diamond for any application that demands lower WF thin films or diamond-based samples with NEA. DFT calculations were performed to determine the most stable position and coverage of Sn on bare and oxygen terminated diamond (100). It was seen that most of the sites whether on bare or oxygen terminated diamond, exhibited NEA with large adsorption energies. There is a predominant covalent nature between the Sn (and SnO) and surface C atoms, hence stronger bonding. A QML of Sn on bare diamond resulted in an NEA of - 0.39 eV with a large adsorption energy of - 4.27 eV while a HML of Sn has resulted in much larger NEA (-1.43 eV) and adsorption energy (-4.4 eV). On the oxygen

terminated surface (OTD), a HML of Sn in ketone configuration resulted in an NEA of -1.37 eV with a much larger adsorption energy of -6.03 eV, which is expected due to the fact that oxygen inclusion increases sticking coefficient and hence bond strength between the atoms. It was determined from the EP and PDOS calculations that due to the shift in the electron density towards the more electronegative species or in other words due to the phenomenon of charge re-distribution because of Sn adsorption, there is an accumulation of negative charge on or near the surface carbon atoms which results in NEA and lower WF at the surface of diamond (100).

Chapter 5

An Investigation into lithium based surface termination and the mobility of Lithium atoms on the diamond surface at various annealing temperatures.

Summary

Most of the material for this chapter has been taken from the publication;

***S. Ullah**, L. Cullingford, T. Zhang, J.R. Wong, G. Wan, M. Cattelan, N.A. Fox, "An investigation into the surface termination and near-surface bulk doping of oxygen-terminated diamond with lithium at various annealing temperatures", MRS Adv. (2021).*

These manuscript were written through contributions of all authors as mentioned below. All authors have given approval to the final version of the manuscript.

***Sami Ullah**: Investigation, Methodology, Conceptualization, Software, Visualization, Writing - original draft. **L. Cullingford**: Investigation, Validation. **T. Zhang**: Investigation, Validation. **J.R. Wong**: Investigation, Validation. **Gary Wan**: Validation, Resources, Writing - review & editing. **Mattia Cattelan**: Conceptualization, Resources, Data curation, Writing - review & editing. **Neil Fox**: Writing - review & editing, Supervision, Funding acquisition.*

In this chapter, a chemical route for the surface termination of oxygen terminated diamond with lithium atoms is presented enabling an investigation into the mobility of Li atoms on the surface of oxygen terminated diamond at higher annealing temperatures. The work in this chapter describes crucial pieces of information on Li based surface termination of diamond which would be useful later in developing a tin and lithium (oxide) based heterostructure termination of diamond, presented in chapter 6. Results in the form of spectroscopic techniques (angle resolved X-ray photoelectron spectroscopy- ARXPS) have been presented to describe the mobility or the movement of lithium near the surface of diamond (near surface bulk of diamond) and how it would affect the physical and electronic structure of diamond at elevated temperatures, a crucial piece of information that makes this a novel and insightful study.

5.1 Introduction

Tuning of the electrical properties of diamond by controlled doping of elements like oxygen, nitrogen, lithium, sodium or boron [51-52], has multiplied the interest in diamond research. Li-doped diamond films are believed to be a potential approach to create n-type semiconducting diamond with low resistivity and room temperature (RT) dopant activation. Theoretical studies predict the potential of Li to act as a shallow donor [129-130]. The energy gap between the Li donor levels to conduction band of diamond is less than 0.3 eV [131] but effective Li doping is very difficult to obtain. One of the reasons for this is the low solubility of Li in diamond [132]. Researchers have previously attempted to incorporate Li into the diamond lattice by the processes of implantation [133-134], diffusion [135-136], and by gas phase in chemical vapor deposition (CVD) [137-138]. Othman et al. [101] have demonstrated the possibility of doping diamond with higher concentrations of dopants Li and N using lithium nitride suspension and gaseous ammonia, respectively. Their method resulted in a higher concentration of both species than those reported by previous diffusion and ion implantation studies, with no lattice damage.

Besides, as discussed in the introductory chapter and as will be seen later, tuning the conductivity of diamond, surface terminations can induce NEA (e.g. H, Cs, Li, etc.) and hence provide ways to tune the WF.

Oxygenation also plays a role in WF changes, as has been found in the cases of Si and Ge. Oxygen is also able to modify surface dipoles created by alkali metal adsorption. In the case of diamond, the lightest alkali metal, Li, on diamond surfaces has been observed to lower the WF of and at the same time form stronger bonds with the surface than the heavier alkali metals.

This has been demonstrated by O'Donnell [100] who performed the first ab initio calculations for Li adsorbed onto the C(100)-2×1 and C(100)-1×1:O surfaces. The results

showed a large NEA and high binding energy per Li atom for the system consisting of a full monolayer of Li, adsorbed on a fully oxygenated diamond (100) surface. These results indicate that the properties of Li adsorption on diamond generally agree with those of heavier alkali metals on silicon, diamond, and germanium. O'Donnell demonstrated the formation of a stable Li-O termination of diamond by physical vapor deposition of a monolayer of Li on the diamond surface which develops and exhibits NEA even at an elevated temperature of 800 °C [77] as has been mentioned in chapter 2.

The aim of the research reported in this chapter is to demonstrate an alternative method for the introduction and coordination of Li atoms with oxygen atoms on the diamond surface to establish a NEA. As mentioned earlier the introduction of Li atoms into diamond lattice has been demonstrated [101], but here the exploration is concerned with the novel and facile chemical means to realize a more controlled approach of creating a stable –O-Li dipole which will lead to NEA condition uniformly over the diamond surface. This study would also pave a way to visualize for the first time the effect of temperature on the concentration of Li atoms in the diamond and on the Li-O species on the surface of diamond sample which is crucial to forming a heterojunction based on Sn and Li on oxygen terminated diamond surface with a purpose of forming an enhanced and effective functional diamond surface.

5.2 Materials and Methods

Boron doped polycrystalline diamond (BDD) with dimensions of 10×10 mm, 0.6 mm thickness and HPHT Nitrogen doped single crystal (111) with dimensions of 3×3 mm and 0.3 mm thickness were used as the substrates. The process of nitrogen and boron doping is described elsewhere [101].

The substrates were acid washed with a solution of sulphuric acid (H_2SO_4) and potassium nitrate KNO_3 to remove any metallic contaminants present on the surface, this process

also terminated the surfaces with oxygen [139]. The substrates were hydrogen plasma treated in a microwave plasma at 900 °C for 2 min, followed by 2 min at 500 °C as described in [57]. This served to smoothen the diamond surface and has been proven to terminate the sample with hydrogen [60]. Lithium nitride (Li_3N), a source of Li, was obtained commercially as a powder from CERAC (99.5% purity, 250 μm particle size). It has already been established that the stability of Li_3N suspension with any oxygen free liquid increases with an increase in polarity of that liquid, with chloroform being the best of all [101]. So, a stable suspension containing 85 mg of Lithium nitride powder suspended in a solution of 5 mg of polyoxyethylene ether (POE) in 5 ml of chloroform was prepared. It resulted in a reddish-brown suspension which was sonicated for 1 hour in an ultrasonication bath.

The surface quality of both diamond substrates was analyzed with Raman spectroscopy for bulk damage to the sp^3 character or evidence of strong graphitization. The lithium nitride solution was drop cast on the surface of both substrates at a volume of 10 μL using a μ-pipette. The substrates were mounted in the NanoESCA facility and were annealed at different temperatures ranging from 500 °C to 850 °C under ultra-high vacuum (UHV) conditions.

XPS measurements were acquired with samples at RT with a monochromatic Al Kα source (1486.7 eV) in as prepared condition and after each annealing step. A pass energy of 20 eV was used, for an overall energy resolution of 600 meV. The angle between sample and electron analyser has been set to 45°. After annealing at 750°C and 850° C additional XPS measurements at more normal angle, i.e. 25°, were acquired, allowing more in-depth analysis of the sample.

5.3 Results and Discussion

Raman Spectroscopy was employed to establish the extent of graphitization and defect generation resulting from sample cleaning. Figure 5.1 indicates that there is no significant loss of sp^3 property on the surface of the HPHT diamond. No signs of significant graphitization or loss of sp^3 character was observed in HPHT diamond, however there is a small peak around 1540 cm^{-1}, which corresponds to the defect clusters in BDD diamond and could not be removed with acid washing. The acid wash did not create any visible defects while getting rid of the surface impurities and graphitized portions.

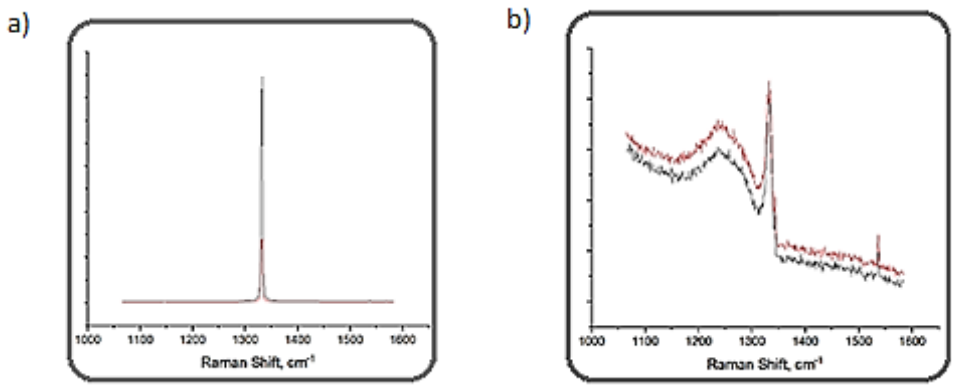

Figure 5.1: a) Raman spectra of HPHT Single crystal; b) Raman spectra of Polycrystalline Diamond using 785 nm laser. Black and red spectra represent before and after cleaning, respectively.

XPS gives us qualitative and quantitative information of the sample surface such as percentage composition and oxidation state of surface species. Figure 5.2 a) and b) show the O1s and Li1s peaks at different annealing temperatures. The deconvolution of the O1s peaks reveals the presence of a mix of ether and carbonyl bonds (a problem that we will discuss in chapter 7) while another peak for metal oxide can be seen at a lower binding energy of 530.8 ± 4 eV which can be attributed to lithium oxide group (Li_2O) [140]. At higher annealing temperatures we see a decrease in the peak area of O1s, indicating loss of oxygen. The metal oxide peak increases in area at 650 °C and thereafter starts decreasing at higher temperatures.

a)

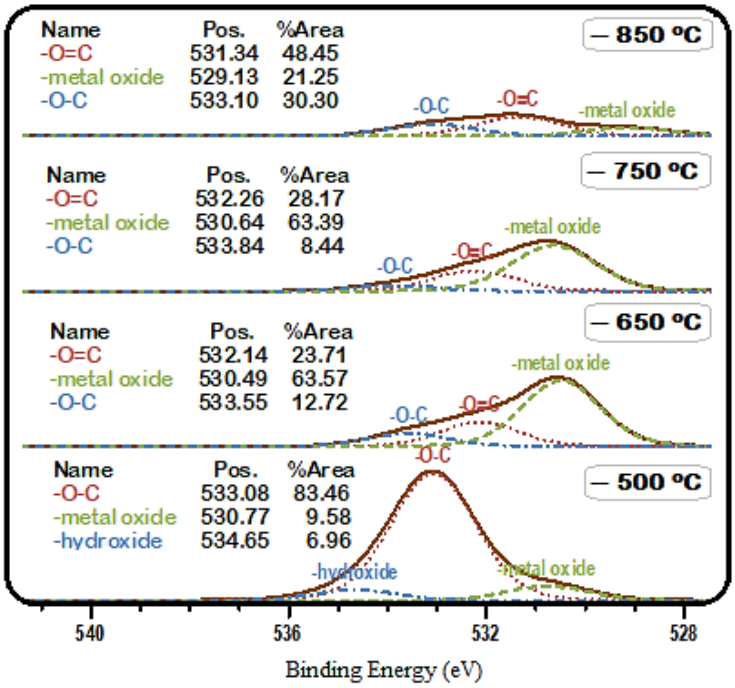

b)

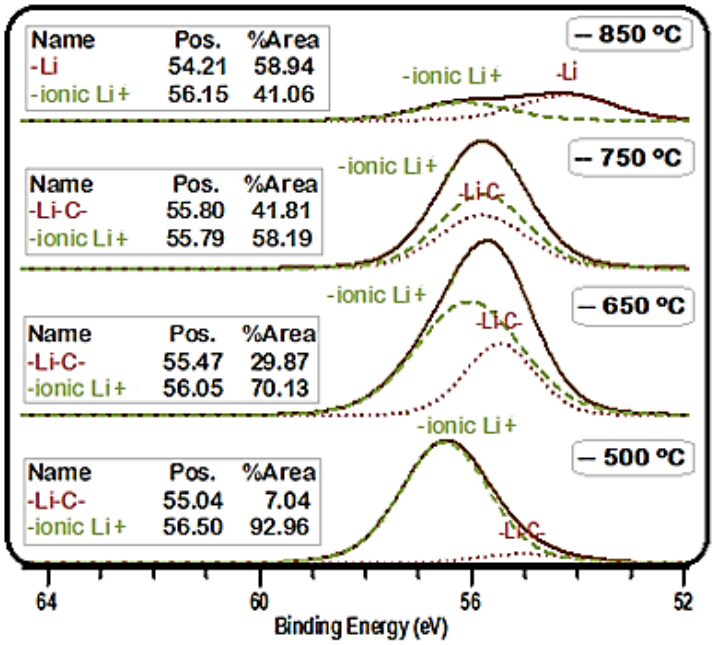

Figure 5.2: a) O 1s peaks and b) Li 1s peak; showing deconvoluted peaks at various annealing temperatures.

However, some of the oxygen is still retained at 850 °C which points towards the stability of oxygen terminated diamond surface as the oxygen doesn't completely escape with metal atoms but binds to the carbon atoms on the surface of diamond.

A similar trend can be seen in Li1s peaks where a deconvolution of the peak reveals the presence of ionic Li^+ component along with another low binding energy (B.E.) peak which can be attributed to the metallic Li diffused into the near surface bulk of diamond. However, this point cannot be proven by mere analysis of Li1s peak. For this reason, the ARXPS was performed in which the sample was tilted to an emission angle of 25° (to the normal of the sample surface) where it is less surface sensitive (LSS position) as demonstrated in Figure 5.3 a). Figure 5.3 b) and c) reveals the deconvoluted C1s peak at the annealing temperatures of 750 °C and 850 °C with XPS emission angle of 45° (slightly more surface sensitive, MSS) and 25° (LSS). The peak deconvolution at 750 °C reveals the presence of a diamond peak (boron doping) at 284.6 eV [57], a peak for single bonded carbon (-C-O-) at 285.6 eV and another peak around 283 eV which was attributed to the metal carbide bond [141], in this case [-Li-C-], although the peaks are very small with considerable uncertainty in the peak areas. The contribution of the metal carbide peak in LSS mode was found to be 2.04% of the total peak area while in the surface sensitive mode it was just 0.13% of the total peak area (a difference of more than 90%). This is interesting as it can be true only if Li has diffused into the near surface bulk of diamond. Othman et al. have demonstrated the successful co-doping of Li-N in the diamond crystal [101] using the same chemical process of Li deposition. Hence a stable interstitial doping [130] of the substrate with Li atoms at higher annealing temperatures is demonstrated along with the formation of stable Li-O- termination of diamond surface using the chemical route. A similar trend is seen when the sample is heated at 850 °C annealing temperature where the peak area of -M-C- peak in BS mode

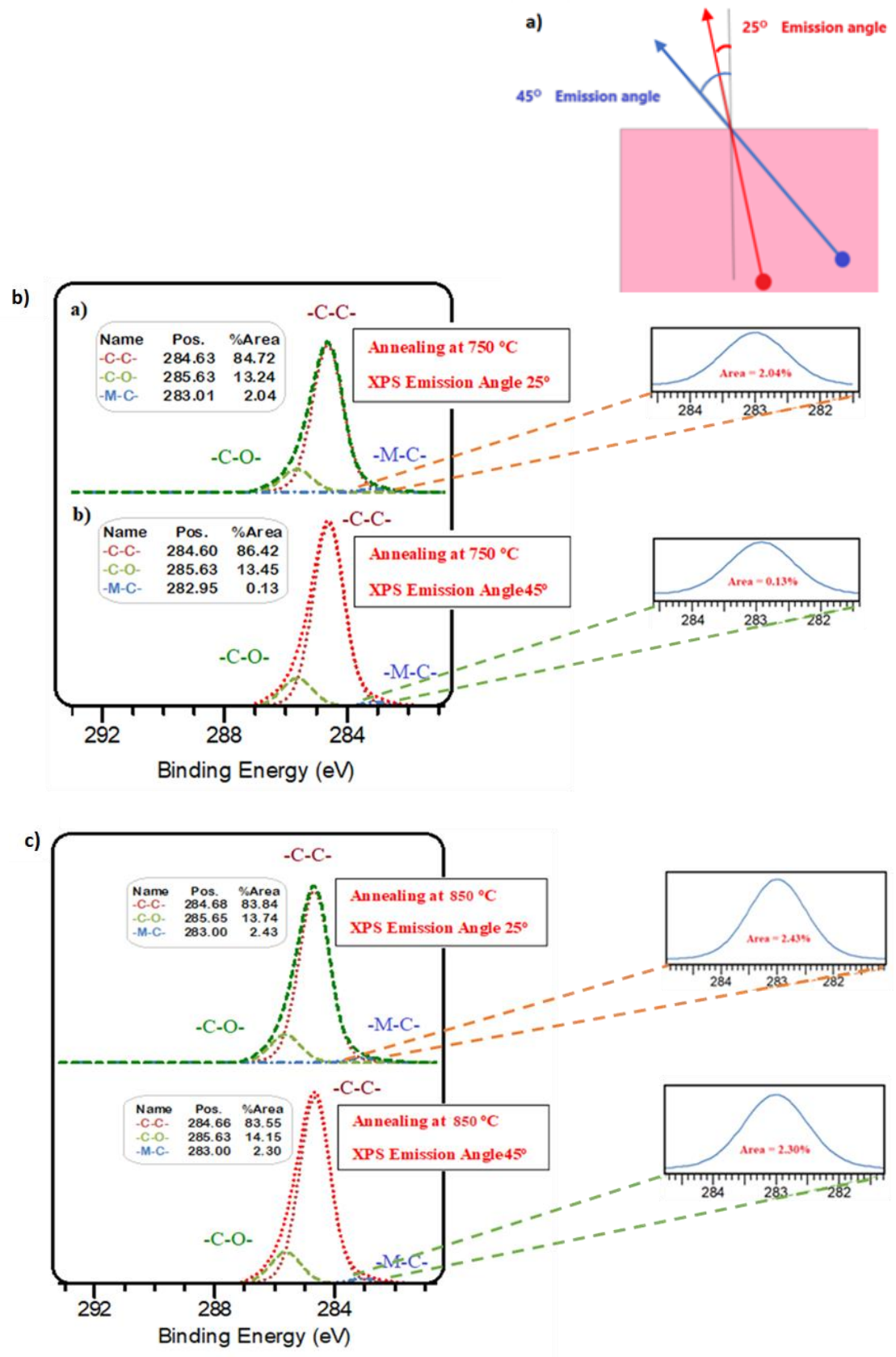

Figure 5.3: a) ARXPS showing (LSS) and (MSS) modes at 25° and 45° to the normal of the sample. b) ARXPS of C1s peak in the LSS mode (25°) and MSS mode (45°) at 750 °C. c) ARXPS of C1s peak in the LSS mode (25°) and MSS mode (45°) at 850 °C.

is more than 5% than in SS mode which shows that at 850 °C the Li in the bulk positions have diffused out to the surface. At 850 °C, the metal carbide peak in Figure 5.3 c) can be seen to decrease in area. At 850 °C, however, the significant decrease in the peak areas of O1s and Li1s in Figure 5.2 a) and b) is seen which was attributed to not only the expulsion of Li atoms from within the near surface bulk of diamond but also the desorption of Li-O- groups from the surface. This represents the complete dissociation of C^{+}-$(O\text{-}Li)^{-}$ structure on the surface of diamond, which is further strengthened by the fact that C1s peak is also seen to saturate towards ~285 eV with maximum intensity. The O1s peak can also be seen again shifting towards higher binding energy with decreased intensity (expulsion of O and Li from the surface) at the same temperature, a point that will be discussed later.

The discussion on the peak areas can be summarised by Figure 5.4 a) and b) in the form of the stoichiometric ratios between O:C, O: Li and C: Li for both samples. These were calculated by normalising the photoemission line areas by the relative sensitivity factors and plotted at different annealing temperatures from RT to 850 °C. The bar diagram shows that as the annealing temperature is increased, the Li:C ratio increases from 500 °C to 650 °C and then decreases slightly to 750 °C and then significantly at 850 °C both in LSS and MSS modes. It can also be seen that N doped diamond shows more stable response to higher annealing temperature than B doped polycrystalline diamond. This could be due to many grain boundaries which can affect the incorporation and diffusion of Li into the near surface bulk in polycrystalline diamond than in single crystal diamond. The O:C ratio has been seen to decrease with annealing temperature while Li:O first increases and then decreases beyond 750 °C. A similar trend has been seen in case of nitrogen doped HPHT diamond. This phenomenon is explained in the discussion section

of this chapter after the important and crucial findings have been discussed first. Figure 5.5 b) shows the B.E. shift of C1s, O1s and the C:O relative shift.

a)

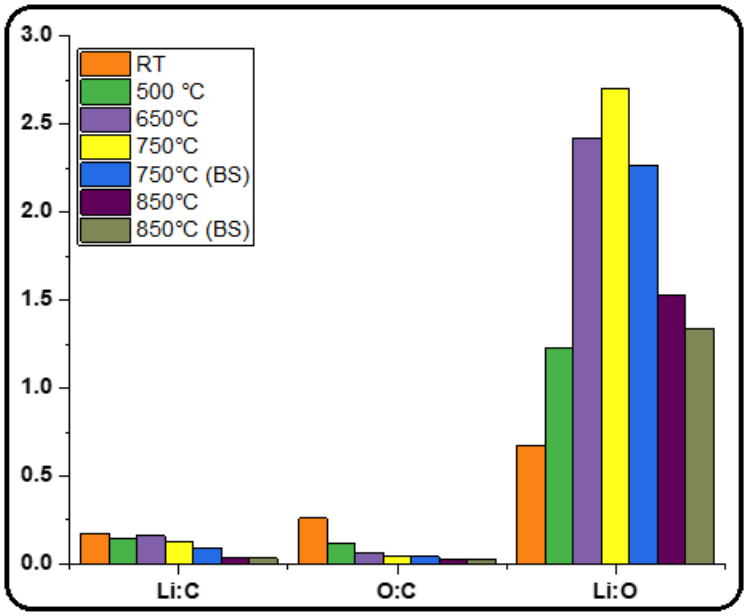

b)

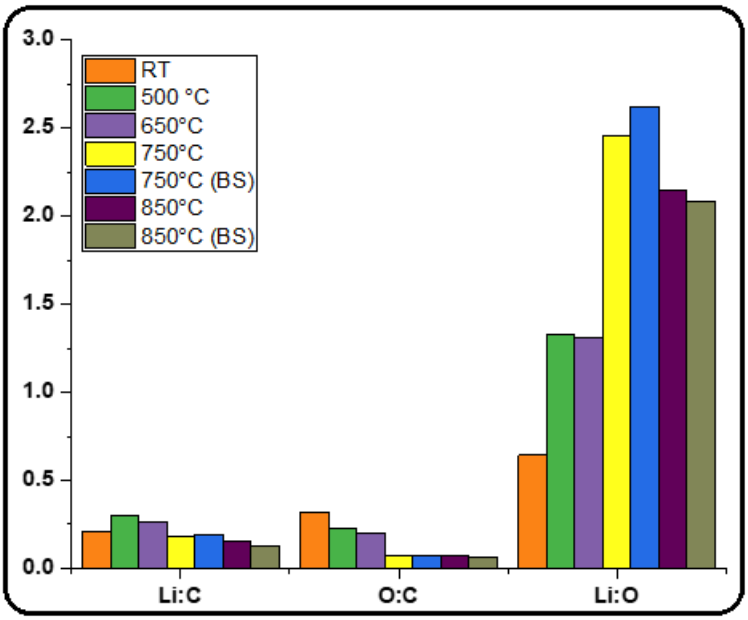

Figure 5.4: a) The relative intensities of Li:C, O:C and Li:O ratios; for Boron doped polycrystalline diamond. b) Relative intensities of Li:C, O:C and Li:O ratios for Nitrogen doped single crystal diamond.

A peak shift occurs due to the formation of surface dipole between the higher electronegative species O and the lower electronegative C atoms which results in the

formation of C+ - O^- dipole as demonstrated in figure 5.5 a). When Li atoms interact with O it results in the transfer of more charge and hence negative potential on O atoms which leads to a lower B.E. as can be seen in the figure 5.2 a) and figure 5.5 b) where peak shifts of O have an upward trend. A similar trend can be seen in C atoms. The Li diffusion into the near surface bulk region of diamond would increase the electric potential on the C atoms and hence a shift of C atoms towards lower B.E. (this can also be seen as an upward trend in C1s shift in figure 5.5 b). A plateau was seen in case of C1s peak shift at the annealing temperature of 650 °C which indicates a saturation point has been reached. O atoms reach their maximum shift at 650 °C, thereafter the shift decreases slightly. This can be interpreted in the following way. The near surface bulk of diamond reaches a saturation point of retaining Li atoms at 650 °C which continues through 750 °C while the maximum interaction occurs between Li and O atoms at the surface at 650 °C indicating the formation of a sub monolayer of -O-Li- termination (Li_2O) on the surface of diamond. After 750 °C, the Li atoms start coming out of the diamond bulk and at the same time Li-O- surface groups start desorbing from the surface resulting in the shift of C1s peak towards higher B.E. (a downward trend in B.E. of C1s). Similarly, the surface bonded O also shifts slightly towards higher binding energy due to Li leaving the surface along with the desorbing O atoms at higher annealing temperature of 850 °C. The shift and asymmetry in C1s peak of diamond surface with functionalisation has been attributed to the surface band bending and surface state formation. This can be calculated using Maier's approach [66]. Using the B.E. of the C1s bulk core level component and the fixed energy separation of 283.9 ± 0.1 eV between the VBM and the C1s core level, the VBM values at various annealing conditions were calculated as shown in figure 5.5 c). CBM was calculated by adding experimental band gap value of 5.47 eV to the VBM. There is a slight upward band bending of 0.05 eV at annealing temperature of 650 °C at which saturation of Li-O bonding and Li diffusion into near surface diamond bulk occurs which

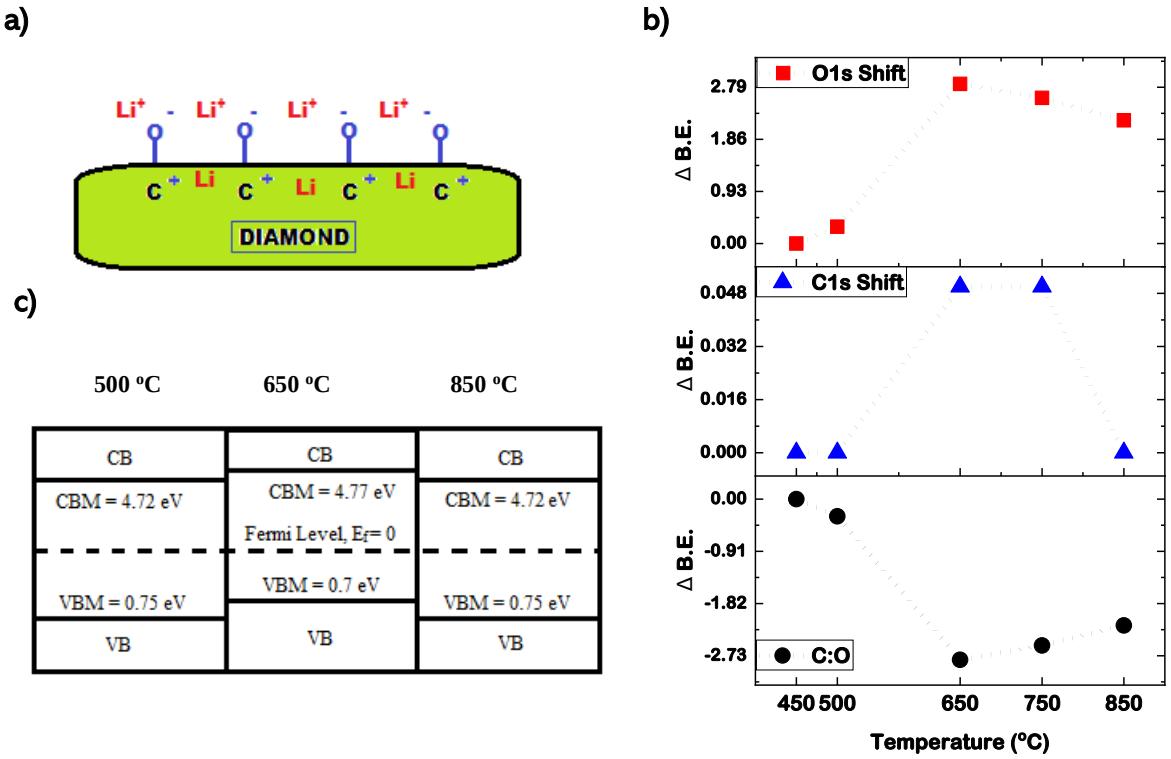

Figure 5.5: a) O-C dipole representation of the diamond surface showing the dipole between C-O due to charge transfer between the species. b) O1s, C1s and C:O relative shifts showing a saturation point at 650 °C and significant changes at 850 °C as explained. c) The band structure of diamond showing the position of VBM and CBM at 500 °C, 650 °C and 850 °C.

then bends again downwards (similar to the XPS peak shift) at 850 °C due to the expulsion of Li atoms from diamond bulk and desorption of Li-O- groups from the surface. This upward band bending due to Li diffusion could be detrimental to some of the properties of the diamond surfaces intended for their use in thermionic emission or other cleaner energy production use.

5.4 Discussion

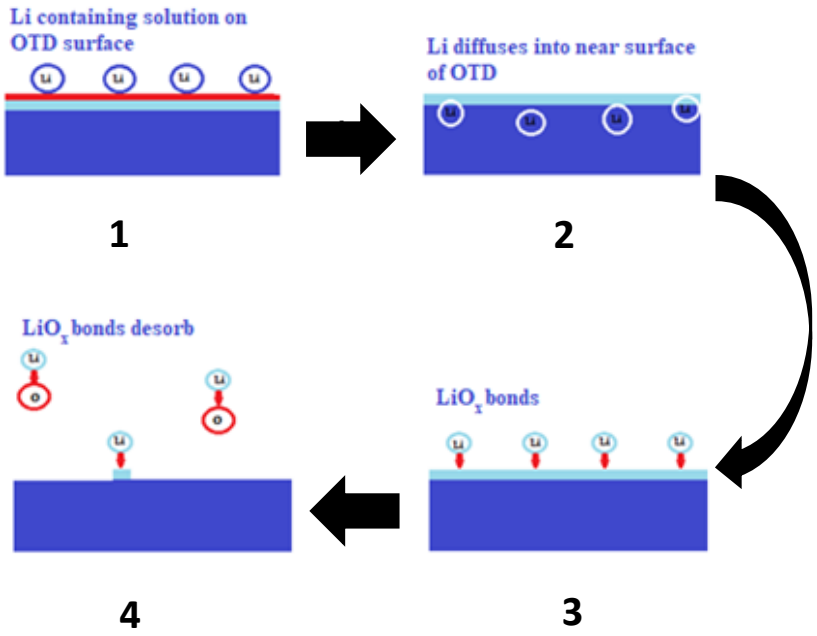

Figure 5.6: The process of O-Li adsorption and Li diffusion into the near surface diamond bulk at the initial annealing temperatures and desorption of -O-Li- *groups at higher annealing temperatures.*

A possible explanation summarizing the results obtained could be, as diagrammatically shown in figure 5.6, that initially upon annealing at 500 °C, Li starts to break out of the solution and starts bonding with the oxygen which is present on the surface of the diamond. These are bonded as a mix of ether and carbonyl bonds to form a -O-Li- termination (Li_2O) on the diamond surface. The existence of solely ether or ketone terminated diamond surface is far from the achievements in this very field of research. The ether and carbonyl bonds each have their own effect on the surface structure and properties of the diamond surface [142] as has been seen in the DFT studies mentioned in the chapter 4. Hence in order to have a very discreet study of any metal termination (or even oxygen termination) on the surface of diamond and to achieve distinct properties based on different differently bonded surface oxygen, we need to focus our research on exclusively forming either an ether terminated oxygen surface, or a ketone terminated diamond surface or find some ways to transform either of the two into one type of oxygen

termination. Some of the Li atoms enter the interstitial sites inside the near surface diamond bulk and impart negative potential to the C atoms. As annealing temperature increases to 650 °C the Li-O bonding reaches saturation, and we see a change in C1s peak shift and band structure changes. The stability of Li termination on the surface of diamond and Li atoms inside the diamond bulk has been established before [58, 101]. No change occurs at 750 °C until the annealing temperature is further increased to 850 °C where the Li which is mobile inside the diamond lattice [101, 130] starts diffusing and forms -O-Li groups many of which desorb at the same temperature from the surface [119]. Thus, a chemical route of creating O-Li termination on the surface of diamond and diffusion of Li atoms into the near surface bulk, was determined. This was stable and existent up to 850 °C.

An increase in the surface conductivity can be expected with increasing Li concentration in the near surface bulk as a shift in the VBM and conduction band minimum was seen (figure 5.5 c). Moreover, Li also increases the electron density near the surface of the diamond and hence changes the surface conductivity as well. This trend can be seen up to 650 °C and falls drastically at 850 °C at which point the Li has almost fully desorbed from the near surface bulk of diamond as seen in Figure 5.3 c).

Lithium and lithium oxide termination of diamond has been shown to induce NEA on the surface of the diamond and hence decrease the WF significantly up to a temperature of 800 °C [6, 119]. Hence, a decrease in the WF of the diamond surface in our sample up to 750 °C, is expected. Up to this temperature O-Li bonds are stable on the diamond surface before they desorb at 850 °C. This provides an insight into the stability of Li on the surface of oxygen terminated diamond. Li and lithium oxide termination of diamond hence are unstable beyond 750 – 850 °C temperature regime which is one of the crucial points that needs to be considered for any future into lithium-based termination of

diamond. As we will discuss in chapter 6, the stability of Li (and hence its oxide form) is increased by the inclusion of Li atoms into the heavy metal oxide layers which in our case is SnO on the surface of diamond. This point can perhaps be generalised to all the alkali metals and heavy metal oxide based heterostructures on the surface of diamond or other substrates as well which point not only towards the increased stability of alkali metals on the surface of substrates (like diamond) but also present surprising properties such as ultra-low WF, increased secondary electron yield, decreased surface roughness, etc. Not only that, with this piece of study a new research area of intercalated alkali and heavy metals (and their oxides) opens up for the efficient and more stable surface termination of wide band gap substrates like diamond.

5.5 Conclusion

The interaction between Li, O and C species on the surface of diamond was visualised with increasing annealing temperature. This study is motivated by a need to identify a temperature-stable metal oxide functionalised diamond surface for use in vacuum thermionic energy converter devices. The possible intercalation of Li inside the diamond sample has also been demonstrated. Li was shown to reach the surface of the diamond crystal as the temperature is increased to form a stable ethyl termination up to 850 °C. This is a novel and easy chemical approach of forming such terminations as previously it has only been demonstrated using PVD methods. This work has been able to confirm O-Li functionalisation by this method from the relative intensity and shifts in XPS peaks from XPS analysis of BDD and Nitrogen doped HPHT single crystal samples. Such findings could serve as an insight into the alloy termination of diamond with alkali and other higher order metals, some of which (e.g. Sn_2Li_5) have been predicted to lower the WF significantly.

Chapter 6

Structure and electronic properties of Tin monoxide and lithiated tin oxide terminated diamond (100) and its comparison with lithium oxide terminated diamond

Summary

Most of the material for this chapter has been taken from the publication.

***S. Ullah**, G. Wan, C. Kouzios, C. Woodgate, M. Cattelan, N.A. Fox, "Structure and electronic properties of Tin monoxide (SnO) and lithiated SnO terminated diamond (100) and its comparison with lithium oxide terminated diamond", Appl. Surf. Sci. 559 (2021) 149962.*

These manuscripts were written through contributions of all authors as mentioned below. All authors have given approval to the final version of the manuscript.

***Sami Ullah**: Investigation, Methodology, Conceptualization, Software, Visualization, Writing - original draft. **Gary Wan**: Validation, Resources, Writing - review & editing. **Christos Kouzios**: Investigation, Writing - review & editing. **Cameron Woodgate**: Investigation, Validation. **Mattia Cattelan**: Conceptualization, Resources, Data curation, Writing - review & editing. **Neil Fox**: Writing - review & editing, Supervision, Funding acquisition.*

In this chapter, an introduction to the metal oxide and heterostructure based terminations of diamond has been presented along with the techniques to experimentally perform such studies. The Lithium oxide-based termination, tin monoxide based termination and tin/lithium oxide (heterostructure) based terminations have been realised (experimentally formed) on the surface of diamond, leading to the negative electron affinity and lower work function on the diamond surface. A solution to the much-debated issue of "reliably" forming tin monoxide rather than tin dioxide (a more stable form of tin oxide) is presented. It has been established that heterostructures based on alkali and heavy metal alloys on the surface of diamond presented an interesting interaction that not only led to the interesting properties but also the improved stability of alkali metals and improved electron emissions from the surface of diamond which is a remarkable outcome that opens a new chapter, in the diamond research, of heterostructure based terminations of diamond. All of this has been shown to be an outcome of advanced spectroscopic techniques on NanoESCA platform at the University of Bristol, UK.

6.1 Introduction

In chapter 4, it was established theoretically that the Sn atoms form an effective NEA imparting termination of diamond (100) surface with QML and HML coverages more dominant in terms of stability. There is a predominant covalent nature between the Sn and surface C, O atoms, hence stronger bonding. A QML of Sn on bare diamond has resulted in NEA with a large adsorption energy while a HML of Sn on OTD has resulted in much larger NEA and adsorption energy which is expected due to the fact that oxygen inclusion increases sticking coefficient and hence bond strength between the atoms. These positive insights encourage the deposition of Sn on the surface of diamond and the observation of NEA and WF using the physical deposition methods and novel spectroscopic techniques, respectively, as will be discussed later.

As has been discussed earlier various metal terminations have produced interesting results on the surface of diamond. Hydrogen termination has been demonstrated to impart a NEA value of -1.3 eV measured experimentally to the diamond surface [57, 60, 143]. However, besides being widely studied, hydrogen terminated diamond surface suffers from the problem of instability due to hydrogen desorption at higher temperatures [11]. When either H desorbs or is replaced by O, the NEA character is lost. Another problem with hydrogen terminated surfaces is water adsorption on H-terminated surfaces which leads to charge transfer and hence upward band bending [144- 145] which again causes loss of NEA. As an alternative, a monolayer or sub monolayer coverage of some of the electropositive group I and II metals [68, 69, 146, 147] and first row transition metals (TMs) [70, 71, 118, 120, 148] on the bare and oxygenated diamond surface have been found to be a suitable candidate for diamond surface termination. Since most of these metals do not form a stable monovalent bond with the surface C atoms, hence oxygen termination on diamond (OTD) surface becomes necessary as O inclusion increases the sticking coefficient between the surface species. The key here is to induce

stronger bonding between the metal layer and the underlying diamond surface and hence a large surface dipole. In other words metal oxygen and carbon oxygen bonds have been found to be stronger and highly stable than metal carbon bonds [74, 75]. All other metal terminations like Cs, Al, transition metals, etc., although result in NEA and lower WF, but face the similar problem of instability at elevated temperatures. However, as has been mentioned in chapter 2, stable low WF surfaces in thermionic emission devices are required to work at higher temperatures. Kane M O'Donnell [77] have been able to demonstrate air stable lithium (Li) -O terminated NEA diamond surface successfully with controlled atomic layer coverage and stability at 800 °C. However, the problems associated with Li such as explosive nature, instability beyond 800 °C, entering the near surface bulk sites of diamond thereby changing the diamond properties demand developing investigating novel non-toxic, eco-friendly, non-risky, abundantly available element (metal) for diamond surface termination which is tin (Sn). Not only that these problems also demand developing methods to increase the stability of Li on the surface of diamond.

Tin (Sn), a same group element with Si and Ge, being a novel termination that we explore in this study has been ignored as a potential candidate for the studies on metal and metal oxide termination on the diamond surface. Recently, Si termination on diamond (100) has been found to result in an NEA of 0.86 ± 0.1 eV while Ge terminated diamond has resulted in an NEA of 0.71 eV. However, Si terminated diamond is unsuitable for the ambient environment due to its high reactivity and any application in the atmospheric environment would need a protective SiO_2 coating on the top. Tin and Tin oxide (monoxide) is expected to modify the surface structure of diamond and enhance the electronic properties of diamond as the theoretical DFT based investigation has already revealed in chapter 4. As a known fact and as mentioned before in the same chapter,

SnO is a capable and promising p-type semiconductor with an experimental, small indirect bandgap of 0.7 eV [81] and a direct energy gap that ranges from 2.5 to 3 eV [82], Sn is abundantly available with non-toxic nature. Sn vacancy has been found to be the main source of p-type nature of SnO which can be altered by proper doping. On top of that in the bulk form Sn, alloyed with alkali metals (Li, Na, etc.) in a specific stoichiometric ratio has been found to possess ultra-low WF in bulk form e.g. Sn_2Li_5 has been found to possess a WF of 1.25 eV [83].

Moreover, it has been found theoretically that lithiation of pristine SnO layers results in the formation of stable layered "sandwich type" structure with Li_xO layers in between the Sn atomic planes [88] which makes it interesting to explore experimentally as well. Such stable structures combined with or on top of the diamond substrates and their interaction with the diamond surface would be an interesting area to investigate with the purpose to demonstrate a highly stable and high temperature resistant, NEA imparting termination on the surface of diamond which is the scope of this chapter.

The possibility of depositing SnO as a stable and efficient NEA imparting termination on the surface of diamond (100) is investigated experimentally, supporting the important results with the data from the theoretical investigation using the DFT code. It is also demonstrated that stable SnO is formed on the surface of diamond (100), reliably, by PVD technique, shedding light on heavy metal oxide terminations and their effect on electron affinity. Reliable formation of a stable SnO layer and discerning it from the SnO_2 (a widely studied and more stable form of tin oxide) has been deemed as one of the unfulfilled goals in this aspect of material research as the surety of obtaining a phase pure SnO has been lacking due to non-availability of a reference. A range of surface science techniques discussed in chapter 3 have been used to characterise the formation of SnO on the surface of diamond.

Using the similar techniques, the Li is deposited and its interaction with SnO is investigated. Through a range of surface science techniques, we have characterised the formation of SnO and SnO_x/Li_2O termination on the surface of diamond.

6.2 Methods

6.2.1 Diamond preparation

High Pressure High Temperature (HPHT) boron doped single crystal diamonds (purchased from Element Six (145-500-0248 and MM 111/4010) with a boron doped layer on top was used in this experiment. Boron doped layer was grown in hot filament chemical vapor deposition reactor, described in chapter 3, using a gas mixture comprising H_2, CH_4 (both Air Liquide, Ltd) at a flow rate of 200 and 2 standard cubic centimetres per minute (sccm), respectively, i.e. 1% CH_4 in H_2 and 5% B_2H_6 in H_2 (BOC Group, plc) with a flow rate of 0.1 sccm for epitaxial B-doped layers on single crystal diamond. The treatment was carried out for 60 minutes at a pressure of 20 Torr and a temperature of ~2300 K which enables a deposition of a good quality diamond thin film at a growth rate of ~0.5 μmh^{-1}. BDD overlayers grown in the same reactor under the same conditions has previously been shown to contain a boron concentration of up to ~10^{20} cm^{-3}, measured from a depth profile using secondary ion mass spectroscopy [149]. The cleaning of the sample surface along with hydrogen termination was done by microwave plasma method, described in chapter 3, using a pure hydrogen plasma at 900 °C for 2 minutes, followed by another 2 minutes at 500 °C as described in [57]. The samples were treated with ozone for 30 minutes to render it O-terminated which was later made evident by XPS analysis.

6.2.2 Ultra-high Vacuum techniques

The film deposition and analysis of the sample were carried out completely under Ultra-high Vacuum (UHV) conditions in interconnected chambers described in chapter 3.

Before starting any analysis or deposition, samples were cleaned by annealing the sample at a temperature of 300°C for 60 minutes under UHV conditions to remove water and adventitious carbon contamination [150].

6.2.3 Thin film deposition

Sn metal deposition was achieved by e-beam deposition, as described in chapter 3. Tin granules were evaporated from a molybdenum crucible. The thickness calibration was optimized by a quartz micro-balance. 0.8 ML of tin was deposited at a temperature (substrate) of 327 °C on the surface of diamond (100).

Li deposition was achieved using a thermal evaporator, as described in the same chapter (3) which consisted of a boron-nitride crucible resistively heated by a tungsten filament. A thermocouple was present in the evaporator to monitor crucible temperature. The crucible deposition temperature was set to 410°C.

Molecular oxygen dosing was performed at an oxygen pressure of 1.5×10^{-6} mbar. Atomic oxygen dosing was achieved by dosing O_2 trough a gas cracker at 1.5×10^{-6} mbar.

6.2.4 Analysis methods

A series of surface analyses were performed at each step of the sample preparation, i.e. X-ray photoelectron spectroscopy (XPS), Spot profile analysis – Low energy electron diffraction SPA-LEED, Ultra violet photoelectron spectroscopy (UPS), WF maps, Angle resolved photoemission spectroscopy (ARPES). All of these techniques are individually described in chapter 3.

XPS was carried out using a monochromatic Al K_α source (1486.7 eV) and the electron analyser at 45° to the sample normal.

SPA-LEED was used with electrons at 100 eV to investigate the surface roughness and reconstructions.

UPS and full wave vector ARPES were carried out using monochromatized He I and He II sources with energy of 21.2 eV and 40.8 eV, respectively. WF mapping was done using a non-monochromatic mercury (Hg) lamp source of ≈5.2 eV. WF maps of the samples were generated from fitting EF-PEEM images close to the WF cut-off edge, using a pixel-by-pixel sigmoid fit. The lateral resolution of the WF map was less than 150 nm.

6.3 Results and discussion

Here the results are presented in the form of XPS, SPA-LEED, UPS, WF data. A very brief introduction to the main techniques used in this chapter (and as discussed in chapter 3 in detail) are presented here. XPS, a core level spectroscopic technique, helps to analyse the top few atomic layers of the diamond surface qualitatively and quantitatively. It also helps to determine the stoichiometry of the surface species along with nature of the dipole formed on the surface of diamond. SPA-LEED gives information on the surface structure of diamond in the form whether there was any surface transformation or more specifically surface reconstruction due to metal adsorption. It also helps to determine the quality of the film produced on the surface of diamond. UPS and ARPES aids in determining the band structure, hence revealing electron affinity and band bending due to metal deposition on the surface of diamond while WF maps help to determine the WF of the surface and determine any transformation of the surface due to metal film deposition.

Some of the important results from the DFT calculations, performed in chapter 4, are presented here briefly at various places to support the XPS and WF data on SnO terminated diamond. The XPS and UPS data for Li-O-terminated diamond are also presented here briefly as this work has been done already in detail [6, 151], to compare

it with SnO- terminated and SnO_x/Li_2O-terminated diamond surface. The differently terminated surfaces will present different photoemission properties with Li-O-terminated diamond already known to possess NEA [58, 151] while SnO terminated diamond and SnO_x/Li_2O terminated diamond will be a new exploration.

6.3.1 Lithium oxide terminated diamond

Li was deposited on oxygen terminated single crystal diamond (B-doped C(100)-(1×1):O) [152] in different conditions, at RT and subsequently annealed at 500 °C and 800 °C. Quantitative XPS information shown in Table 6.1 shows that the Area % of Li was reduced by the 60 minutes 500°C annealing, and completely removed by a 15 minute 800°C anneal. Oxygen was also largely removed at 800°C, indicating that the carbon-oxygen bonds were broken rather than the Li-O bonding due to a small amount of oxygen remaining with no detectable Li remaining.

To understand the process of O-Li adsorption and removal with annealing temperature on the surface of diamond, component analysis of the oxygen peak is shown in figure 6.1. A component at low binding energy is linked to the O-Li peak in figure 6.1 b). The component became the most relevant after annealing at 500 °C implying that the lithium is distributed on the surface, however SPA- LEED acquisition (Figure 6.2) shows no new visible reconstruction other than the same B-doped C(100)-(1×1):O, which could mean a (1x1) reconstruction or amorphous layer on the surface which is counter-intuitive as Li has been found to form (2x1) reconstruction on the surface of diamond (100) [77, 151]. However, we believe it to be retention of (1x1) reconstruction, in which LiO groups form nanoclusters of islands on the diamond surface which doesn't cause surface reconstruction, rather than an amorphous layer due to the fact that 500 °C is too high of an annealing temperature for an amorphous LiO layer to exist especially when we see

much of excess Li going away (expelled) at such a high temperature and due to the fact that the surface species are expected to form a pattern at such temperature.

Table 6.1. Quantitative XPS survey peak information showing that the amount of Li is reduced by the 500°C anneal and removed by the 800°C anneal.

Sample	Peak	Area %
Pre Li	O 1s	6.4
	C 1s	93.6
	Li 1s	-
Li Deposited	O 1s	8.67
	C 1s	80.35
	Li 1s	10.98
500 °C Anneal	O 1s	5.26
	C 1s	87.88
	Li 1s	6.68
800 °C Anneal	O 1s	0.51
	C 1s	99.49
	Li 1s	-

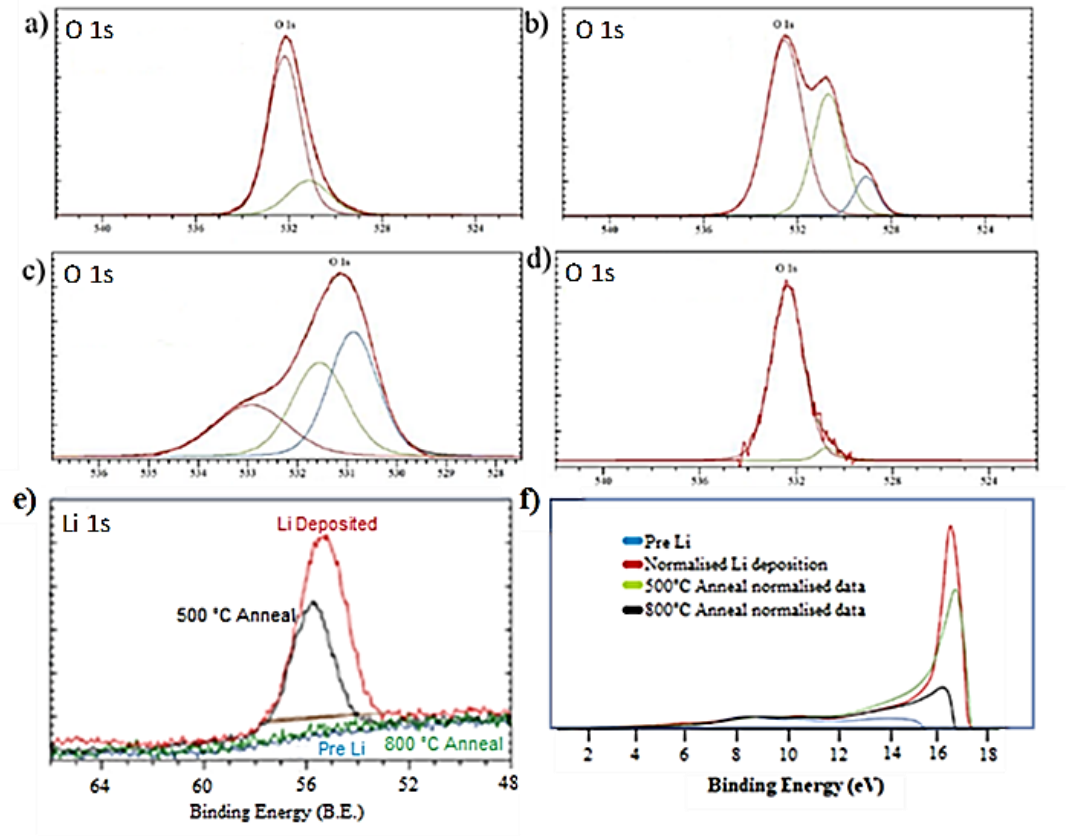

Figure 6.1: XPS Oxygen 1s peaks with fitted components showing all changes in size, shape and position in a) Pre Li, b) Li deposited, c) 500°C anneal, d) 800°C anneal and e) Li peak shape changes with annealing temperature. f) UPS spectrum for LiO terminated diamond.

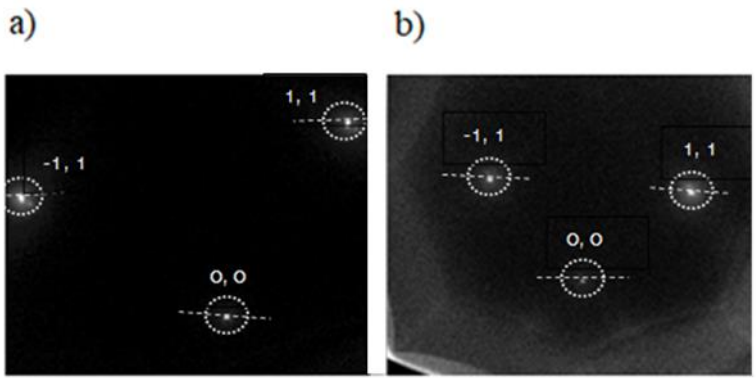

Figure 6.2: SPA-LEED images of a) Oxygen terminated diamond; b) Li_2O terminated diamond after annealing temperature of 500 °C for 1 hour revealing 1 × 1 reconstruction of the surface. SPA-LEED was taken with an electron energy of 100 eV. The 1 × 1 spots are marked by the white circles, while the intensity of each spot was measured along the white dashes at the respective points. Spa-LEED images show the order at the surface is retained after SnO termination on the surface of diamond and also after Li deposition.

With 500°C annealing the component peaks shift towards the higher binding energies with a large apparent O-Li component at 530.9 ± 3 eV [140] while Li is at 56 eV [119]. During the annealing, heating evolves 'bulk' lithium with a different bond energy to Li-O, perhaps approaching a sub-monolayer, evidence of which can be seen in the reduction of Li peak intensity and area in Figure 6.1 e).

6.3.2 Tin oxide terminated surface

In order to analyse the SnO_x/Li_2O terminated diamond structure later, first we have to study the formation of SnO on the surface of diamond. DFT calculations have revealed the possibility of terminating the diamond (100) surface with Sn atoms and the suitable configurations of Sn on OTD, worthwhile to be repeated here briefly. It was seen that Sn produces NEA on the surface of OTD (100) in nearly all configurations. Larger adsorption energies were obtained at QML (0.25 ML) and HML (0.5 ML) of Sn on oxygen terminated diamond (both ether and ketone of oxygen termination were considered). Sn was seen to prefer a position on top of oxygen rather than in between (bridge) the two oxygen atoms. A very low adsorption energy was obtained with the FML (1 ML) of Sn on diamond which could be because of the large size of Sn atoms and increased electrostatic repulsion between them, hence no bonding occurring between the Sn atoms and the surface C atoms of diamond. The two most stable configurations of Sn in QML and HML configuration can be seen in figure 6.3. An NEA of -1.37 eV was obtained with an E_a of -6.03 eV at HML of Sn on top of carbonyl oxygen atoms while an electron affinity (EA) of 0.16 eV with an E_a of -6.45 eV was obtained for QML of Sn in the same configuration. However, for a QML of Sn i.e., 1 Sn atom, on top of OTD (ether terminated), an NEA value of -0.86 eV was obtained with an E_a of -5.9 eV.

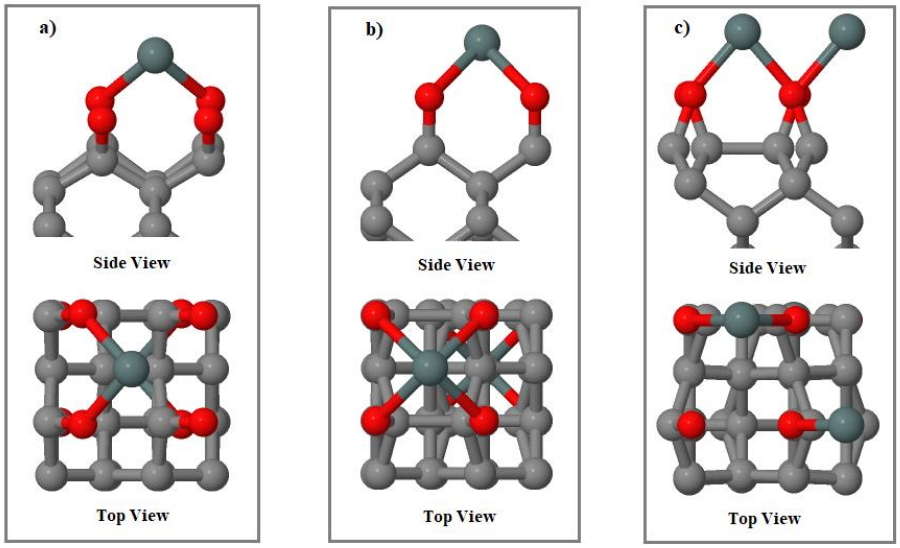

Figure 6.3: Geometry optimised output structures showing a) QML (1 atom) of Sn on the oxygen (ether) terminated diamond which has resulted in no surface reconstruction. b) QML (1 atom) Sn on the oxygen (ketone/carbonyl) terminated diamond; the breaking of ketone bond has resulted in the surface reconstruction between the C atoms. c) HML where 1 Sn is in between the two O (ketone) atoms hence resulted in reconstruction (or C-C bond) on the surface whereas the other Sn atom in on top of another O atom. All of these configuration show NEA with a large E_a. This figure is reproduced with colour modification from chapter 4.

6.3.3 Deposition of Tin on OTD

Sn was deposited using e-beam deposition technique at a temperature of 327 °C on the surface of OTD (100) which is slightly higher than the melting point of Sn, increasing the possibility for the rearrangement of Sn atoms on the surface of diamond. A quartz microbalance was used to optimise the sub monolayer deposition of Sn on the surface of B-doped C(100)-(1×1):O.

Initially after the deposition, a metallic peak of Sn was observed at a lower binding energy of 484.9 eV [153] along with an oxide peak at a higher binding energy of 485.5 eV [154]. The presence of the two peaks implies partial oxidation of thin sub monolayer Sn film or clusters to form SnO nanocluster (oxides) on the surface of diamond (100) as Sn has been shown to form nano-oxides on the surface of other substrates e.g. Pt [155] in different patterns. The ideal case in our study would be to form a continuous layer of SnO on the surface of diamond.

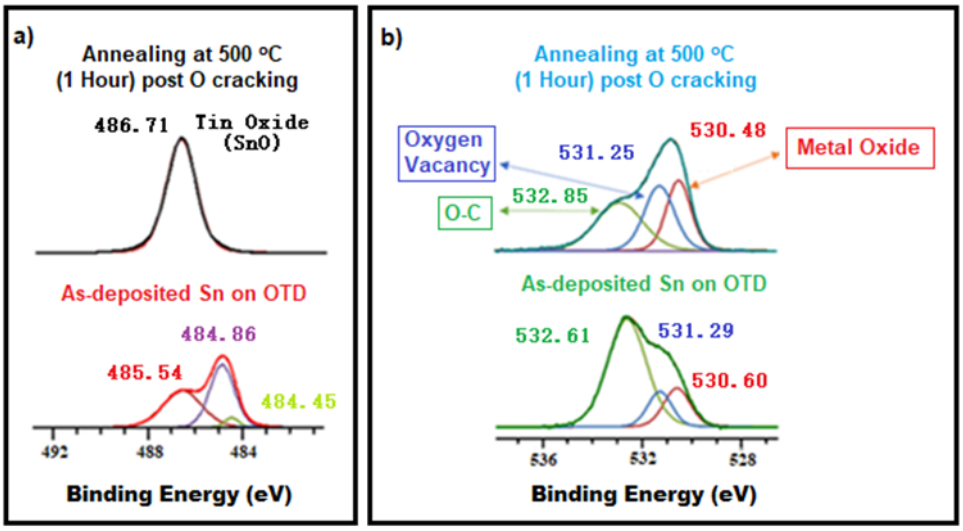

Figure 6.4: XPS of the sample at each process step showing a) Transition of Sn from metallic and oxide combination to pure oxide phase using oxygen cracking and annealing. b) Change in Oxygen peaks during the process. We have a peak for metal oxide and an oxygen vacancy peak at 530.5 eV and 531.3 eV [7].

The sample was initially annealed at 600 °C for 60 minutes without any significant changes in the film. Atomic oxygen exposure by oxygen cracking was found to be the most effective method in our experiments to transform metallic Sn into SnO than the molecular oxygen exposure. The sample was exposed to the atomic oxygen (oxygen cracking) for 70 minutes at a pressure of ~10^{-6} mbar at the RT and then annealed at 500 °C for 60 minutes again. As can be seen in figure 6.4, the presence of a O 1s component at lower binding energy along with the Sn3d oxide peak confirms the controlled formation of SnO termination on the surface of diamond, while another oxygen vacancy peak, responsible for the p-doping of SnO film, at slightly higher binding energy has been reported by B. E. Park et al. [7]. Oxygen vacancies are point defects and contribute to the high conductance of metal oxides due to being a source of excessive electrons. Tin oxides (SnO_x) are known to exhibit intrinsically high amounts of oxygen vacancies due to the multivalence of Sn cation [7]. We believe that we have been able to form SnO rather than SnO_2 on diamond (100) due to the presence of Sn4d spin orbit doublet and the fact that any further process (Li deposition and annealing in our case as described in the next

section) results in the Sn4d spin orbit doublet retaining its shape for SnO adsorbed layers as can be seen in figure 6.5, while as it transforms into a 4 peak structure for SnO_2 [156].

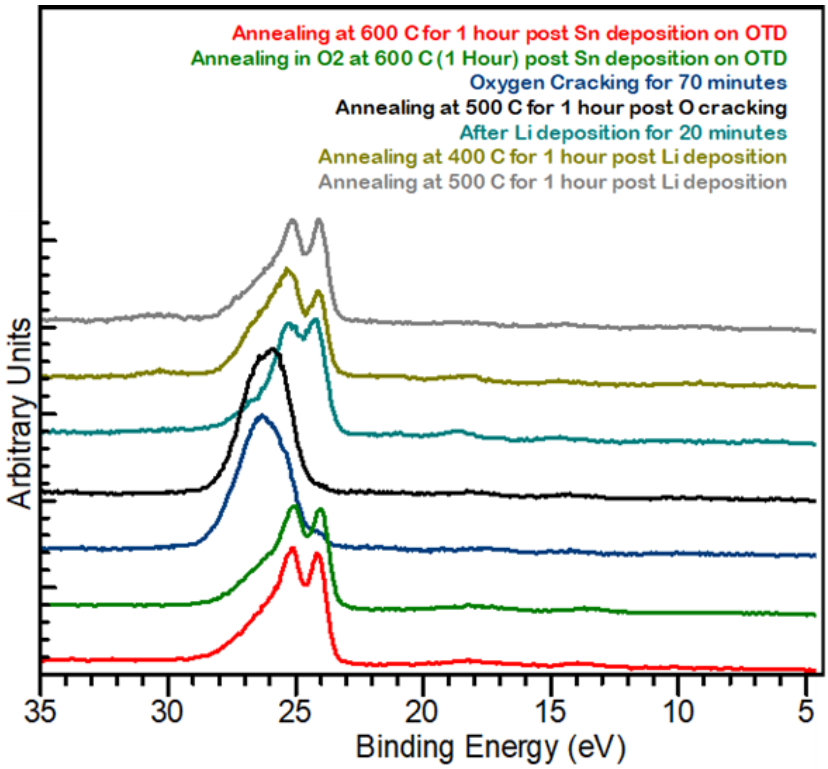

Figure 6.5: Sn4d spectra at various surface processes, confirms the presence of SnO rather than SnO_2 on the surface of diamond. The presence and retention of Sn4d spin orbit doublet (rather than 4 peaks as in case of SnO_2) before and after introducing Li, respectively, shows the presence of SnO rather than SnO_2 which is an important piece of information and could serve as a reference for future research/ study into tin oxide-based materials.

These results could serve as a reliable reference for SnO which has been lacking ever since. Molecular oxygen was used to oxidise the sample along with annealing at a temperature of 600 °C for 60 minutes, however it did not show any significant change. This finding indicates that atmospheric conditions probably will not have a significant effect on the SnO termination on the surface of diamond which indicates increased stability of the termination in the ambient conditions. Stability is a necessary condition for application in device fabrication outside the UHV environment.

In order to reveal the surface structure of the SnO terminated diamond or in other words the changes in the surface due to SnO termination SPA-LEED was performed as described

in chapter 3. The SPA-LEED data proves that the (1x1) reconstruction of the diamond (100) is retained throughout the process. No other visible reconstructions are found. The width and profile of the LEED spots in figure 6.8 shows the broadening of the LEED spots after the SnO formation on the surface of B-doped C(100)-(1×1):O diamond. This, in our opinion, confirms the claim that SnO deposits as nanoclusters that just broaden the diamond (100) LEED integral spots. The spa-LEED data is reinforced by the geometry optimised structures obtained in case of both QML and HML of Sn on OTD in different configurations. The reconstruction of the diamond (100) surface or in other words C-C bonding was seen only in a few configurations e.g., in figure 6.3 b) where a carbonyl or ketone bond exists between surface C and O. Sn bonds with the surface O, resulting in the breaking of ketonic or carbonyl bond between surface C and O and formation of C-C bond and hence a 2×1 reconstruction. In all the situation where surface O was bonded in ether configuration to surface C, no reconstruction was seen. No reconstruction was seen due to Sn-Sn bonding in case of HML coverage either which could be attributed to the relatively bigger size of Sn and hence a repulsion as mentioned before.

In order to gain a firm understanding of the surface structure and bonding, the difference in the electrostatic potential between OTD and Sn-OTD surfaces in different configurations (i.e., ether and carbonyl) were investigated using DFT calculations.

Figure 6.6 a) and b) shows the electrostatic potential at the surface of ether terminated diamond and when QML of Sn is added to it, respectively. A potential difference of 1.4 eV was obtained in this case which corresponds to the binding energy shift (ΔB.E.) of 1.07 eV in the surface C1s obtained experimentally. This along with the SPA- LEED analysis makes us believe that Sn atoms have assumed a QML or HML coverage on the ether terminated diamond.

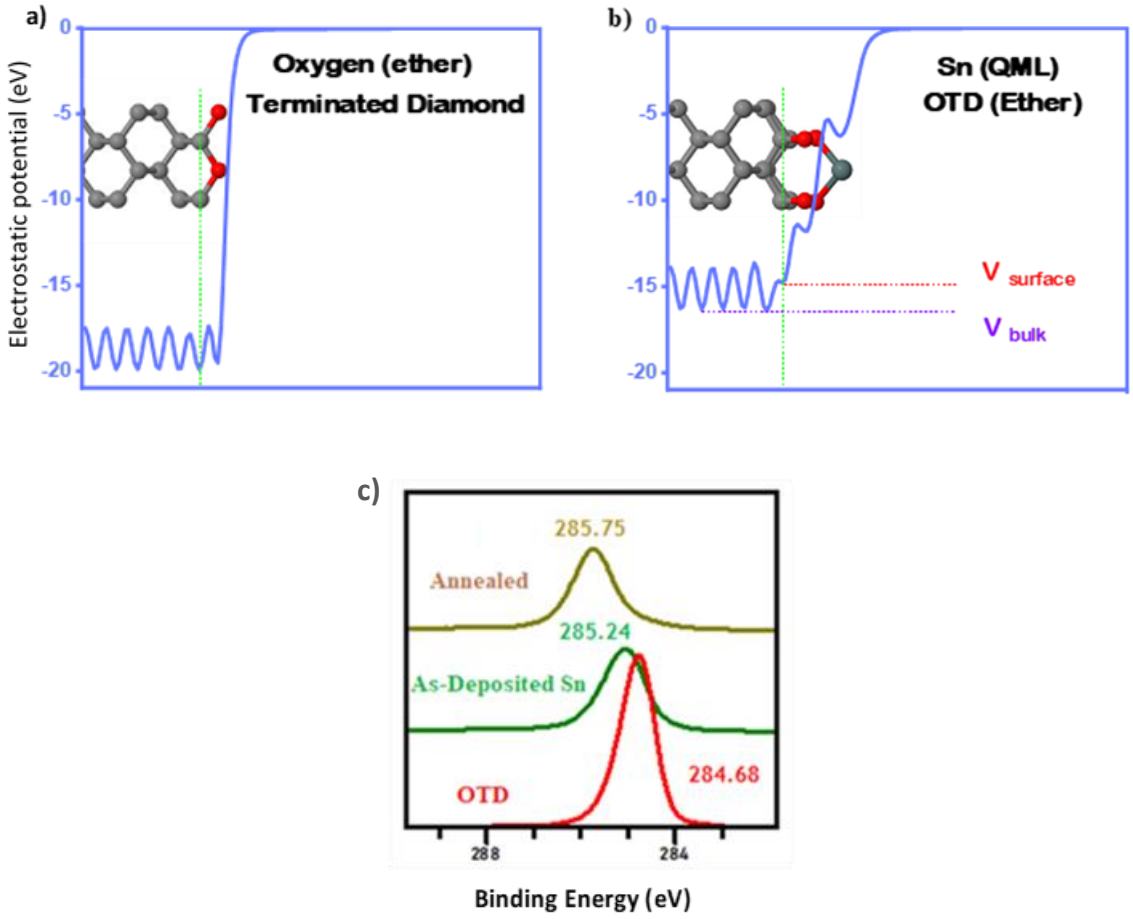

Figure 6.6: a), b) Electrostatic potential diagram showing variation of potential on the surface of diamond from the bulk diamond in oxygen (ether) terminated diamond and Sn (QML) OTD (ether) terminated diamond, respectively. c) XPS peaks for surface carbon (C1s) showing the shift in XPS peak.

This might also indicate that Sn bonds weakly to the OTD surface, as has been seen in case of Al also [76], as ether configuration has slightly lower adsorption energy than ketone/carbonyl one. The bond length didn't vary much between different configurations. C-O Mulliken bond populations between 0.64 to 0.77 were obtained which is significantly implies a single bond. Moreover, Mulliken charges on Sn and O atoms indicate ionic bonds between the surface species (Sn and ether oxygen). As we move from QML to HML, the nature of the bond changes from ionic to a covalent one and hence more NEA, which generally happens with increasing the coverage of metal atoms

on the diamond surface. HML, in our case, has been seen to give the maximum NEA and the largest adsorption energy.

6.3.4 Lithium deposition on Tin monoxide terminated diamond

Lithium was deposited at RT on the SnO terminated diamond. The lithiation of pristine SnO layers, as observed by A. Pedersen [88] in a theoretical study, results in the formation of stable layered Li_xO structure and the expelled tin atoms form atomic planes to separate the Li_xO layers [88].

We have found that as soon as the lithium deposits on the SnO terminated surface of diamond, the reduction of SnO occurs in which Li draws the oxygen atoms from SnO and results in expelled Sn atoms which can be seen in the form of metallic peaks in figure 6.7, confirming the theoretical predictions made by A. Pedersen [88]. Table 6.2 sums up the key results of stoichiometry of the key elements involved in the experiments calculated from the relative peak areas which shows the formation of SnO initially on the diamond surface and then Li_2O/SnO_x on the surface of diamond after lithium deposition and annealing. Tin oxide in the last stage includes a defective oxygen stoichiometry likely due to the oxygen deprivation as a result of lithium inclusion which is also seen in figure 6.7. The Li inclusion like H^+ bombardment in [7] is expected to reduce and eliminate the oxygen vacancies (seen in the form of lowering and later disappearing of Ov peak size) after annealing, as the mobile Li reduces SnOx. Thus, we have no peak for Ov, a large peak for LiO group and another peak SnOx.

The formation of the Li_2O/SnO_x junction was facilitated by annealing the sample at 500 °C. The Li_2O oxide peak increases at the expense of the non-stoichiometric component at 530.5 eV; the Sn oxide peak at 531.3 eV decreases which results from the fact that with an increase in temperature, the oxygen atoms are exchanged between Sn and Li. The formation of Li_2O and the release of metallic Sn atoms indicates the possibility of the

formation of 2D planes between lithium oxide layers in a multilayer structure as has been indicated by A. Pedersen [88].

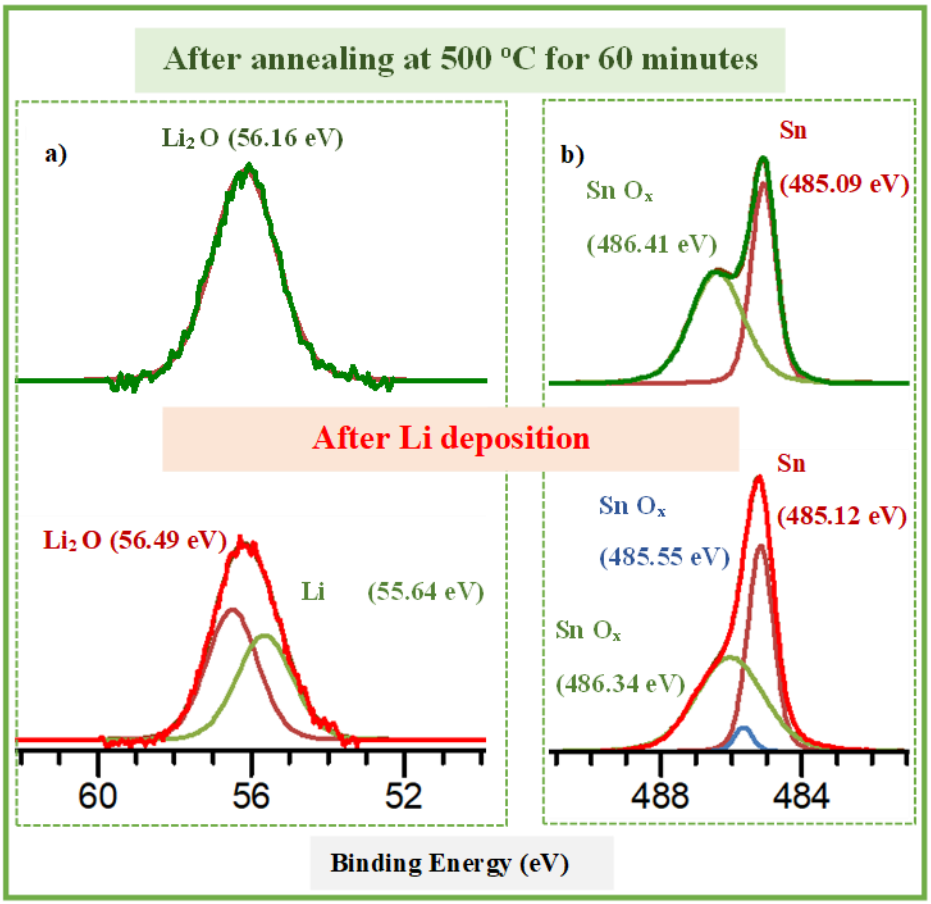

Figure 6.7: a) Lithium peaks (deconvoluted using U2 Tougaard background and FWHM widths of 1.7 eV ± 0.1 eV for oxide peaks), b) Sn Peaks (deconvoluted using Shirley background and FWHM of 1.8 eV ± 0.1 eV for oxide peak; As soon as Li was deposited, lithium reduced the tin oxide giving a peak for metallic tin while also giving another peak for lithium oxide. We can also see a clear peak for lithium oxide and SnO after annealing at 500 °C which confirms the formation of Li_2O/SnO_x heterojunction. Only Li 1s and Sn 3d 5/2 peaks are shown for clarity.

Table 6.2. Summing up the key stoichiometric ratios of the elements involved in the experiment, calculated using the individual peak areas and their corresponding differential photoelectron cross section.

Treatment	Sn:O	Li:O
As deposited Sn	1.25	-
Annealing at 500 °C for 60 minutes post O cracking	0.82	-
Annealing at 500 °C for 60 minutes post deposition	3.35	2.35

Pederson et al. have theoretically realised the structures of $Li_{1/2}OSn$, LiOSn, and Li_2OSn by lithiating the SnO layers at different lithium concentrations which has also shed light on the volume expansions in the process. All of these three phases or structures have been seen to maintain the SnO crystal structure with Sn planes surrounding the central LiO_x layer which challenges the previously thought idea of Sn atoms agglomerating into clusters in LiO_x matrix upon lithiation of SnO layers. This is relevant to our research as this would mean non agglomeration and also decumulation or dispersal (if any) of SnO clusters on the surface of diamond due to the inclusion of Li atoms and hence increased uniformity of the Sn based thin layers on the surface of diamond. This could also open the door for further research into the possible intercalation of Li atoms into SnO planes in bulk form which would open novel chapters and lead to further insight into the research area of energy storage especially Li ion battery research which is one of the major focus of material scientists worldwide.

Spa-LEED (figure 6.8) data reveals no further reconstruction on the surface of diamond (100) either due to SnO termination or heterostructure formation. This fact is also enhanced by the spot width analysis which shows the broadening of the LEED spots due to SnO and heterostructure termination without any surface reconstruction. It could be attributed to the presence of a fine monolayer or a sub-monolayer nanocluster formation

that doesn't result in the surface carbon bonds or the elements of surface species to form any new bonds that could change the surface structure.

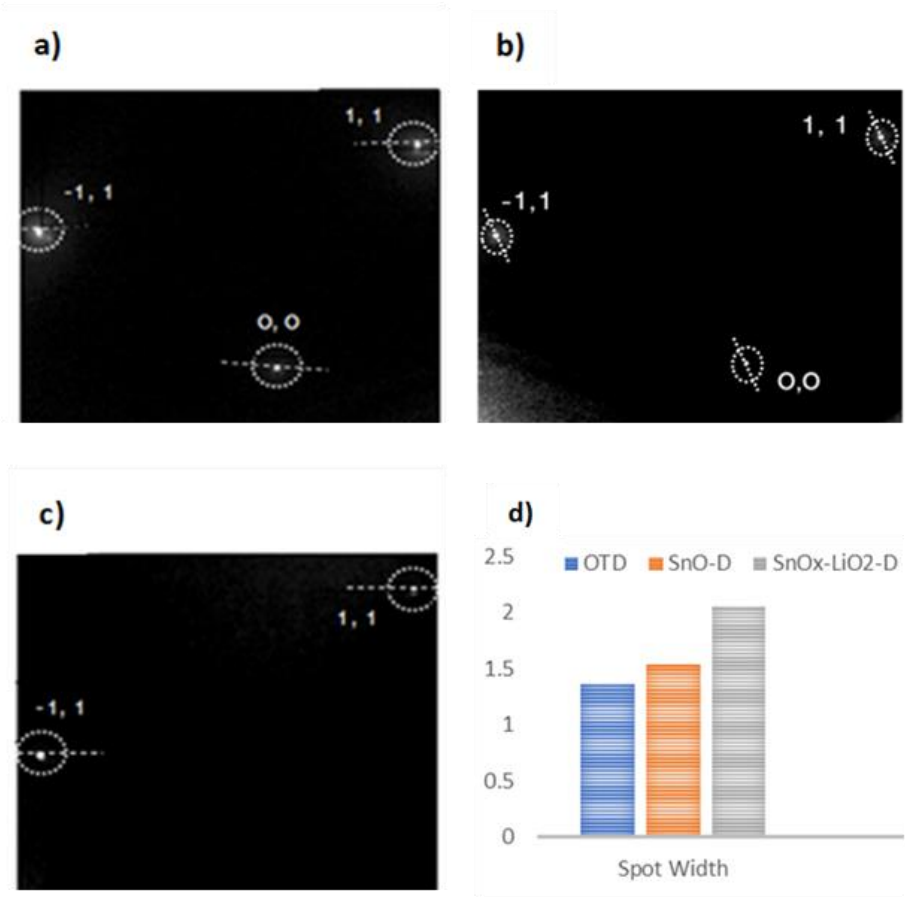

Figure 6.8: SPA-LEED images of a) Oxygen terminated diamond; b) SnO terminated diamond; c) SnO/Li_2O terminated diamond after annealing temperature of 500 °C for 1 hour revealing 1 × 1 reconstruction of the surface. SPA-LEED was taken with an electron energy of 100 eV. The 1 × 1 spots are marked by the white circles, while the intensity of each spot was measured along the white dashes at the respective points. Spa-LEED images show the order at the surface is retained after SnO termination on the surface of diamond and also after Li deposition; d) Spot width analysis of oxygen terminated, SnO terminated and Li_2O/SnO_x terminated diamond surfaces, obtained using the intensity profile of each spot in figure 6.8 and then measuring the width at the centre of each intensity peak, showing the increase in the width of the LEED spots which is typical of a fine monolayer/ sub-monolayer layer nanoparticles (or nano-oxides /nanoclusters) which just broaden the LEED integral spots.

6.3.5 UPS data for Lithium oxide, Tin oxide terminated diamond and heterostructure (tin oxide/lithium oxide) terminated diamond

He I UPS was performed after every process in order to have an ultra-surface sensitive acquisition and determine the WFs. The WF can be also determined by fitting the EF-PEEM image acquisitions close to the WF threshold (see figure 6.9). Within our lateral

resolution of about 150nm we found homogenous change in the WF across the sample. The particles on the surface, which broaden the LEED spots (Figure 6.8) are therefore much smaller than our lateral resolution. Average WFs for various process steps for the Sn 3d and Li 1s spectra are also shown in Table 6.3. This shows that WF is reduced when Li is deposited and annealed at 500°C. The annealing further reduces WF by ~0.2 eV due to possible removal of bulk Li as suggested from the XPS. WF reduces from 5.9 eV to 3.93eV through the surface treatments. Figure 6.13 shows the UPS graphs of the LiO-terminated, SnO and SnO_x/Li_2O terminated diamond surface at every step revealing the WF of the material.

Table 6.3: Average WFs for various process steps for the Sn 3d and Li 1s spectra. Li deposition was done on Sample 1 while other processes as mentioned were carried out on sample 2. WF was calculated using averaging function on the WF maps.

Treatment	WF (±1)
Pre Li (Sample 1)	5.90
After Li Deposition (Sample 1)	4.12
500°C Anneal (Sample 1)	3.93
800°C Anneal (Sample 1)	4.55
Oxygen Terminated Diamond (Sample 2)	5.9
SnO Terminated Diamond (Sample 2)	4.1
Li_xO/SnO Terminated Diamond (Sample 2)	3.9
SnO_x/ Li_2O (Sample 2) / 500°C Anneal	3.6

At 800 °C, as has been seen in the XPS, much of the oxygen also goes away along with all Li as Li-O resulting in the diamond being almost completely unterminated, hence an increase in the WF.

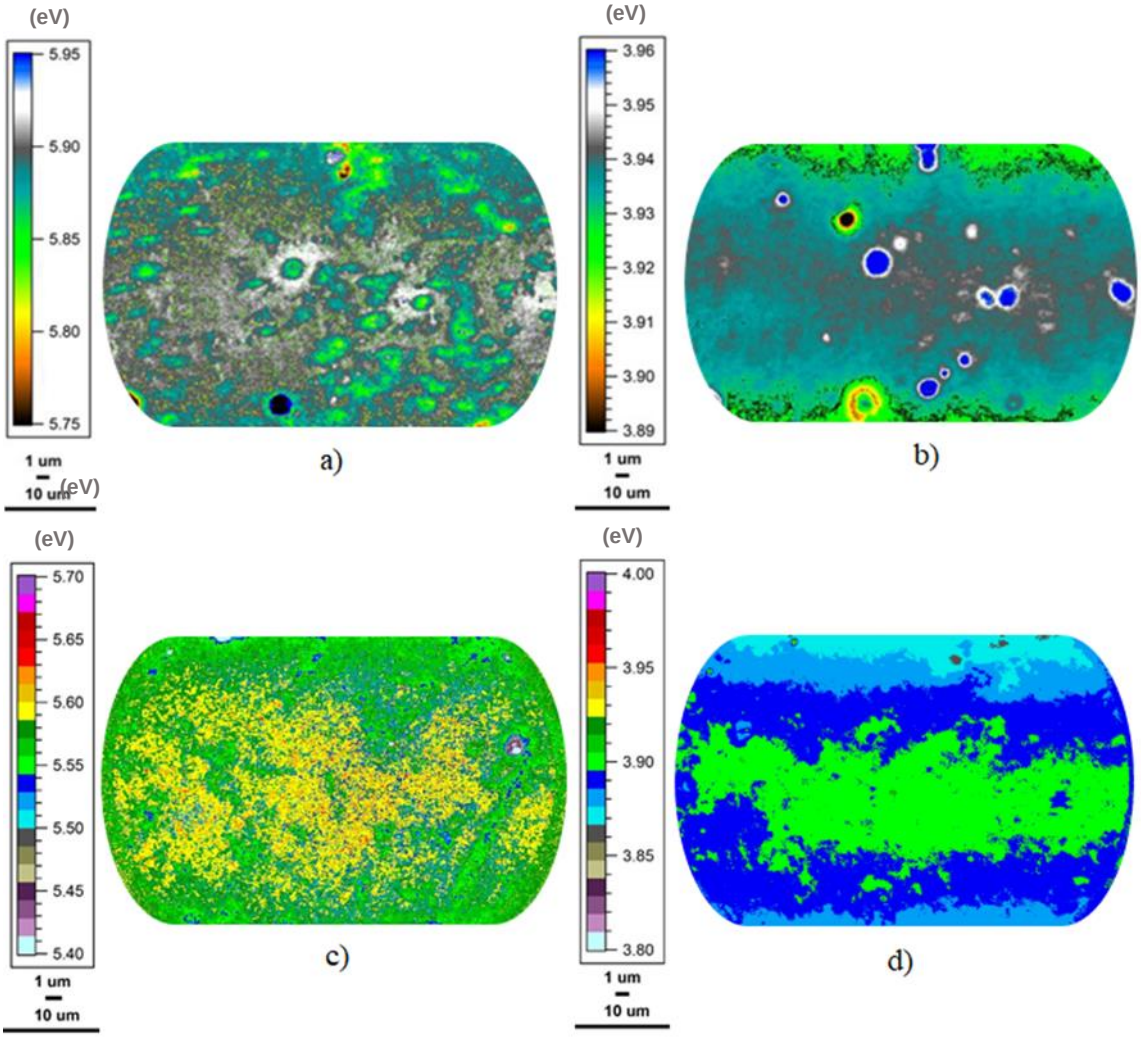

Figure 6.9: PEEM work-function maps of a) Oxygen terminated diamond before Li deposition; b) Li-O terminated diamond; c) Oxygen terminated diamond before SnO and Li deposition; d) Li_2O/SnO_x deposited diamond; revealing the homogenous surface/ termination with the lowest WF of < 3.9 eV. The field of view is cut because the WF is different at the top and bottom of the image due to the parabolic energy dispersion done by the two analysers in NanoESCA (PEEM).

The presence of NEA on LiO terminated diamond has been demonstrated earlier, however in our case it was about -0.60 eV (calculated using equation 6.1 and VBM position from UPS). A discussion on NEA and VBM will be discussed in next section. In case of SnO_x/Li_2O terminated diamond surfaces, the WF reduces from 5.9 eV to 4.3 eV when only SnO was deposited on the surface of diamond (100) which is due to the shift in the charge density between the surface species in a way that imparts NEA to the diamond surface as can be shown later. WF is further reduced to 3.9 eV when lithium is deposited on the surface.

With an increase in annealing temperature to 500 °C, a WF of 3.7 eV was obtained which is lower than O-Li terminated diamond at that temperature.

This further decrease in WF could be due to the loss of excess lithium during the annealing process as seen in case of O-Li terminated diamond. Furthermore, we have calculated the amount of lithium lost with annealing in both samples and it turned out that 47% of lithium was lost at an annealing temperature of 500 °C for O-Li terminated diamond while only 15 % was lost in the case of SnO_x/Li_2O terminated diamond (figure 6.10).

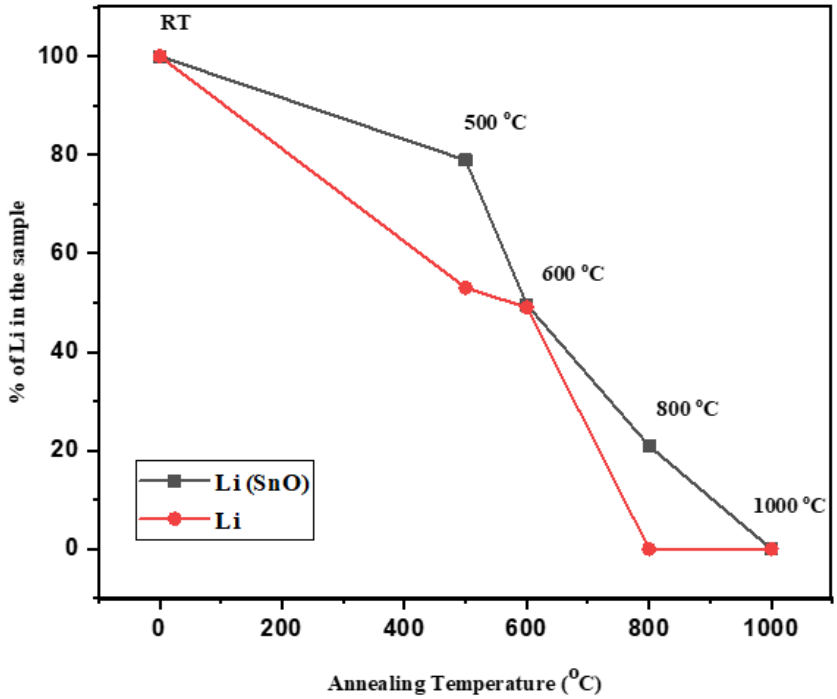

Figure 6.10: Percentage of Li in the sample after various annealing steps which demonstrates the relative stability of Li on oxygen terminated diamond and SnO terminated diamond. This graph was obtained using the relative areas of the Li 1s and Sn 1s high resolution peaks. As we can see stability of Li is stronger in case of Li_2O/SnO_x terminated diamond than in the LiO terminated diamond. Also Li was seen to exist up to 1000 °C in the former case compared to the latter. This could give an insight into the successful intercalation of Li into SnO planes as has been mentioned already.

This implies an increased stability of lithium on the surface of diamond with tin oxide. This is also evidenced by the retention of Li by the sample with tin oxide even at a temperature of 1000 °C, as can be seen in figure 6.10, while Li was totally lost at 800 °C in case of LiO terminated diamond. Another problem with LiO termination of diamond

is that Li enters the interstitial sites at higher temperatures which was found earlier [101] and in our study with a different sample as well, causing a significant amount of doping and hence upward band bending in the diamond (100). This band bending can significantly alter the bulk properties of diamond. With SnO terminated diamond, Li is less likely to enter the diamond bulk due to the presence of heavy and large sized Sn atoms present on the surface of diamond. This can be evidenced by a significant amount of downward band bending in our samples with Sn as explained in the next section. This can give more efficient termination of diamond with heterostructures for higher stability and lower WF.

6.4 Discussion on VBM and NEA

ARPES was done near the top of the valence band to reveal the band structure of the samples and to observe the band bending in the diamond surface due to the metal oxide terminations. However, an increase in the background noise increases the difficulty in visualizing the band structure as can be seen in figure 6.11.

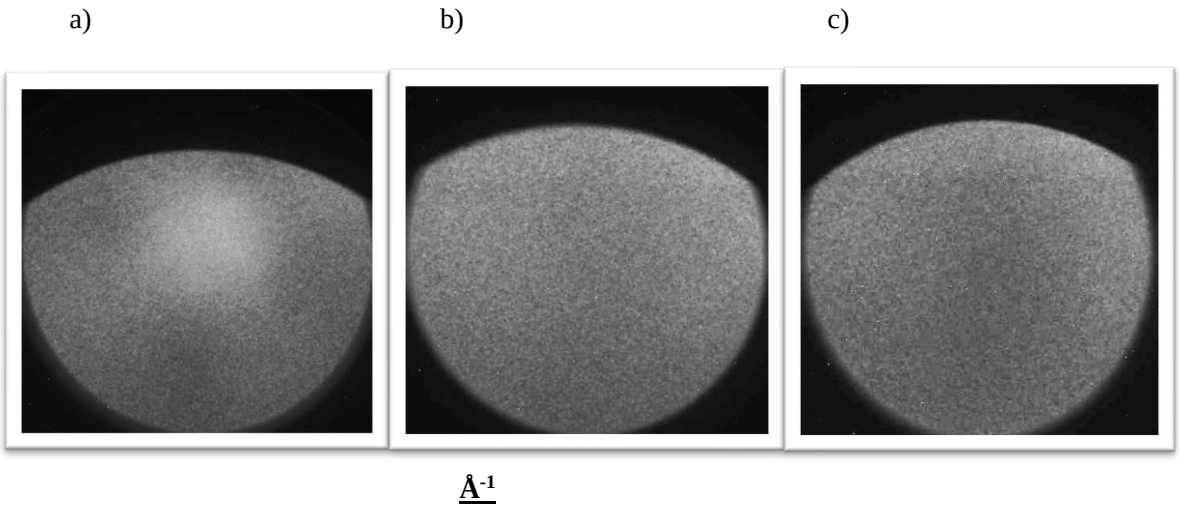

Figure 6.11: a) ARPES for oxygen terminated diamond; the structure for the bulk diamond is faintly visible in the centre. b) ARPES for SnO terminated diamond; no ARPES seen. c) ARPES for Li_2O/SnO_x terminated diamond; no ARPES seen. ARPES was obtained using a pass energy of 50 eV and scanning between B.E. of -0.5 to 4 eV with a step of -0.05 eV. These figures were generated by averaging the intensity over the whole B.E.

In spite of this, full wave vector ARPES allowed us to determine the VBM (VBM) position more precisely [57], although it was determined using UPS and Maier 's method [34]

$$\chi = \Phi + \alpha - E_g \qquad \text{---------- (6.1)}$$

also, as can be seen in figure 6.12. The intensity at the centre of ARPES at various steps was plotted against the binding energy (B.E.) which leads to the determination of VBM position at the point where the signal dropped to the background level. The VBM position found due to the above mentioned methods is presented in table 6.4 for comparison with NEA calculated using the equation.

Where χ is electron affinity, Φ is WF, E_g is band gap energy and α is the difference between fermi energy level and VBM. Since the VBM values obtained using full wave vector ARPES are more precise, these were used to calculate the values of NEA.

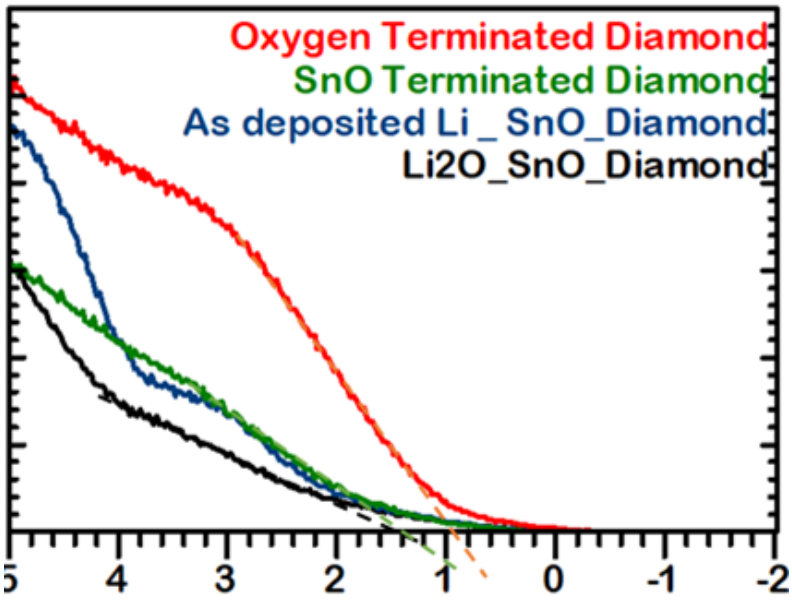

Figure 6.12: UPS spectra of the diamond (100) showing the Fermi edge of the sample at various process steps. The VBM position is determined by extrapolating the low binding energy (leading) edge of the measured valence band into the measured background. The background intensity is represented by the state free area in the band gap. The intersection resulting as a result of the interpolation is assumed to be the energy where density of states (DOS) reaches close to zero (0) i.e. VBM.

*Table 6.4. Electronic structure information at different terminations of diamond (100). * indicates the values used for calculating the electron affinity (EA) value (by taking their average). VBM was determined using three different methods which showed the same trend. Data for H- terminated diamond is included for comparison.*

Sample	VBM (ARPES) (eV)	VBM (UPS) (eV)	Maier's Method (eV)	WF (eV) (±0.1)	EA (eV)	Stability
OTD	0.8*	0.9*	0.75	5.9	1.28 (PEA)	Starts stabilising at 800 °C
HTD [57, 60, 143]	----------				- 1.30 (NEA)	Desorbs at > 700 °C
LiO-D	0.9*	1.05*	0.47	3.93	-0.60 (NEA)	Desorbs at 800 °C
SnO-D	1.4*	1.3*	1.75	4.1	-0.02 (NEA)	Desorbs completely at >1000 °C
Li/Sn-OTD	1.5*	1.4*	1.85	3.6	-0.42 (NEA)	Desorbs completely at >1000 °C

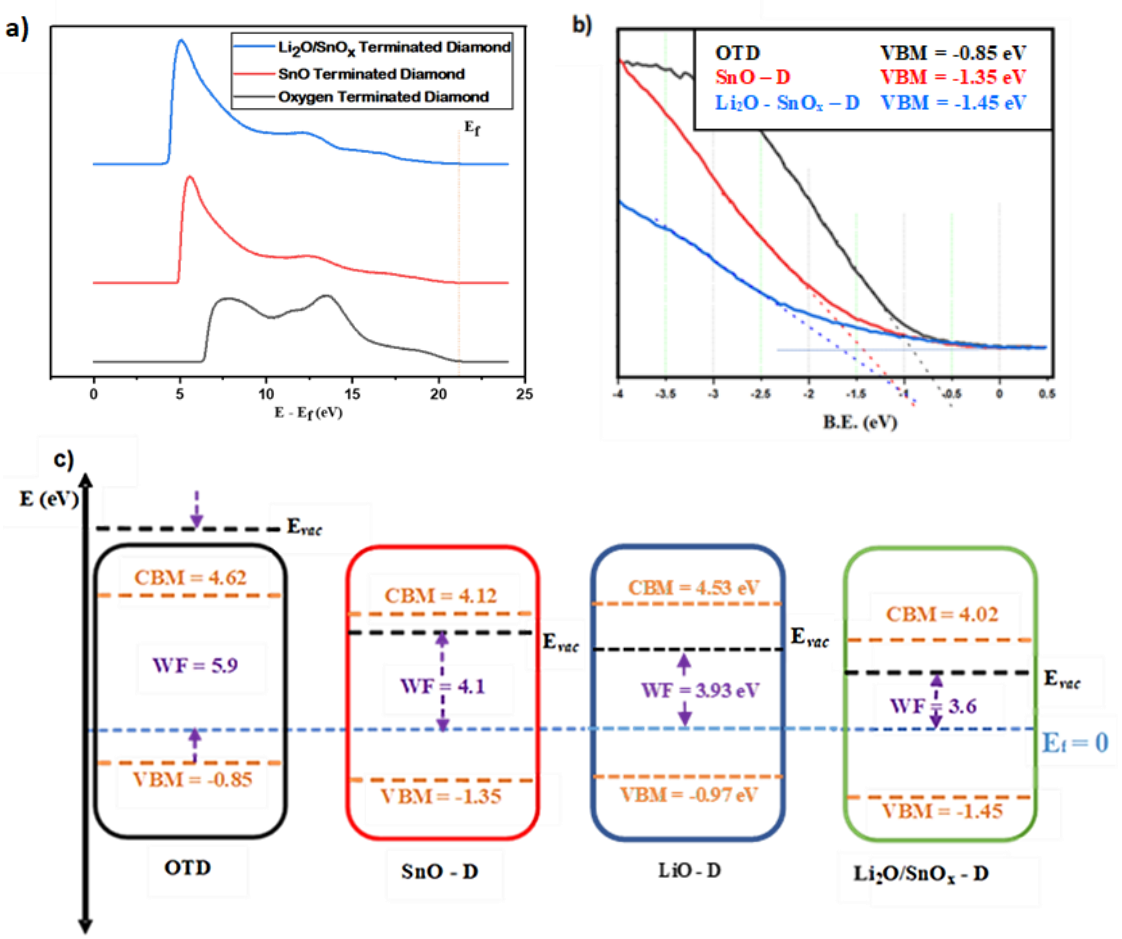

Figure 6.13: a) UPS graphs for LiO- terminated and SnO_x/Li_2O terminated Diamond surface at various process steps. The spectra were produced using a monochromatic 21.2 eV He-I source. WF decreases with the process steps, finally giving a WF reduction of 2.3 eV. b) VBM position determined using ARPES at 3 process steps. c) A schematic diagram showing the downward band bending of diamond (100) due to the various terminations. A band gap of 5.47 eV was assumed in calculating the energy levels.

The electronic structure of differently terminated diamond (100) is shown in figure 6.13 c) which shows a considerable band bending when LiO, SnO and Li_2O - SnO_x is formed on the surface of diamond (100). VBM position was determined using ARPES (as discussed above in figure 6.13 b)), UPS (by extrapolating the low binding energy leading edge of the valence band linearly into the measured background) (figure 6.12) and by Maier's Method. Although different methods of determining the VBM position gave slightly different values which could be due to errors in the calculation and extrapolation, similar trends in band bending were seen in all the methods. SnO terminated diamond

(100) was seen to have an NEA of -0.02 eV which is less than the theoretically calculated values for QML (-0.86 eV) and HML (-1.37 eV). This could be due to the problems associated with obtaining a smooth and contaminant free surface before metal termination. An increased value of NEA = - 0.42 eV is obtained with the lithiation of SnO terminated diamond or in other words with the formation of Li_2O-SnO_x terminated diamond (100) which calls for improvements to be made in the surface processing steps so that a lower value of NEA and hence WF could be obtained for efficient termination based on a heterostructure between alkali and heavy metals. Although H terminated and LiO terminated diamond surfaces present much higher NEA, however, these terminations desorb at lower temperatures than seen in case of other Sn and heterostructure based terminations.

In order to determine the efficiency in thermionic emission, the UPS spectra results were normalized by the illuminated area and integrated to calculate the quantity of secondary electrons. The integration has been carried out in a zone representative of the secondary electrons. Although O-Li terminated diamond has higher electron yield at every temperature than SnO_x/Li_2O terminated diamond, the decrease in the electrons was more rapid in the former than in the latter sample which also shows the increased stability of Li_2O - SnO_x terminated diamond over the O-Li terminated one. Li termination has already been found to exhibit NEA [119] while the SnO terminated diamond in our study showed a very small value of NEA.

6.5 Thermionic testing

In order to realise the future of SnO nano cluster terminated diamond surfaces in thermionics, a few runs of thermionic emission on the thermionic kit and using the method described in chapter 3 was performed with SnO terminated diamond acting as an emitter and later as collector as well. The results from this sample were compared

with those of hydrogen terminated diamond for establishing how close the response was to the much accepted hydrogen terminated diamond. For this small experiment, samples of single crystal diamond were grown using CVD with nitrogen doping (as it has been seen to produce a stable outcome) on the molybdenum substrates. The samples were terminated with SnO nanoclusters in the same way as before. The samples were loaded in the thermionic kit and testing was performed at a pressure of 10^{-7} mbar, using a program controlled temperature ramp from 400 °C – 700 °C – 400 °C at a rate of 1 °C per second and keeping the sample at 700 °C for 50 seconds shown in figure 6.14 to investigate any surface desorption effects. The distance between the emitter and the collector was maintained at 100 and 200 µm.

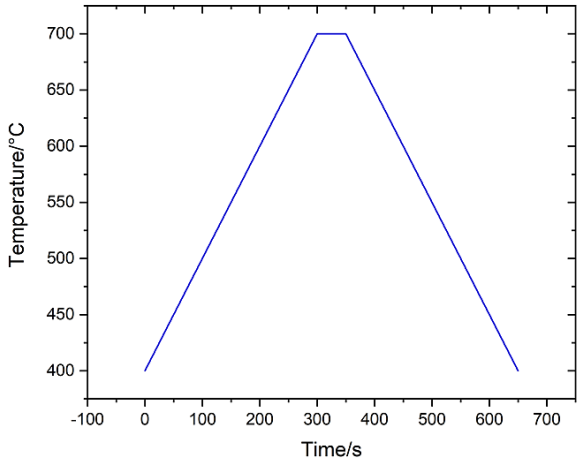

Figure 6.14: The temperature profile/ ramp used for performing the thermionic runs on the hydrogen and SnO terminated diamond in all case.

Figure 6.15 shows the thermionic emission outcome of H and SnO terminated diamond at the distances of 100 and 200 µm between the emitter and the collector. It was seen that the highest current output from the SnO terminated sample in both cases reached a maximum up to 2 mA which is far greater than H terminated diamond in this experiment. The response of SnO terminated diamond to the increasing temperature is much better than H terminated diamond. There is however, a considerable surface species desorption at 700 °C in the case when the distance between the emitter and collector is 200 µm.

This could be due to poor diamond film quality or improper SnO deposition which should be corrected by using a single crystal diamond surface and properly optimised SnO deposition. Nevertheless, this small experiment has confirmed what was said earlier regarding the scope of SnO as an alternative of H terminated diamond at higher temperatures and in many ways as described in the earlier sections.

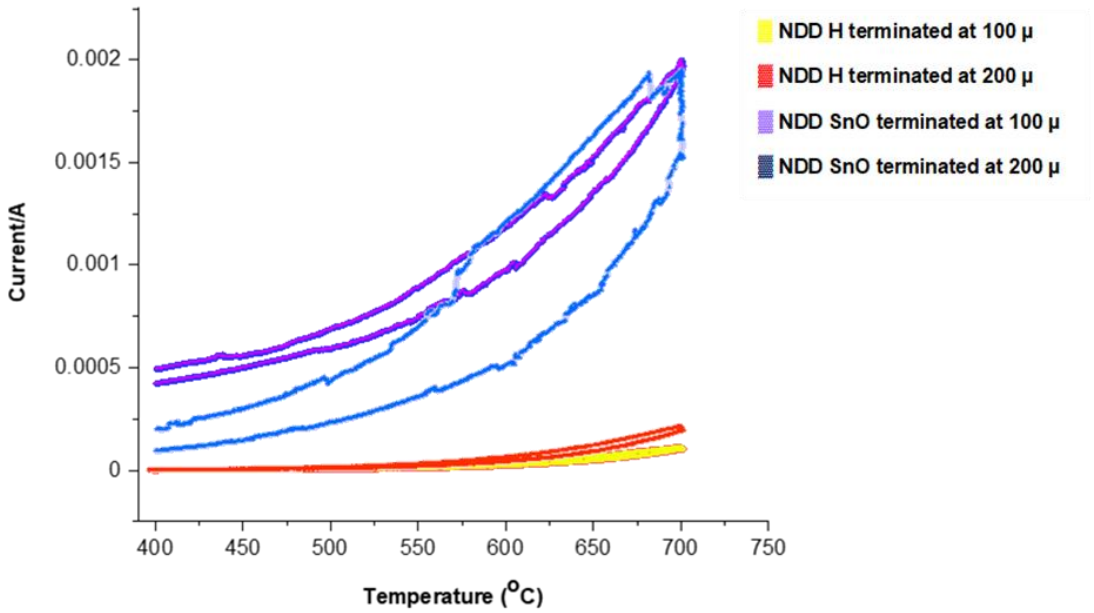

Figure 6.15: A set of thermionic profiles illustrating the difference in current output between hydrogen, and SnO terminated nitrogen doped diamond at a sample distance of 100 and 200 µ between the emitter and the collector.

Using SnO terminated polycrystalline diamond as a cathode has resulted in totally different results were in terms of current output the SnO terminated diamond lies in between H terminated and O terminated diamond which is expected theoretically as O terminated diamond has PEA and hence has lowest current output. Thus it shows that SnO termination on the surface of diamond actually does enhance the capabilities of diamond (polycrystalline and single crystal as well) as a emitter device which can be used in thermionics.

6.6 Tin and Tin/Lithium based Heterostructure terminated diamond

Although it has been known and mentioned earlier that the inclusion of oxygen in between the metal atom and the surface carbon atom increases the sticking coefficient

and hence increases the bonding strength and stability of the surface species. This results into the efficient NEA imparting and WF lowering termination of diamond surface for its use in various fields such as thermionic emission conversion in our case. This was also observed in case of Sn in this study as has been demonstrated in earlier sections and has also been observed with Li and other metals [157]. We have already shown in chapter 4 the possibility and positive outcome of Sn termination on the bare surface of diamond using DFT based studies which did not only show the generation of NEA imparting dipole on the surface of diamond but also beckoned towards the superior bonding and charge distribution between the surface species i.e. C and Sn. To demonstrate this experimentally, a sub-monolayer of Sn was deposited using e-beam deposition in the same way as shown in the methods section of this chapter on the surface of a bare diamond (cleaned) at various thicknesses that is QML, HML and FML with annealing performed in between these steps as can be inferred from figure 6.16 and table 6.5. It was learned by performing the characterisation at various steps, following the methods mentioned in the section 6.2 of this chapter and also in chapter 3, that Sn deposition at QML indeed results in the formation of metal carbide (tin carbide) bonds through XPS peak analysis i.e. multiple peaks were observed both in C and Sn that could be attributed to the metal carbide (tin carbide at lower B.E. and C-H at higher B.E.) and a small oxide peak in Sn as seen in figure 6.16 a) and b). SPA-LEED revealed the 2×1 initial surface structure (figure 6.16 c), d) and e)) for the bare diamond surface which was observed throughout the process except after QML of metal (Sn) deposition and 250 °C anneal (1 hour), the LEED pattern was dimmed which could indicate amorphous or non-crystalline surface species due to metal deposition which means the Sn atoms have not re arranged into an ordered layer perfectly.

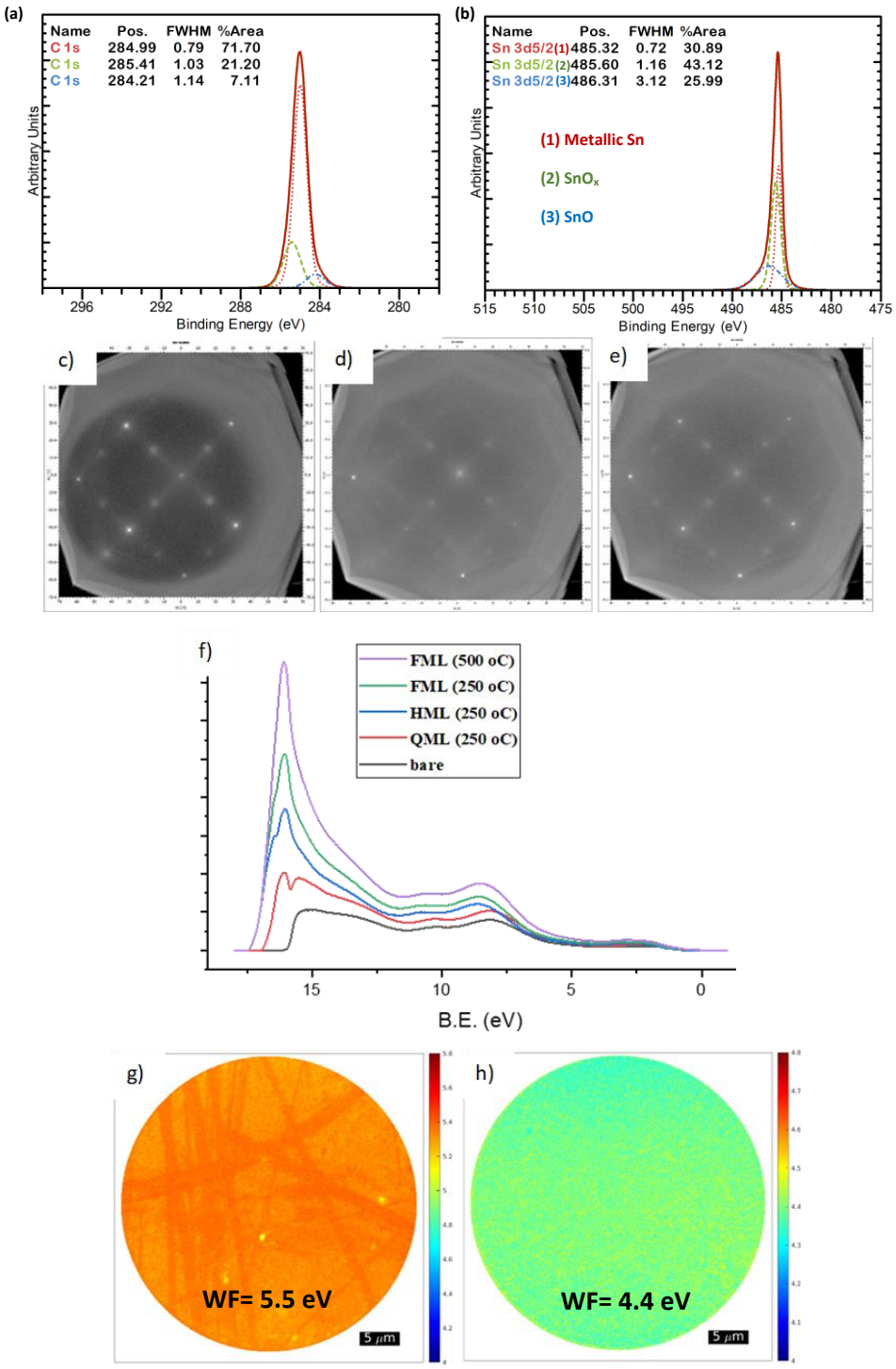

Figure 6.16: a), b) XPS of sample revealing multiple peaks in C1s and Sn 3d that could be attributed to metal (tin) carbide formation. There is a small oxide peak as well which could be due to contamination. Only Sn3d 5/2 peaks have been shown and Sn 3d 3/2 peaks are omitted for the sake of clarity. c), d), e) SPA-LEED images of bare diamond, QML deposited and 250 °C annealed (1 hour) sample, FML deposited and 500 °C annealed (1 hour) sample, respectively, reveals high temperature requirement to enhance the surface structure. f) UPS image of the sample revealing the NEA peak appearing initially at QML deposition which reduces later at 1 ML deposition. g) and h) WF maps of bare diamond and QML deposited, 250 °C annealed diamond showing WF reduction up to 1 eV.

*Table 6.5: Electronic structure information at different terminations of diamond (100). *Values indicate the averaged ones (between UPS and Maer's method VBM values). VBM was determined using three different methods which showed the same trend.*

Sample	WF (± 0.1 eV)	VBM (from UPS) (± 0.1 eV)	Maer's method (VBM) (± 0.1 eV)	Av. VBM	EA (from UPS and av. *)
Bare	**5.5**	**0.77***	**1.17***	**0.97**	**0.8 / 1***
QML & 250 ºC	**4.4**	**0.23***	**1***	**0.62**	**- 0.84 / - 0.45***
HML & 250 ºC	**4.4**	**0.21***	**1***	**0.61**	**- 0.86 / - 0.46***
FML & 250 ºC	**4.3**	**0.16***	**1***	**0.58**	**- 1.01 / - 0.59***
FML & 500 ºC	**4.4**	**0.38***	**0.9***	**0.64**	**- 0.69 / - 0.43***

Later it was seen at 1 ML and 500 °C annealing (1 hour), though we get a clear LEED with 2×1 surface pattern, which suggests using higher temperature annealing to improve surface structure. However, we have seen Sn starts to go away at higher temperatures as seen in case of Sn-O terminated diamond as well during optimisation through a considerable peak area reduction (although oxygen increases the sticking coefficient of a metal on diamond in case of metal oxides than metals of bare diamond). The indications of NEA, as can be seen in the UPS image in figure 6.16 f) and lowering of WF by almost 1 eV (figure 6.16 g) and h)) after annealing at 250 °C were also observed as can be inferred from the data presented in table 6.5 also. However, no further significant changes in WF were seen with further Sn deposition i.e. at HML or FML or with further annealing. This is quite contrary to what we have seen in case of SnO terminated diamond

and it could be attributed to the oxygen's ability to participate towards forming an efficient metal oxide (in our case SnO) layer on the surface of diamond.

As part of our inquisition, we have tried to form metal heterostructure with Sn/Li on the surface of diamond but unfortunately after performing multiple unsuccessful runs with negative outcomes it was learned that our Li source in the deposition chamber was actually oxidised and hence there was no way of controlling the contamination other than changing the Li source. This would ultimately fall into the future work of this project and thesis.

6.7 Conclusions

We have demonstrated the possibility of forming SnO terminated diamond using DFT calculation. NEA values of - 0.86 eV and -1.37 eV were obtained with QML and HML of Sn on oxygen terminated diamond (100). Larger adsorption energies of more than - 6 eV was obtained with various configurations of Sn on OTD which shows that Sn has an ability to form a stable termination on the surface of OTD. This stability was established experimentally as SnO on the surface of diamond was unaffected by molecular oxygen or ambient conditions, a necessary condition for device application. The formation of SnO nano-cluster terminations on the surface of B-doped C(100)-(1×1):O resulted in the downward band bending and lowering of WF by 1.8 eV. An NEA of -0.02 eV was also seen. A considerable amount of downward band bending was seen due to Sn deposition on OTD. SnO was reliably formed instead of SnO_2 which has been a point of debate until now as a reliable reference had been missing. DFT analysis revealed that surface C-C reconstruction due to Sn bonding occurs only in those cases when O atom is bonded to the surface C in a ketone configuration, a larger adsorption and more pronounced NEA was also seen in these cases, which shows Sn prefers to break the ketone bonds than

the ether ones. Experimentally, no reconstruction was seen due to SnO termination of diamond.

Although Li-O terminated diamond shows NEA of -0.60 eV with a WF of 3.93 eV, the lithium content decreases quite rapidly at 500 °C. There is also a problem of Li doping the diamond crystal or occupying the interstitial sites inside the diamond bulk and hence changing the bulk properties considerably. The Li interaction with SnO nanoclusters was observed after depositing Li on the SnO terminated diamond. Li withdrew oxygen from the tin oxide and forms Li_2O along with metallic Sn atoms. This interaction resulted in the increased stability of Li on diamond surface. Only about 15% of Li was lost in case of the Li_2O - SnO_x termination on diamond (100) compared to 47% lost in case of LiO terminated diamond. No surface reconstruction was seen due to Li_2O - SnO_x termination of diamond (100). By elaboration of the UPS data, we also found that the photoelectron yield was decreasing more rapidly in case of pure LiO compared to Li_2O - SnO_x. Li_2O - SnO_x terminated diamond also resulted in an NEA of -0.42 eV and a WF decrease of 2.3 eV. A downward band bending was seen in case of SnO and Li_2O - SnO_x terminated diamond, as opposed to upward band bending in case of LiO terminated diamond (seen in a different study), which implies that tin oxide can be preventing Li from entering the bulk of diamond (doping) and hence preserving the diamond bulk properties.

The results obtained in this study not only provide an insight into the heterostructure termination of diamond but are crucial in developing future efficient terminations for low work-function and NEA on the surface of diamond.

Chapter 7

Summary

Conclusion and Future Work

This short chapter sums up all the key findings in this work obtained through the DFT based theoretical studies and later ultra-high vacuum (UHV) based deposition and spectroscopic characterisation techniques, on the viability of tin based sustainable functionalisation of diamond for efficient and more stable terminations.

The future work section identifies some of the basic problems encountered in diamond based research and other specific issues related to the work reported in this thesis in the form of scope for future investigations in this research area.

7.1 Conclusion

The main aim of the work presented in this thesis is to study tin and its 2D oxide as a candidate material for functionalising the surface of diamond to exhibit a NEA property. The bare unterminated surface of diamond has a positive EA and if left exposed to atmosphere the value will alter depending upon the amount of oxygen or OH taken up by the surface. The main focus of this thesis is the potential use of NEA diamond as the electrode material in TEC devices that convert concentrated heat, such as solar energy, into electrical power. Various elements and their oxides have been investigated as a means to impart the surface of synthetic diamond with NEA. For example, hydrogen terminated diamond is known to induce NEA property on diamond which can withstand temperatures of up to 973.15K [62, 158]. Since NEA diamond materials exhibit measurable thermionic emission at temperatures below red heat (ca 800K), the useful operating temperature range for a diamond TEC lies between this and approximately 1150K for terrestrial applications. One elemental candidate that has been overlooked by researchers is tin and its monoxide.

The first question posed in this study was whether it is possible to have a Sn-terminated surface as Sn atoms have larger size compared to C atoms, a huge electron cloud compared with all other previously researched terminations of diamond which were smaller in size than Sn atoms. To answer this question, a computational study was performed using CASTEP on the University of Bristol's blue crystal 4 supercomputer. The interaction of Sn atoms in quarter monolayer (QML), half mono layer (HML), and full monolayer (FML) disposed on the surface of a bare diamond slab was simulated and compared with a diamond surface on which O and then Sn were coordinated as can be seen in chapter 4. The parameters that were used for ascertaining the successful adsorption were 'exothermic energy' or negative adsorption energy and electron affinity. It was revealed that the most stable and NEA yielding coverage of Sn atoms was QML on the bare surface and HML on the oxygen terminated surface of diamond. The electrostatic potential calculations gave a negative value of electron affinity while partial density of states calculations revealed the predominantly covalent (hence stronger) nature of the bonds between Sn and C atoms on bare diamond and between Sn and O atoms on oxygen terminated diamond. It also came to the light that NEA develops on the surface of diamond due to the charge distribution between the surface species in which negative charge accumulated on or near the surface carbon atoms due to the generation of a surface dipole between Sn and C on the bare diamond surface and between SnO and C

on the oxygen terminated surface. The generation of surface dipole due to the charge accumulation in the vicinity of the surface species was exhibited experimentally in the form of chemical shifts in the XPS peaks of surface species in chapter 6. This was a crucial finding as this meant the theoretical methods had validated Sn as a potential NEA imparting termination of diamond with a large stability. In the most stable and in fact most of the forms, no change in the surface structure due to reconstruction could be seen which did reflect in the experimental investigation later on in chapter 6.

Prior to the studies of Li and Sn on oxygen-terminated diamond presented in this work, it was reported that tin and lithium in a particular stoichiometric ratio of Sn_2Li_5 was found to produce an ultra-low WF material (WF less than 1.25 eV) [83]. Additionally, the addition of trace amounts of oxygen was reported to lower the WF even further. A theoretical study by A. Pederson [88] had already suggested an interesting interaction between the incoming Li atoms and SnO planes where Li atoms take up oxygen from the 2D SnO layers and hence forming Lithium oxide in between the Sn planes which could be termed as 'intercalation'. Findings such as these were enough to motivate a study of Li and SnO based heterostructure on the surface of diamond to evaluate the potential stability for thermionic applications. As a part of this study, Li was deposited on the surface of diamond chemically (described in chapter 6) and it was learnt that when the sample was heated at higher temperatures the Li atoms didn't just settle at the surface but diffused into the near surface bulk of diamond up to the temperature of 750 °C and then came out forming LiO at the surface and later desorbing out from the surface at 850 °C with most of the oxygen atoms as well. This also meant the electronic properties of the diamond sample also changed as the upward band bending was seen in the band structure of diamond surface due to the inclusion of Li atoms into the bulk of diamond. Although the effect was very small and might be viewed as insignificant in this study, it could be amplified if the same process is performed consistently across larger surface areas which could be of significant benefit to the thermionic operation of diamond surfaces. This observation raises the issue of the stability of lithium on the oxygen-terminated diamond surface. And this work has reported evidence of lithium coordinated with oxygen being desorbed from the diamond surface.

Following up on the manner in which Sn and Li were found to interact to form a low WF surface, experimental work featured in Chapter 6 was carried out to construct an atomically thin layer of Sn on an oxygenated diamond surface. It was found that a sub-

monolayer of SnO rather than SnO_2 could be formed under UHV by a sequence of annealing steps and atomic oxygen exposures. An important finding was the temperature stability of the nanostructured layer which showed no degradation when cycled from RT to 1000 °C. Furthermore, the sub-mono layer of SnO was found to induce a NEA of –0.02 eV on the p-type diamond surface causing a reduction in surface WF of 1.8eV. These results suggest that this termination is an attractive alternative to hydrogen or LiO, and which could promote superior thermionic operation on n-type diamond.

For diamond-based collector electrodes, an even lower WF would be desired for TEC operation. To address this requirement work was conducted to develop a heterostructure on the SnO-terminated diamond surface by depositing Li at elevated temperature. It was observed that a SnO_x-Li_2O heterostructure was formed that exhibited NEA (-0.42 eV) and caused a further reduction of 2.3 eV in the surface WF. After annealing this sample at various temperatures, it was seen that the interaction between Sn and Li atoms on the surface of diamond had resulted in the increased stability of Li on diamond surface. Only about 15% of the Li was lost in case of the Li_2O - SnO_x termination on diamond (100) compared to 47% lost in case of LiO terminated diamond at various annealing temperatures. UPS measurements of the secondary electron peak characteristic of NEA diamond confirmed that SnO and Li_2O-SnO_x terminations were more stable retaining larger intensities than LiO. UPS measurements of the secondary electron peak characteristic of NEA diamond confirmed that SnO and Li_2O-SnO_x terminations were more stable retaining larger intensities than LiO.

7.2 Future Work

Although Sn based termination of bare and O-terminated diamond (100) and similarly other metal terminations [35] have been shown, theoretically and experimentally, to impart interesting properties that that could advance the development of diamond-based TEC device technology. However, there are a number of material-related challenges that would need to be addressed through further research to realise a diamond TEC.

One of these is the production of large area, high quality diamond material. It has been shown [109] that emission current output from single crystal material can be improved by a factor of 1000 if means is found to significantly reduce the surface defects that disrupt the coordination of terminating species across the diamond surface.

With this in mind, there have been several recent developments in large area single crystal growth [159]. Also, CVD methods have been proposed in the past that use deuterium in microwave plasmas to achieve atomically flat C(111) diamond surfaces [160]. A study that seeks to explore these aspects for thermionic applications may yield some useful insights that could be applied to the SnO-based materials featured in this work. Surface roughness produces surface states in the band structure and hence alter the surface properties of diamond considerably for example these lead to low carried mobility in transistors [161], interference with the quantum applications [162]. Another challenge that has been identified in this work and as described in chapter 4 concerns the oxygen termination of the diamond surface. It is known that oxygen atoms bond to the surface of diamond either in ether configuration where each oxygen atom takes a 'bridge' position between two surface carbon atoms with a single bond between these or an 'on top' position where the O atoms coordinate with the surface carbon atoms with a double bond. However, to achieve a singly terminated diamond, for example, has proven to be very difficult to achieve. Most of the time the outcome of every oxygen termination process that has been explored until now is the mix of both ether and ketone bonding which is problematic as there are different bond energies and hence adsorption energies associated with ether terminated and ketone terminated diamond surfaces as demonstrated in Chapter 3 of this thesis. This leads to improper and imperfect optimisations of surface termination on diamond and hence unreliable outcomes with metal based surface terminations. However, from the plasma, chemical, photochemical, electrochemical and thermal treatments to produce an oxygen terminated surface, electrochemical method has shown most promising approach for achieving a single type of termination and more work would be needed to develop this approach [1].

Linked to the method of oxygen terminating the diamond surface is the issue of its stability on the diamond surface. We have observed in our experiments the loss of oxygen at various temperatures during the annealing of the sample. It was seen in the XPS that there was a considerable peak reduction in case of oxygen at higher temperatures in many samples as can be seen in figure 7.1. The research question that needs to be addressed is whether this is to do with the in efficient adsorption of oxygen on the surface of diamond and how this is influenced by using single crystal material exhibiting significantly lower surface defect densities and the use of electrochemical oxidation and more work would be needed to develop this approach.

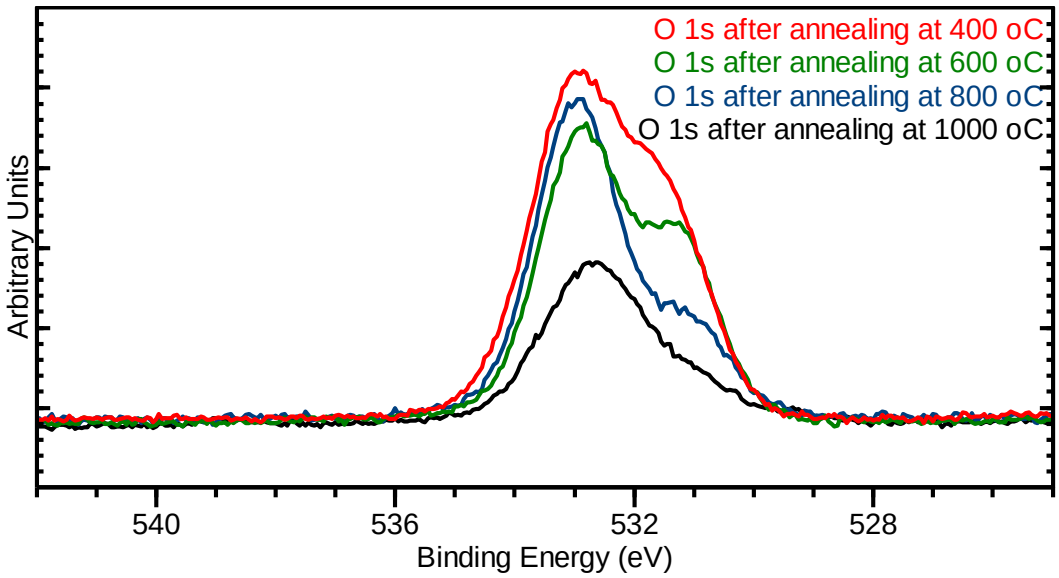

Figure 7.1: XPS peaks of O at various annealing temperatures; showing the reduction in the peak area with the annealing at higher temperatures due to the oxygen loss. This spectra were obtained after metal (Sn) deposition on the surface of diamond which could mean Sn atoms are taking away O atoms from the surface which otherwise is expected to be stable at this temperature range.

Interest in the low electron WF in alloys of Li and Sn metals(e.g. Sn_2Li_5), as reported in a paper by Alchagirov and co-workers [83] has been identified in this thesis as a potential compound for realising a termination that produces a stronger NEA on diamond and larger reduction in WF.

Some preliminary work has been conducted towards realising such a material but experiments to date have proved challenging and compounds with the correct stoichiometry have not been made to imitate this. In this work, the co-surface termination of diamond with Sn/Li system on bare and oxygen terminated was explored for different configurations.

Figure 7.2 shows the most significant configurations or systems in terms of their stability and electron affinities which were comparable to the Sn and Li terminated bare and oxygen terminated diamond (100). Although this beckons towards the positive outcome in this piece of study however, when these structures were further analysed, it came out that there was a complex interaction among the surface species.

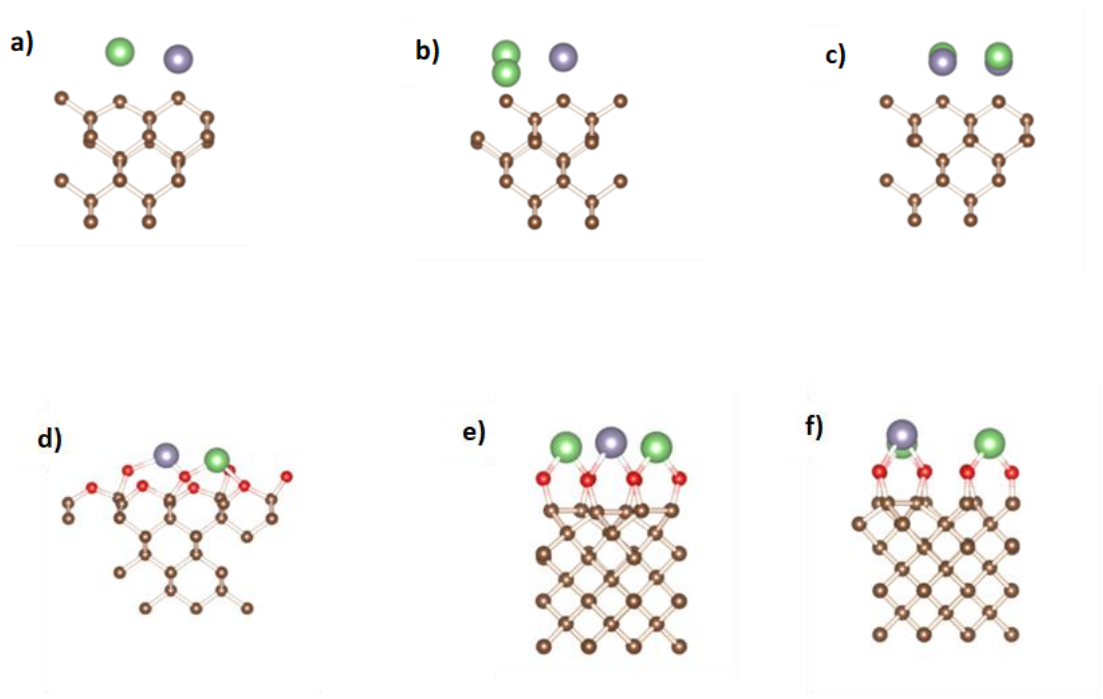

Figure 7.2: Describing various Sn/Li based heterostructure terminations on bare diamond (100) with Sn:Li as 1:1 in a) with an electron affinity of -1.5 eV , 1:2 in b) with bridge or ether bonds between these and with an electron affinity of -1.39 eV and 2:2 in c) with same ether / bridge configuration and with an electron affinity of -0.89 eV; and oxygen terminated diamond (100) with Sn and Li in 1:1 ratio in d) and ether/ bridge configuration initially and with an electron affinity of -1.48 eV, 1:2 ratio in e) and ether/ bridge configuration initially and with an electron affinity of -1.87 eV and 1:2 ratio in f) and ketone / on top initially and with an electron affinity of -1.64 eV.

Sn mostly produced a covalent bond with surface C atoms and O atoms while Li atoms in most cases produced ionic bonds (as per the Mulliken charge analysis). The charge density was seen to shift in such a way that surface carbon atoms always had a negative charge on or near them, also seen in chapter 3. No direct bonding between the surface C atoms and Li atoms was seen in many cases. Sn was seen to possess a negative charge in some cases along with surface C atoms, although it is expected to contribute electrons to the surface of diamond and hence accumulate a positive charge. All this demands a molecular dynamics based study into this piece of research so that a properly optimised theory around this topic can be produced.

Another piece of future work would be to test these surface structures (that is Sn and heterostructure (Sn/Li) based termination on the bare and oxygen terminated diamond) on the surface of diamond (111) substrate. Diamond (111) has been seen to possess many remarkable properties when it comes to termination with different material

especially with graphene. It is expected to give more efficient outcome than its C(100) and C(110) counterpart with metal and metal oxide terminations (here Sn and SnO).

Also the experiments reported in this thesis were performed on boron doped diamond (BDD) due to the fact that boron doping renders the surface of diamond p doped, hence conductive and usable in XPS. However, we have seen better and more stable response of diamond with XPS at higher annealing temperatures in chapter 4. Hence, it is believed that the outcome with Sn, SnO and SnO_x/LiO_2 on the surface of diamond would be more stable and probably more efficient with a N doped diamond, an indication towards which is also given by the thermionic emission output in the conclusion section of this chapter.

Bibliography

[1] M. C. James, "Aluminium and Oxygen Termination of Diamond for Thermionic Applications," no. October 2019, 2019.

[2] B. W. Paul M, "Diamond thin films: a 21st-century material," *Trans. R. Soc. Lond. A*, vol. 358, pp. 473–495, 2000.

[3] "Characterization of Electron Emission From Diamond Surfaces For Energy Conversion Devices," 2020.

[4] S. Ullah *et al.*, "An investigation into the surface termination and near-surface bulk doping of oxygen-terminated diamond with lithium at various annealing temperatures," *MRS Adv.*, pp. 1–10, Apr. 2021, doi: 10.1557/s43580-021-00060-x.

[5] S. Ullah, G. Wan, C. Kouzios, C. Woodgate, M. Cattelan, and N. Fox, "Structure and electronic properties of tin monoxide (SnO) and lithiated SnO terminated diamond (100) and its comparison with lithium oxide terminated diamond," *Appl. Surf. Sci.*, vol. 559, p. 149962, 2021, doi: https://doi.org/10.1016/j.apsusc.2021.149962.

[6] K. M. O'Donnell *et al.*, "Diamond surfaces with air-stable negative electron affinity and giant electron yield enhancement," *Adv. Funct. Mater.*, vol. 23, no. 45, pp. 5608–5614, 2013, doi: 10.1002/adfm.201301424.

[7] B. E. Park, J. Park, S. Lee, S. Lee, W. H. Kim, and H. Kim, "Phase-controlled synthesis of SnO x thin films by atomic layer deposition and post-treatment," *Appl. Surf. Sci.*, vol. 480, pp. 472–477, Jun. 2019, doi: 10.1016/j.apsusc.2019.03.013.

[8] bchoate, "Waste Heat Recovery: Technology and Opportunities in U.S. Industry".

[9] T. L. Martin, "Lithium oxygen termination as a negative electron affinity surface on diamond : a computational and photoemission study," no. July, 2011, [Online]. Available: http://ethos.bl.uk/OrderDetails.do?uin=uk.bl.ethos.559712

[10] W. Shen, Y. Pan, S. Shen, H. Li, Y. Zhang, and G. Zhang, "Electron affinity of boron-terminated diamond (001) surfaces: a density functional theory study," *J.*

Mater. Chem. C, vol. 7, p. 9756, 2019, doi: 10.1039/c9tc02517k.

[11] K. M. O'Donnell, T. L. Martin, and N. L. Allan, "Light metals on oxygen-terminated diamond (100): Structure and electronic properties," *Chem. Mater.*, vol. 27, no. 4, pp. 1306–1315, 2015, doi: 10.1021/cm5043155.

[12] A. K. Tiwari, J. P. Goss, P. R. Briddon, N. G. Wright, A. B. Horsfall, and M. J. Rayson, "Effect of different surface coverages of transition metals on the electronic and structural properties of diamond," *Phys. Status Solidi Appl. Mater. Sci.*, vol. 209, no. 9, pp. 1697–1702, Sep. 2012, doi: 10.1002/pssa.201200027.

[13] J. Cook *et al.*, "Consensus on consensus: a synthesis of consensus estimates on human-caused global warming," *Environ. Res. Lett.*, vol. 11, no. 4, p. 048002, Apr. 2016, doi: 10.1088/1748-9326/11/4/048002.

[14] D. Lüthi *et al.*, "High-resolution carbon dioxide concentration record 650,000-800,000 years before present," *Nature*, vol. 453, no. 7193, pp. 379–382, May 2008, doi: 10.1038/NATURE06949.

[15] "World Population Prospects - Population Division - United Nations." https://population.un.org/wpp/Download/Standard/Population/ (accessed Jun. 26, 2022).

[16] J. Gütschow *et al.*, "The PRIMAP-hist national historical emissions time series," *Earth Syst. Sci. Data*, vol. 8, no. 2, pp. 571–603, Nov. 2016, doi: 10.5194/ESSD-8-571-2016.

[17] J. Gütschow, A. Günther, and M. Pflüger, "The PRIMAP-hist national historical emissions time series (1750-2019) v2.3.1," Sep. 2021, doi: 10.5281/ZENODO.5494497.

[18] IPCC, "Framing and Context," *Glob. Warm. 1.5°C*, pp. 49–92, May 2022, doi: 10.1017/9781009157940.003.

[19] "Climate Change | United Nations." https://www.un.org/en/global-issues/climate-change (accessed Jun. 30, 2022).

[20] "What does Trump actually believe on climate change? - BBC News." https://www.bbc.co.uk/news/world-us-canada-51213003 (accessed Jun. 26,

2022).

[21] "The Paris Agreement | UNFCCC." https://unfccc.int/process-and-meetings/the-paris-agreement/the-paris-agreement (accessed Jun. 30, 2022).

[22] "Fossil Fuels - Our World in Data." https://ourworldindata.org/fossil-fuels (accessed Jun. 26, 2022).

[23] "HOME - UN Climate Change Conference (COP26) at the SEC – Glasgow 2021." https://ukcop26.org/ (accessed Jun. 30, 2022).

[24] "Introduction - UN Climate Change Conference (COP26) at the SEC – Glasgow 2021." https://ukcop26.org/uk-presidency/ (accessed Jun. 30, 2022).

[25] A. Fenwick, O., Jones, "No TitleMaterials for the Energy Transition roadmap: Materials Thermoelectric Energy Conversion Materials," *September*, 2020. https://www.royce.ac.uk/materials-for-the-energy-transition-thermoelectric-energy-conversion

[26] D. Hoye, R.L.Z, Stranks, S.D., Khripko, "Materials for the Energy Transition roadmap: Materials for Photovoltaic Systems," *Henry Royce Institute*. https://www.royce.ac.uk/content/uploads/2020/09/M4ET-Materials-for-Photovoltaic-Systems-roadmap.pdf

[27] N. Stephens, I.E.L, Athanassopoulou, "No TitleMaterials for the Energy Transition roadmap: Materials for Low-Carbon Production of Hydrogen and Related Energy Carriers and Chemical Feedstocks," *Henry Royce Institute*. https://www.royce.ac.uk/content/uploads/2020/09/M4ET-Materials-for-low-carbon-production-of-hydrogen-and-related-energy-carriers-and-chemical-feedstocks-.pdf

[28] I. M. Moya, X., Ilevbare, "No TitleMaterials for the Energy Transition roadmap: Caloric Energy Conversion Materials," *Henry Royce Institute*. https://www.royce.ac.uk/content/uploads/2021/10/M4ET-Caloric-Energy-Conversion-Materials-roadmap.pdf

[29] D. E. H. J. Gernaat, H. S. de Boer, V. Daioglou, S. G. Yalew, C. Müller, and D. P. van Vuuren, "Climate change impacts on renewable energy supply," *Nat. Clim. Chang. 2021 112*, vol. 11, no. 2, pp. 119–125, Jan. 2021, doi: 10.1038/s41558-020-00949-9.

[30] Irena, "The Power to Change: Solar and Wind Cost Reduction Potential to 2025," 2016, Accessed: Jun. 30, 2022. [Online]. Available: www.irena.org

[31] K. Solaun and E. Cerdá, "Climate change impacts on renewable energy generation. A review of quantitative projections," *Renew. Sustain. Energy Rev.*, vol. 116, p. 109415, Dec. 2019, doi: 10.1016/J.RSER.2019.109415.

[32] S. Obara and R. Tanaka, "Waste heat recovery system for nuclear power plants using the gas hydrate heat cycle," *Appl. Energy*, vol. 292, p. 116667, Jun. 2021, doi: 10.1016/J.APENERGY.2021.116667.

[33] B. M. Nichols, J. E. Butler, J. N. Russell, and R. J. Hamers, "Photochemical functionalization of hydrogen-terminated diamond surfaces: A structural and mechanistic study," *J. Phys. Chem. B*, vol. 109, no. 44, pp. 20938–20947, Nov. 2005, doi: 10.1021/JP0545389/SUPPL_FILE/JP0545389SI20050907_063200.PDF.

[34] L. Maier, F. and Ristein, J. and Ley, "Electron affinity of plasma-hydrogenated and chemically oxidized diamond (100) surfaces," *Phys. Rev. B*, vol. 64, no. 16, p. 165411, 2001.

[35] M. C. James, F. Fogarty, R. Zulkharnay, N. A. Fox, and P. W. May, "A Review of Surface Functionalisation of Diamond for Thermionic Emission Applications," *Carbon*. 2020. doi: 10.1016/j.carbon.2020.09.019.

[36] F. Fogarty, "Renewable energy : low temperature thermionic emission from modified diamond surfaces," 2020, Accessed: May 28, 2021. [Online]. Available: http://hdl.handle.net/1983/95996647-2d8a-487f-adce-ee5f98fea033

[37] M. A. Cayless, "Thermionic generation of electricity," *Br. J. Appl. Phys.*, vol. 12, no. 9, p. 433, Sep. 1961, doi: 10.1088/0508-3443/12/9/303.

[38] J. Ryan Smith, "Increasing the efficiency of a thermionic engine using a negative electron affinity collector," *J. Appl. Phys.*, vol. 114, no. 16, p. 164514, Oct. 2013, doi: 10.1063/1.4826202.

[39] G. HATSOPOULOS, "THERMIONIC ENERGY CONVERSION," Sep. 1966, doi: 10.2514/6.1966-2318.

[40] A. C. Marshall, "A reformulation of thermionic theory for vacuum diodes," *Surf.*

Sci., vol. 517, no. 1–3, pp. 186–206, Oct. 2002, doi: 10.1016/S0039-6028(02)02063-0.

[41] G. L. Bennett, "Look at the Soviet space nuclear power program," *Proc. Intersoc. Energy Convers. Eng. Conf.*, vol. 2, pp. 1187–1194, 1989, doi: 10.1109/IECEC.1989.74620.

[42] M. Kataoka *et al.*, "Enhanced thermionic electron emission from a stacked structure of phosphorus-doped diamond with a nitrogen-doped diamond surface layer," *Phys. status solidi*, vol. 213, no. 10, pp. 2650–2653, Oct. 2016, doi: 10.1002/PSSA.201600173.

[43] W. F. Paxton, A. Steigerwald, M. Howell, N. Tolk, W. P. Kang, and J. L. Davidson, "The effect of hydrogen desorption kinetics on thermionic emission from polycrystalline chemical vapor deposited diamond," *Appl. Phys. Lett.*, vol. 101, no. 24, Dec. 2012, doi: 10.1063/1.4772069.

[44] W. F. Paxton, S. Ravipati, M. M. Brooks, M. Howell, and J. L. Davidson, "Thermionic Emission from Diamond Films in Molecular Hydrogen Environments," *Front. Mech. Eng.*, vol. 3, p. 18, Dec. 2017, doi: 10.3389/FMECH.2017.00018/BIBTEX.

[45] W. F. Paxton, M. Howell, W. P. Kang, and J. L. Davidson, "Influence of hydrogen on the thermionic electron emission from nitrogen-incorporated polycrystalline diamond films," *J. Vac. Sci. Technol. B, Nanotechnol. Microelectron. Mater. Process. Meas. Phenom.*, vol. 30, no. 2, p. 021202, Mar. 2012, doi: 10.1116/1.3684982.

[46] F. A. M. Koeck, R. J. Nemanich, A. Lazea, and K. Haenen, "Thermionic electron emission from low work-function phosphorus doped diamond films," *Diam. Relat. Mater.*, vol. 18, no. 5–8, pp. 789–791, May 2009, doi: 10.1016/j.diamond.2009.01.024.

[47] K. Uppireddi, T. L. Westover, T. S. Fisher, B. R. Weiner, and G. Morell, "Thermionic emission energy distribution from nanocrystalline diamond films for direct thermal-electrical energy conversion applications," *J. Appl. Phys.*, vol. 106, no. 4, p. 043716, Aug. 2009, doi: 10.1063/1.3204667.

[48] G. Xiao, G. Zheng, M. Qiu, Q. Li, D. Li, and M. Ni, "Thermionic energy conversion

for concentrating solar power," *Applied Energy*, vol. 208. Elsevier Ltd, pp. 1318–1342, Dec. 15, 2017. doi: 10.1016/j.apenergy.2017.09.021.

[49] F. A. M. Koeck, J. M. Garguilo, and R. J. Nemanich, "On the thermionic emission from nitrogen-doped diamond films with respect to energy conversion," in *Diamond and Related Materials*, Nov. 2004, pp. 2052–2055. doi: 10.1016/j.diamond.2004.06.027.

[50] F. A. M. Köck, J. M. Garguilo, B. Brown, and R. J. Nemanich, "Enhanced low-temperature thermionic field emission from surface-treated N-doped diamond films," *Diam. Relat. Mater.*, vol. 11, no. 3–6, pp. 774–779, Mar. 2002, doi: 10.1016/S0925-9635(02)00006-7.

[51] E. B. Lombardi, A. Mainwood, and K. Osuch, "Ab initio study of lithium and sodium in diamond," *Phys. Rev. B - Condens. Matter Mater. Phys.*, vol. 76, no. 15, Oct. 2007, doi: 10.1103/PhysRevB.76.155203.

[52] N. Jiang, A. Hatta, and T. Ito, "Nitrogen doping effects on electrical properties of diamond films," *Japanese J. Appl. Physics, Part 2 Lett.*, vol. 37, no. 10 A, Oct. 1998, doi: 10.1143/jjap.37.l1175.

[53] M. N. R. Ashfold, J. P. Goss, B. L. Green, P. W. May, M. E. Newton, and C. V. Peaker, "Nitrogen in Diamond," *Chemical Reviews*, vol. 120, no. 12. American Chemical Society, pp. 5745–5794, Jun. 24, 2020. doi: 10.1021/acs.chemrev.9b00518.

[54] B. C. Djubua and N. N. Chubun, "Emission Properties of Spindt-Type Cold Cathodes with Different Emission Cone Material," *IEEE Trans. Electron Devices*, vol. 38, no. 10, pp. 2314–2316, 1991, doi: 10.1109/16.88516.

[55] W. F. Paxton, A. Steigerwald, M. Howell, N. Tolk, W. P. Kang, and J. L. Davidson, "The effect of hydrogen desorption kinetics on thermionic emission from polycrystalline chemical vapor deposited diamond," *Appl. Phys. Lett.*, vol. 101, no. 24, p. 243509, Dec. 2012, doi: 10.1063/1.4772069.

[56] F. A. M. Koeck and R. J. Nemanich, "Sulfur doped nanocrystalline diamond films as field enhancement based thermionic emitters and their role in energy conversion," in *Diamond and Related Materials*, Nov. 2005, pp. 2051–2054. doi: 10.1016/j.diamond.2005.09.001.

[57] G. Wan, M. Cattelan, and N. A. Fox, “Electronic structure tunability of diamonds by surface functionalization,” *J. Phys. Chem. C*, 2019, doi: 10.1021/acs.jpcc.8b11232.

[58] K. M. O’Donnell *et al.*, “Diamond Surfaces with Air-Stable Negative Electron Affinity and Giant Electron Yield Enhancement,” *Adv. Funct. Mater.*, vol. 23, no. 45, pp. 5608–5614, Dec. 2013, doi: 10.1002/adfm.201301424.

[59] K. M. O’Donnell, T. L. Martin, and N. L. Allan, “Light Metals on Oxygen-Terminated Diamond (100): Structure and Electronic Properties,” *Chem. Mater.*, vol. 27, no. 4, pp. 1306–1315, Feb. 2015, doi: 10.1021/cm5043155.

[60] J. B. Cui, J. Ristein, M. Stammler, K. Janischowsky, G. Kleber, and L. Ley, “Hydrogen termination and electron emission from CVD diamond surfaces: A combined secondary electron emission, photoelectron emission microscopy, photoelectron yield, and field emission study,” *Diam. Relat. Mater.*, vol. 9, no. 3, pp. 1143–1147, 2000, doi: 10.1016/S0925-9635(99)00279-4.

[61] S. J. Sque, R. Jones, and P. R. Briddon, “Structure, electronics, and interaction of hydrogen and oxygen on diamond surfaces,” *Phys. Rev. B - Condens. Matter Mater. Phys.*, vol. 73, no. 8, p. 085313, Feb. 2006, doi: 10.1103/PhysRevB.73.085313.

[62] P. K. Baumann and R. J. Nemanich, “Surface cleaning, electronic states and electron affinity of diamond (100), (111) and (110) surfaces,” *Surf. Sci.*, vol. 409, no. 2, pp. 320–335, Jul. 1998, doi: 10.1016/S0039-6028(98)00259-3.

[63] M. Rutter and J. Robertson, “Ab initio calculation of electron affinities of diamond surfaces,” *Phys. Rev. B - Condens. Matter Mater. Phys.*, vol. 57, no. 15, pp. 9241–9245, Apr. 1998, doi: 10.1103/PhysRevB.57.9241.

[64] K. M. O’Donnell, T. L. Martin, N. A. Fox, and D. Cherns, “Ab initio investigation of lithium on the diamond C(100) surface,” *Phys. Rev. B - Condens. Matter Mater. Phys.*, vol. 82, no. 11, p. 115303, Sep. 2010, doi: 10.1103/PhysRevB.82.115303.

[65] Z. Sun *et al.*, “Boron-terminated diamond (100) surfaces with promising structural and electronic properties,” *Phys. Chem. Chem. Phys.*, vol. 22, no. 15, pp. 8060–8066, Apr. 2020, doi: 10.1039/d0cp00121j.

[66] F. Maier, J. Ristein, and L. Ley, "Electron affinity of plasma-hydrogenated and chemically oxidized diamond (100) surfaces," *Phys. Rev. B - Condens. Matter Mater. Phys.*, vol. 64, no. 16, p. 165411, Oct. 2001, doi: 10.1103/PhysRevB.64.165411.

[67] D. Takeuchi *et al.*, "Direct observation of negative electron affinity in hydrogen-terminated diamond surfaces," *Appl. Phys. Lett.*, vol. 86, no. 15, pp. 1–3, Apr. 2005, doi: 10.1063/1.1900925.

[68] K. P. Loh, J. S. Foord, R. G. Egdell, and R. B. Jackman, "Tuning the electron affinity of CVD diamond with adsorbed caesium and oxygen layers," *Diam. Relat. Mater.*, vol. 6, no. 5–7, pp. 874–878, Apr. 1997, doi: 10.1016/s0925-9635(96)00737-6.

[69] J. L. Nie, H. Y. Xiao, X. T. Zu, and F. Gao, "First principles calculations on Na and K-adsorbed diamond(1 0 0) surface," *Chem. Phys.*, vol. 326, no. 2–3, pp. 308–314, Aug. 2006, doi: 10.1016/j.chemphys.2006.02.005.

[70] P. K. Baumann and R. J. Nemanich, "Characterization of cobalt-diamond (100) interfaces: electron affinity and Schottky barrier," *Appl. Surf. Sci.*, vol. 104–105, pp. 267–273, Sep. 1996, doi: 10.1016/S0169-4332(96)00156-0.

[71] A. K. Tiwari, J. P. Goss, P. R. Briddon, N. G. Wright, A. B. Horsfall, and M. J. Rayson, "Effect of different surface coverages of transition metals on the electronic and structural properties of diamond," *Phys. status solidi*, vol. 209, no. 9, pp. 1697–1702, Sep. 2012, doi: 10.1002/pssa.201200027.

[72] A. K. Tiwari, J. P. Goss, P. R. Briddon, N. G. Wright, A. B. Horsfall, and M. J. Rayson, "Electronic and structural properties of diamond (001) surfaces terminated by selected transition metals," *Phys. Rev. B - Condens. Matter Mater. Phys.*, vol. 86, no. 15, Oct. 2012, doi: 10.1103/PhysRevB.86.155301.

[73] S. Petrick and C. Benndorf, "Potassium adsorption on hydrogen- and oxygen-terminated diamond(100) surfaces," *Diam. Relat. Mater.*, vol. 10, no. 3–7, pp. 519–525, Mar. 2001, doi: 10.1016/S0925-9635(00)00440-4.

[74] Y. Luo, *Comprehensive handbook of chemical bond energies*. 2007. Accessed: Nov. 08, 2019. [Online]. Available: https://content.taylorfrancis.com/books/download?dac=C2009-0-19699-

5&isbn=9781420007282&format=googlePreviewPdf

[75] B. Ruscic, D. Feller, and K. A. Peterson, “Active Thermochemical Tables: dissociation energies of several homonuclear first-row diatomics and related thermochemical values,” 2015, pp. 191–202. doi: 10.1007/978-3-662-47051-0_17.

[76] M. C. James, A. Croot, P. W. May, and N. L. Allan, “Negative electron affinity from aluminium on the diamond (1 0 0) surface: A theoretical study,” *J. Phys. Condens. Matter*, vol. 30, no. 23, p. 235002, May 2018, doi: 10.1088/1361-648X/aac041.

[77] K. M. O’Donnell *et al.*, “Diamond Surfaces with Air-Stable Negative Electron Affinity and Giant Electron Yield Enhancement,” *Adv. Funct. Mater.*, vol. 23, no. 45, pp. 5608–5614, Dec. 2013, doi: 10.1002/adfm.201301424.

[78] A. Schenk *et al.*, “Formation of a silicon terminated (100) diamond surface,” *Appl. Phys. Lett.*, vol. 106, no. 19, 2015, doi: 10.1063/1.4921181.

[79] A. K. Schenk *et al.*, “The surface electronic structure of silicon terminated (100) diamond,” *Nanotechnology*, vol. 27, no. 27, p. 275201, Jul. 2016, doi: 10.1088/0957-4484/27/27/275201.

[80] M. J. Sear *et al.*, “Germanium terminated (1 0 0) diamond,” *J. Phys. Condens. Matter*, vol. 29, no. 14, p. 145002, Apr. 2017, doi: 10.1088/1361-648X/aa57c4.

[81] W. Zhou and N. Umezawa, “Band gap engineering of bulk and nanosheet SnO: An insight into the interlayer Sn-Sn lone pair interactions,” *Phys. Chem. Chem. Phys.*, vol. 17, no. 27, pp. 17816–17820, Jul. 2015, doi: 10.1039/c5cp02255j.

[82] J. Geurts, S. Rau, W. Richter, and F. J. Schmitte, “SnO films and their oxidation to SnO2: Raman scattering, IR reflectivity and X-ray diffraction studies,” *Thin Solid Films*, vol. 121, no. 3, pp. 217–225, Nov. 1984, doi: 10.1016/0040-6090(84)90303-1.

[83] B. B. Alchagirov, R. K. Arkhestov, and F. F. Dyshekova, “Electron work function in alloys with alkali metals,” *Tech. Phys.*, vol. 57, no. 11, pp. 1541–1546, 2012, doi: 10.1134/S1063784212110023.

[84] K. J. Saji, K. Tian, M. Snure, and A. Tiwari, "2D Tin Monoxide—An Unexplored p-Type van der Waals Semiconductor: Material Characteristics and Field Effect Transistors," *Adv. Electron. Mater.*, vol. 2, no. 4, pp. 1–9, 2016, doi: 10.1002/aelm.201500453.

[85] A. K. Geim and I. V. Grigorieva, "Van der Waals heterostructures," *Nature*, vol. 499, no. 7459, pp. 419–425, Jul. 2013, doi: 10.1038/nature12385.

[86] K. E. Aifantis, S. Brutti, S. A. Hackney, T. Sarakonsri, and B. Scrosati, "SnO2/C nanocomposites as anodes in secondary Li-ion batteries," *Electrochim. Acta*, vol. 55, no. 18, pp. 5071–5076, Jul. 2010, doi: 10.1016/j.electacta.2010.03.083.

[87] W. Dong *et al.*, "A Robust and Conductive Black Tin Oxide Nanostructure Makes Efficient Lithium-Ion Batteries Possible," *Adv. Mater.*, vol. 29, no. 24, Jun. 2017, doi: 10.1002/adma.201700136.

[88] A. Pedersen and M. Luisier, "Lithiation of Tin Oxide: A Computational Study," *ACS Appl. Mater. Interfaces*, vol. 6, no. 24, pp. 22257–22263, Dec. 2014, doi: 10.1021/am506108s.

[89] S. J. Clark *et al.*, "First principles methods using CASTEP," *Zeitschrift fur Krist.*, vol. 220, no. 5–6, pp. 567–570, May 2005, doi: 10.1524/zkri.220.5.567.65075.

[90] F. Giustino, "Materials Modelling using Density Functional Theory," *Oxford Univ. Press*, pp. 1–19, 2014.

[91] & R. O. M. Born, "(," *Ann. Phys.*, vol. 84, p. 457, 1927.

[92] D. Vanderbilt, "Soft self-consistent pseudopotentials in a generalized eigenvalue formalism," *Phys. Rev. B*, vol. 41, no. 11, pp. 7892–7895, Apr. 1990, doi: 10.1103/PhysRevB.41.7892.

[93] M. Fuchs and F. Der Mpg, "Comparison of exchange-correlation functionals : from LDA to GGA and beyond," *J. Chem. Physics,* no. November, 2005.

[94] J. P. Perdew, K. Burke, and M. Ernzerhof, "Generalized gradient approximation made simple," *Phys. Rev. Lett.*, vol. 77, no. 18, pp. 3865–3868, Oct. 1996, doi: 10.1103/PhysRevLett.77.3865.

[95] A. J. Cohen, P. Mori-Sánchez, and W. Yang, "Insights into Current Limitations of

Density Functional Theory," *Science (80-.).*, vol. 321, no. 5890, pp. 792–794, Aug. 2008, doi: 10.1126/science.1158722.

[96] H. J. Monkhorst and J. D. Pack, "Special points for Brillouin-zone integrations," *Phys. Rev. B*, vol. 13, no. 12, pp. 5188–5192, Jun. 1976, doi: 10.1103/PhysRevB.13.5188.

[97] R. S. Mulliken, "Electronic Population Analysis on LCAO–MO Molecular Wave Functions. I," *J. Chem. Phys.*, vol. 23, no. 10, pp. 1833–1840, Oct. 1955, doi: 10.1063/1.1740588.

[98] A. J. Morris, R. J. Nicholls, C. J. Pickard, and J. R. Yates, "OptaDOS: A tool for obtaining density of states, core-level and optical spectra from electronic structure codes," *Comput. Phys. Commun.*, vol. 185, no. 5, pp. 1477–1485, 2014, doi: 10.1016/j.cpc.2014.02.013.

[99] C. J. Fall, N. Binggeli, and A. Baldereschi, "Deriving accurate work functions from thin-slab calculations," *J. Phys. Condens. Matter*, vol. 11, no. 13, pp. 2689–2696, Apr. 1999, doi: 10.1088/0953-8984/11/13/006.

[100] K. M. O'Donnell, T. L. Martin, N. A. Fox, and D. Cherns, "Ab initio investigation of lithium on the diamond C(100) surface," *Phys. Rev. B - Condens. Matter Mater. Phys.*, vol. 82, no. 11, Sep. 2010, doi: 10.1103/PhysRevB.82.115303.

[101] M. Z. Othman, P. W. May, N. A. Fox, and P. J. Heard, "Incorporation of lithium and nitrogen into CVD diamond thin films," *Diam. Relat. Mater.*, vol. 44, pp. 1–7, Apr. 2014, doi: 10.1016/J.DIAMOND.2014.02.001.

[102] X. Zhang, "Investigation of Heavily Boron Doped Diamond Thin Film for Electronic Devices," *PhD Thesis, Univ. Bristol*, 2017.

[103] V. A. Shershulin *et al.*, "Size-dependent luminescence of color centers in composite nanodiamonds," *Phys. status solidi*, vol. 212, no. 11, pp. 2600–2605, Nov. 2015, doi: 10.1002/PSSA.201532204.

[104] M. C. Patt, *Bulk and surface sensitive energy-filtered photoemission microscopy using synchrotron radiation for the study of resistive switching memories*, vol. 122. 2016.

[105] R. Messier, "Thin Film Deposition Processes," *MRS Bull.*, vol. 13, no. 11, pp. 18–

21, 1988, doi: 10.1557/S0883769400063879.

[106] F. Izumi, “Pattern-fitting structure refinement of tin(II) oxide,” *J. Solid State Chem.*, vol. 38, no. 3, pp. 381–385, Jul. 1981, doi: 10.1016/0022-4596(81)90068-2.

[107] N. Fairley *et al.*, “Systematic and collaborative approach to problem solving using X-ray photoelectron spectroscopy,” *Appl. Surf. Sci. Adv.*, vol. 5, p. 100112, Sep. 2021, doi: 10.1016/J.APSADV.2021.100112.

[108] M. Escher *et al.*, “NanoESCA: A novel energy filter for imaging x-ray photoemission spectrosocpy,” *J. Phys. Condens. Matter*, vol. 17, no. 16, Apr. 2005, doi: 10.1088/0953-8984/17/16/004.

[109] H. Dominguez-Andrade, A. Croot, G. Wan, J. A. Smith, and N. A. Fox, “Characterisation of thermionic emission current with a laser-heated system,” *Rev. Sci. Instrum.*, vol. 90, no. 4, p. 045110, Apr. 2019, doi: 10.1063/1.5088150.

[110] A. Croot, G. Wan, A. Rowan, H. D. Andrade, J. A. Smith, and N. A. Fox, “Beta Radiation Enhanced Thermionic Emission from Diamond Thin Films,” *Front. Mech. Eng.*, vol. 3, p. 17, Nov. 2017, doi: 10.3389/fmech.2017.00017.

[111] S. Nunez-Sanchez, H. D. Andrade, J. Harwood, I. Bickerton, N. A. Fox, and M. J. Cryan, “Molybdenum gratings as a high-temperature refractory platform for plasmonic heat generators in the infrared,” *Micro Nano Lett.*, vol. 13, no. 9, pp. 1325–1328, Sep. 2018, doi: 10.1049/MNL.2018.0156.

[112] D. Takeuchi, S.-G. Ri, H. Kato, C. E. Nebel, and S. Yamasaki, “Negative electron affinity on hydrogen terminated diamond,” *Phys. status solidi*, vol. 202, no. 11, pp. 2098–2103, Sep. 2005, doi: 10.1002/pssa.200561927.

[113] D. Petrini and K. Larsson, “A theoretical study of the energetic stability and geometry of hydrogen- and oxygen-terminated diamond (100) surfaces,” *J. Phys. Chem. C*, vol. 111, no. 2, pp. 795–801, Jan. 2007, doi: 10.1021/jp063383h.

[114] G. Speranza *et al.*, “XPS and UPS in situ study of oxygen thermal desorption from nanocrystalline diamond surface oxidized by different process,” *Diam. Relat. Mater.*, vol. 20, no. 4, pp. 560–563, Apr. 2011, doi: 10.1016/j.diamond.2011.03.001.

[115] L. Diederich, P. Aebi, O. M. Küttel, and L. Schlapbach, “NEA peak of the differently

terminated and oriented diamond surfaces," *Surf. Sci.*, vol. 424, no. 2, pp. 1–7, 1999, doi: 10.1016/S0039-6028(99)00210-1.

[116] M. Kaviani, P. Deák, B. Aradi, T. Frauenheim, J. P. Chou, and A. Gali, "Proper surface termination for luminescent near-surface NV centers in diamond," *Nano Lett.*, vol. 14, no. 8, pp. 4772–4777, Aug. 2014, doi: 10.1021/nl501927y.

[117] P. K. Baumann and R. J. Nemanich, "Electron emission from metal-diamond (100), (111) and (110) interfaces," *Diam. Relat. Mater.*, vol. 7, no. 2–5, pp. 612–619, Feb. 1998, doi: 10.1016/s0925-9635(97)00256-2.

[118] P. K. Baumann and R. J. Nemanich, "Electron affinity and Schottky barrier height of metal-diamond (100), (111), and (110) interfaces," *J. Appl. Phys.*, vol. 83, no. 4, pp. 2072–2082, Feb. 1998, doi: 10.1063/1.366940.

[119] K. M. O'Donnell *et al.*, "Photoelectron emission from lithiated diamond," *Phys. Status Solidi Appl. Mater. Sci.*, vol. 211, no. 10, pp. 2209–2222, 2014, doi: 10.1002/pssa.201431414.

[120] P. K. Baumann and R. J. Nemanich, "Characterization of copper-diamond (100), (111), and (110) interfaces: Electron affinity and Schottky barrier," *Phys. Rev. B*, vol. 58, no. 3, pp. 1643–1654, Jul. 1998, doi: 10.1103/PhysRevB.58.1643.

[121] M. C. James, P. W. May, and N. L. Allan, "*Ab initio* study of negative electron affinity from light metals on the oxygen-terminated diamond (1 1 1) surface," *J. Phys. Condens. Matter*, vol. 31, no. 29, p. 295002, Jul. 2019, doi: 10.1088/1361-648X/ab18ef.

[122] F. Fogarty and F. Fogarty, "Renewable Energy – Low Temperature Thermionic Emission from Modified Diamond Surfaces," no. February, 2020.

[123] M. De *et al.*, "The (100), (111) and (110) surfaces of diamond: an abï¿¿initio B3LYP study," *Mol. Phys.*, vol. 112, no. 7, pp. 1030–1039, 2014, doi: 10.1080/00268976.2013.829250.

[124] D. Qi *et al.*, "Tuning the electron affinity and secondary electron emission of diamond (100) surfaces by diels-alder reaction," *Langmuir*, vol. 23, no. 19, pp. 9722–9727, Sep. 2007, doi: 10.1021/la701285h.

[125] J. Furthmüller, J. Hafner, and G. Kresse, "Dimer reconstruction and electronic

surface states on clean and hydrogenated diamond (100) surfaces," *Phys. Rev. B - Condens. Matter Mater. Phys.*, vol. 53, no. 11, pp. 7334–7351, Mar. 1996, doi: 10.1103/PhysRevB.53.7334.

[126] J. Van Der Weide, Z. Zhang, P. K. Baumann, M. G. Wensell, J. Bernholc, and R. J. Nemanich, "Negative-electron-affinity effects on the diamond (100) surface," *Phys. Rev. B*, vol. 50, no. 8, pp. 5803–5806, Aug. 1994, doi: 10.1103/PhysRevB.50.5803.

[127] X. M. Zheng and P. V. Smith, "The stable configurations for oxygen chemisorption on the diamond (100) and (111) surfaces," *Surf. Sci.*, vol. 262, no. 1–2, pp. 219–234, Feb. 1992, doi: 10.1016/0039-6028(92)90473-J.

[128] J. D. Levine, "Structural and electronic model of negative electron affinity on the Si/Cs/O surface," *Surf. Sci.*, vol. 34, no. 1, pp. 90–107, 1973, doi: 10.1016/0039-6028(73)90190-8.

[129] J. P. Goss, R. J. Eyre, and P. R. Briddon, "Theoretical models for doping diamond for semiconductor applications," *Physica Status Solidi (B) Basic Research*, vol. 245, no. 9. pp. 1679–1700, Sep. 2008. doi: 10.1002/pssb.200744115.

[130] S. A. Kajihara, A. Antonelli, J. Bernholc, and R. Car, "Nitrogen and potential n-type dopants in diamond," *Phys. Rev. Lett.*, vol. 66, no. 15, pp. 2010–2013, 1991, doi: 10.1103/PhysRevLett.66.2010.

[131] E. B. Lombardi and A. Mainwood, "A first principles study of lithium, sodium and aluminum in diamond," *Diam. Relat. Mater.*, vol. 17, no. 7–10, pp. 1349–1352, Jul. 2008, doi: 10.1016/j.diamond.2007.12.015.

[132] G. Popovici, R. G. Wilson, T. Sung, M. A. Prelas, and S. Khasawinah, "Diffusion of boron, lithium, oxygen, hydrogen, and nitrogen in type IIa natural diamond," *J. Appl. Phys.*, vol. 77, no. 10, pp. 5103–5106, 1995, doi: 10.1063/1.359320.

[133] R. Job, M. Werner, A. Denisenko, A. Zaitsev, and W. R. Fahrner, "Electrical properties of lithium-implanted layers on synthetic diamond," *Diam. Relat. Mater.*, vol. 5, no. 6–8, pp. 757–760, 1996, doi: 10.1016/0925-9635(95)00458-0.

[134] M. Restle *et al.*, "Lattice sites of ion implanted Li in diamond," *Appl. Phys. Lett.*, vol. 66, no. 20, pp. 2733–2735, May 1995, doi: 10.1063/1.113691.

[135] C. Uzan-Saguy, C. Cytermann, B. Fizgeer, V. Richter, R. Brener, and R. Kalish, "Diffusion of lithium in diamond," in *Physica Status Solidi (A) Applied Research*, Oct. 2002, pp. 508–516. doi: 10.1002/1521-396X(200210)193:3<508::AID-PSSA508>3.0.CO;2-H.

[136] G. Popovici, T. Sung, S. Khasawinah, M. A. Prelas, and R. G. Wilson, "Forced diffusion of impurities in natural diamond and polycrystalline diamond films," *J. Appl. Phys.*, vol. 77, no. 11, pp. 5625–5629, 1995, doi: 10.1063/1.359204.

[137] K. Okumura, J. Mort, and M. Machonkin, "Lithium doping and photoemission of diamond thin films," *Appl. Phys. Lett.*, vol. 57, no. 18, pp. 1907–1909, 1990, doi: 10.1063/1.104008.

[138] H. Sachdev, R. Haubner, and B. Lux, "Lithium addition during CVD diamond deposition using lithium tert.-butanolat as precursor," *Diam. Relat. Mater.*, vol. 6, no. 2–4, pp. 494–500, Mar. 1997, doi: 10.1016/s0925-9635(96)00628-0.

[139] P. W. May, J. C. Stone, M. N. R. Ashfold, K. R. Hallam, W. N. Wang, and N. A. Fox, "The effect of diamond surface termination species upon field emission properties," *Diam. Relat. Mater.*, vol. 7, no. 2–5, pp. 671–676, Feb. 1998, doi: 10.1016/s0925-9635(97)00181-7.

[140] D. Briggs, "X-ray photoelectron spectroscopy (XPS)," *Handb. Adhes. Second Ed.*, pp. 621–622, 2005, doi: 10.1002/0470014229.ch22..

[141] A. V. Shchukarev and D. V. Korolkov, "XPS study of group IA carbonates," *Cent. Eur. J. Chem.*, vol. 2, no. 2, pp. 347–362, 2004, doi: 10.2478/BF02475578.

[142] S. Ullah and N. Fox, "Modification of the Surface Structure and Electronic Properties of Diamond (100) with Tin as a Surface Termination: A Density Functional Theory Study," *J. Phys. Chem. C*, vol. 125, no. 45, pp. 25165–25174, 2021, doi: 10.1021/acs.jpcc.1c05973.

[143] D. Takeuchi, S. G. Ri, H. Kato, C. E. Nebel, and S. Yamasaki, "Negative electron affinity on hydrogen terminated diamond," in *Physica Status Solidi (A) Applications and Materials Science*, Sep. 2005, pp. 2098–2103. doi: 10.1002/pssa.200561927.

[144] F. Maier, M. Riedel, J. Ristein, and L. Ley, "Origin of Surface Conductivity in Diamond," 2000.

[145] D. Takeuchi, M. Riedel, J. Ristein, and L. Ley, "Surface band bending and surface conductivity of hydrogenated diamond," *Phys. Rev. B - Condens. Matter Mater. Phys.*, vol. 68, no. 4, Jul. 2003, doi: 10.1103/PhysRevB.68.041304.

[146] K. P. Loh, X. N. Xie, S. W. Yang, J. S. Pan, and P. Wu, "A spectroscopic study of the negative electron affinity of cesium oxide-coated diamond (111) and theoretical calculation of the surface density-of-states on oxygenated diamond (111)," *Diam. Relat. Mater.*, vol. 11, no. 7, pp. 1379–1384, Jul. 2002, doi: 10.1016/S0925-9635(02)00014-6.

[147] K. W. Wong, Y. M. Wang, S. T. Lee, and R. W. M. Kwok, "Lowering of work function induced by deposition of ultra-thin rubidium fluoride layer on polycrystalline diamond surface," *Appl. Surf. Sci.*, vol. 140, no. 1–2, pp. 144–149, 1999, doi: 10.1016/S0169-4332(98)00582-0.

[148] J. van der Weide, "Schottky barrier height and negative electron affinity of titanium on (111) diamond," *J. Vac. Sci. Technol. B Microelectron. Nanom. Struct.*, vol. 10, no. 4, p. 1940, Jul. 1992, doi: 10.1116/1.586162.

[149] S. C. Halliwell, P. W. May, N. A. Fox, and M. Z. Othman, "Investigations of the co-doping of boron and lithium into CVD diamond thin films," *Diam. Relat. Mater.*, vol. 76, pp. 115–122, Jun. 2017, doi: 10.1016/j.diamond.2017.05.001.

[150] J. J. Lander and J. Morrison, "Low energy electron diffraction study of the (111) diamond surface," *Surf. Sci.*, vol. 4, no. 3, pp. 241–246, May 1966, doi: 10.1016/0039-6028(66)90004-5.

[151] K. M. O'Donnell, T. L. Martin, N. A. Fox, and D. Cherns, "The Li-adsorbed C(100)-(1x1):O diamond surface," in *Materials Research Society Symposium Proceedings*, 2011, pp. 163–168. doi: 10.1557/opl.2011.442.

[152] P. E. Pehrsson and T. W. Mercer, "Oxidation of the hydrogenated diamond (100) surface," *Surf. Sci.*, vol. 460, no. 1–3, pp. 49–66, Jul. 2000, doi: 10.1016/S0039-6028(00)00494-5.

[153] "Core level binding energies for the elements Zr-Te (Z=40-52) - IOPscience." https://iopscience.iop.org/article/10.1088/0022-3719/13/11/008/pdf (accessed Jun. 06, 2020).

[154] D. Shuttleworth, "Preparation of metal-polymer dispersions by plasma

techniques. An ESCA investigation," *J. Phys. Chem.*, vol. 84, no. 12, pp. 1629–1634, 1980, doi: 10.1021/j100449a038.

[155] J. Zheng *et al.*, "From novel PtSn/Pt(110) surface alloys to SnOx/Pt(110) nano-oxides," *Surf. Sci.*, vol. 615, pp. 103–109, Sep. 2013, doi: 10.1016/J.SUSC.2013.05.004.

[156] P. De Padova, R. Larciprete, M. Mangiantini, and M. Fanfoni, "Cr, Sn and Ag SnO2 interface formation studied by synchrotron radiation induced UPS," *J. Electron Spectros. Relat. Phenomena*, vol. 76, no. C, pp. 499–504, 1995, doi: 10.1016/0368-2048(95)02474-3.

[157] M. C. James, M. Cattelan, N. A. Fox, R. F. Silva, R. M. Silva, and P. W. May, "Experimental Studies of Electron Affinity and Work Function from Aluminium on Oxidized Diamond (100) and (111) Surfaces," 2021, doi: 10.1002/pssb.202100027.

[158] L. Diederich, O. M. Küttel, E. Schaller, and L. Schlapbach, "Photoemission from the negative electron affinity (100) natural hydrogen terminated diamond surface," *Surf. Sci.*, vol. 349, no. 2, pp. 176–184, Apr. 1996, doi: 10.1016/0039-6028(95)01117-X.

[159] M. Schreck, S. Gsell, R. Brescia, and M. Fischer, "Ion bombardment induced buried lateral growth: the key mechanism for the synthesis of single crystal diamond wafers," *Sci. Reports 2017 71*, vol. 7, no. 1, pp. 1–8, Mar. 2017, doi: 10.1038/srep44462.

[160] N. Mizuochi, N. Tokuda, M. Ogura, and S. Yamasaki, "Isotope effect of deuterium microwave plasmas on the formation of atomically flat (111) diamond surfaces," *Jpn. J. Appl. Phys.*, vol. 51, no. 9, p. 090106, Sep. 2012, doi: 10.1143/JJAP.51.090106/XML.

[161] T. Matsumoto *et al.*, "Inversion channel diamond metal-oxide-semiconductor field-effect transistor with normally off characteristics," *Sci. Reports 2016 61*, vol. 6, no. 1, pp. 1–6, Aug. 2016, doi: 10.1038/srep31585.

[162] A. Stacey *et al.*, "Nitrogen Terminated Diamond," *Adv. Mater. Interfaces*, vol. 2, no. 10, p. 1500079, Jul. 2015, doi: 10.1002/admi.201500079.